For Reference

NOT TO BE TAKEN FROM THIS ROOM

Ex libris
Universitatis
Albertaensis

QUAECUMQUE VERA

Digitized by the Internet Archive
in 2021 with funding from
University of Alberta Libraries

https://archive.org/details/Byrne1971

THE UNIVERSITY OF ALBERTA

THE APPLICATION OF HYPOELASTIC THEORY TO PROBLEMS IN PLASTICITY

BY

© THOMAS PETER BYRNE

A THESIS
SUBMITTED TO THE FACULTY OF GRADUATE STUDIES
IN PARTIAL FULFILMENT OF THE REQUIREMENTS FOR THE DEGREE
OF DOCTOR OF PHILOSOPHY

DEPARTMENT OF MECHANICAL ENGINEERING

EDMONTON, ALBERTA
FALL, 1971

Thesis
1971F
13D

UNIVERSITY OF ALBERTA

FACULTY OF GRADUATE STUDIES

The undersigned certify that they have read, and recommend to the Faculty of Graduate Studies for acceptance, a thesis entitled "The Application of Hypoelastic Theory to Problems in Plasticity" submitted by Thomas Peter Byrne in partial fulfilment of the requirements for the degree of Doctor of Philosophy.

ABSTRACT

The problems of tension, simple shear and torsion are solved using a hypoelastic constitutive equation similar to the Prandtl-Reuss equation for an elastic-plastic material. It is shown that the hypoelastic solutions give underestimates for the force variables of the classical elastic-plastic solutions in these particular problems.

Simple extension and torsion of a circular and square bar are investigated experimentally for commercially pure aluminum. A work-hardening function is approximated from the results of the tension test. The torsion problem is then solved for both the circular and square cross section using hypoelastic theory. The theoretical and experimental results are compared for the work-hardening material.

ACKNOWLEDGEMENTS

The author wishes to express his gratitude to Dr. J.B. Haddow for the guidance and supervision of this thesis.

Appreciation is extended to the National Research Council and the University of Alberta for the financial support received during the course of this research.

The experimental test specimens were prepared by members of the Mechanical Engineering shop. Mr. R. Haswell assisted in all stages of the experimental work and Mr. F. Christopher was of great value during the instrumentations. Typing of the thesis was done by Miss H. Wozniuk.

The author would also like to thank his wife, Sigrid, for her patience and encouragement.

TABLE OF CONTENTS

Page

CHAPTER I INTRODUCTION 1

CHAPTER II THE RELATION BETWEEN HYPOELASTICITY AND PLASTICITY 3

2.1 The General Hypoelastic Constitutive Equation 3

2.2 An Elastic-Perfectly Plastic Constitutive Equation 10

2.3 A Hypoelastic Constitutive Equation Similar to the Prandtl-Reuss Equation 17

2.4 A Hypoelastic Constitutive Equation Suitable for Some Work-Hardening Materials .. 22

CHAPTER III SOLUTIONS OF SOME HYPOELASTIC PROBLEMS AND COMPARISON WITH CORRESPONDING ELASTIC-PERFECTLY PLASTIC SOLUTIONS 24

3.1 Simple Extension 24

3.2 Simple Shear 26

3.3 Torsion 36

3.3.a Statement of the Problem 36

3.3.b Classical Elastic Torsion 36

3.3.c Hypoelastic Torsion 40

3.3.d Numerical Procedure for a Square Cross-Section 51

3.3.e Results for Torsion of a Square Bar 59

3.3.f Hypoelastic Torsion of a Circular Bar 60

TABLE OF CONTENTS (continued)

Page

CHAPTER IV EXPERIMENTAL CONSIDERATION OF A WORK-HARDENING MATERIAL 73

4.1 Torsion Tests 73

4.1.1 Experimental Apparatus 73

4.1.2 The Test Specimens 75

4.1.3 Calibration and Experimental Procedure 77

4.1.3.a Calibration of the Dynamometer.. 77

4.1.3.b Calibration of Twist Measurement 78

4.1.3.c Experimental Procedure 81

4.1.4 Results of the Torsion Test 81

4.1.5 Comparison Test 83

4.2 Tension Test 85

CHAPTER V SOLUTION OF SOME WORK-HARDENING PROBLEMS AND COMPARISON TO EXPERIMENTAL RESULTS 114

5.1 Determination of the Work-Hardening Function 114

5.2 Simple Shear 117

5.3 Torsion of a Circular Bar 119

5.4 Torsion of a Square Bar 120

5.5 An Elastic-Plastic Constitutive Equation for a Work-Hardening Material 123

TABLE OF CONTENTS (continued)

Page

CHAPTER VI CONCLUSION 134

6.1 Estimation of Errors 134

6.1.1 Errors in Numerical Procedure 134

6.1.2 Experimental Errors 141

6.2 Discussion of Errors 142

6.3 Discussion of Results 143

BIBLIOGRAPHY 152

LIST OF TABLES

Table		Page
3.1	Results for Elastic-Plastic Torsion of a Square Bar	63
4.1	Torque Calibration	88
4.2	Calibration of Angle of Twist for Circular Specimen	89
4.3	Calibration of Angle of Twist for Square Specimen	90
4.4	Experimental Data for Torsion of Circular Bar	91
4.5	Results for Circular Cross-Section	92
4.6	Experimental Data for Torsion of Square Bar	93
4.7	Results for Square Cross-Section	94
4.8	Summary of Results for Circular Bar	95
4.9	Summary of Results for Square Bar	96
4.10	Calibration of Angle of Twist for Comparison Specimen	97
4.11	Experimental Data for Comparison Test	98
4.12	Calculation of Angle of Twist from Spider Voltage Readings	99
4.13	Experimental Data for Tensile Test	100
4.14	Summary of Results for Tensile Test	101
5.1	Estimated Slopes of Tensile Results	127
5.2	Results for Torsion of Circular Bar	128
6.1	Estimation of Maximum Errors in Slopes	149
6.2	Estimation of Maximum Errors in Moments	150

LIST OF FIGURES

Figure		Page
3.1	Simple Extension ($\mu/k = 1000$)	64
3.2	Typical Rectangular Element in Simple Shear	27
3.3	Simple Shear ($\mu/k = 1000, 100, 10$)	65
3.4	Simple Shear ($\mu/k = 1$)	66
3.5	Classical Elastic-Plastic Theory Using the Jaumann Stress Rate ($\mu/k = 1$)	67
3.6	Hypoelastic Theory using the Jaumann Stress Rate ($\mu/k = 1$)	68
3.7	Right Prismatic Bar Under Pure Torsion	37
3.8	Square Cross-Section of the Bar	52
3.9	Typical Gridded Region for Numerical Calculation ..	54
3.10	Moment for Torsion of a Square Bar ($\mu/k = 1000$) ..	69
3.11	Maximum Stress Function for Torsion of a Square Bar ($\mu/k = 1000$)	70
3.12	Maximum Shear Stress for Torsion of a Square Bar ($\mu/k = 1000$)	71
3.13	Moment for Torsion of a Circular Bar ($\mu/k = 1000$).	72
4.1	Spider Apparatus Mounted on Specimen	74
4.2	Lever Arms and Transducers	75
4.3	Calibration of the Dynamometer	77
4.4	Moment Calibration Curve	102
4.5	Calibration of Angle of Twist for Lower Spider of Circular Specimen	103

LIST OF FIGURES (continued)

Figure Page

4.6 Calibration of Angle of Twist for Upper Spider of Circular Specimen 104

4.7 Calibration of Angle of Twist for Lower Spider of Square Specimen 105

4.8 Calibration of Angle of Twist for Upper Spider of Square Specimen 106

4.9 Moment for Torsion of Circular Specimen 107

4.10 Experimental Moment for Torsion of Circular Specimen 108

4.11 Experimental Moment for Torsion of Square Specimen 109

4.12 Calibration of Angle of Twist for Lower Spider of Comparison Specimen 110

4.13 Calibration of Angle of Twist for Upper Spider of Comparison Specimen 111

4.14 Comparison of Angle of Twist Per Unit Length From Strain Gauges and Spider Apparatus 112

4.15 The Tensile Test Specimen 85

4.16 Cross-Sectional View of Tensile Specimen Showing the Location of the Strain Gauges 86

4.17 Experimental Tensile Results for a Work-Hardening Material 113

4.18 The Torsion Specimens 76

5.1 Estimated Slopes of Tensile Results 129

5.2 Theoretical Curve for Simple Tension Problem 130

5.3 Simple Shear - Work-Hardening Material 131

5.4 Torsion of Work-Hardening Material with a Circular Cross-Section 132

LIST OF FIGURES (continued)

Figure Page

5.5 Torsion of Work-Hardening Material with a Square Cross-Section 133

6.1 Work-Hardening Function for Commercially Pure Aluminum 151

6.2 Mohr Circle for the Simple Shear Problem 145

6.3 Typical Element in a Body During Simple Shear 146

NOMENCLATURE

t	time
λ,μ	Lamé constants
E,ν	Young's modulus, Poisson's ratio
$\dot{\lambda},d\lambda$	non-negative scalor factors of proportionality in the theory of plasticity
$a_{\alpha\beta},\alpha_\gamma$	coefficients in the hypoelastic constitutive equation
k	yield stress in pure shear
α^2,K^2	dimensionless constants, $\alpha^2 = 2\mu^2/k^2$, $K^2 = 1/\alpha^2$
f	yield function or plastic potential
g	work-hardening function in the theory of plasticity
H,h	work-hardening functions in the theory of hypoelasticity, $h = H/2J$
H_1,H_2	upper and lower bounds on H
a	semi-width of square cross section in torsion problem radius of circular cross section in torsion problem
Δ_1	mesh size in finite difference procedure for square cross section
$\Delta = \frac{\Delta_1}{a}$	dimensionless mesh size
V	voltage readings taken during experiments
N	number of revolutions of the dividing head
ΔT	equal intervals in dimensionless deviatoric stress during experimental tension test
e_s	estimated error in strains during tension test

NOMENCLATURE (continued)

e_T	truncation error in the slope $d\varepsilon/dT$
e_R	round-off error in the slope $d\varepsilon/dT$
B_i	coefficients in the sine series for the slope $d\varepsilon/dT$ $(i = 1,2,\ldots,15)$
σ_{ij}	stress tensor components
S_{ij}	deviatoric stress tensor components
$\sigma = \frac{\sigma_{kk}}{3}$	hydrostatic part of the stress tensor
$t_{ij} = \frac{\sigma_{ij}}{2\mu}$	dimensionless stress tensor components
$T_{ij} = \frac{S_{ij}}{2\mu}$	dimensionless deviatoric stress tensor components
v_i	velocity vector components
u_i	displacement vector components
e_{ij}	strain tensor components
$\dot{e}_{ij}$	strain rate tensor components
d_{ij}	rate of deformation tensor components
ω_{ij}	spin tensor components
de_{ij}	strain increment tensor components
d'_{ij}	deviatoric rate of deformation tensor components
ε_{ij}	deviatoric strain tensor components
$e = \frac{e_{kk}}{3}$	hydrostatic part of the strain tensor
$d = \frac{d_{kk}}{3}$	hydrostatic part of the rate of deformation tensor
δ_{ij}	kronecker delta components

NOMENCLATURE (continued)

I_R, II_R, III_R	first, second and third invariants respectively of a second order tensor R_{ij}
$R = t_{k\ell}d_{k\ell}$	invariants used throughout the thesis
$N = t_{k\ell}t_{\ell m}d_{mk}$	
$P = t_{k\ell}d_{\ell m}d_{mk}$	
$Q = t_{k\ell}t_{\ell m}d_{mn}d_{nk}$	
$M' = T_{k\ell}d'_{k\ell}$	
$W' = \frac{M'}{\dot{\theta}}$	
$J = II_T$	
$K = III_T$	
W	external work per unit volume
M	torque in the torsion problem
M_1, M_2	upper and lower bounds on M
θ	angle of twist per unit length in the torsion problem
$\dot{\theta}$	rate of angular twist per unit length
ξ	angle of shear in the simple shear problem
Ψ, ψ	stress functions in the torsion problem, $\psi = \Psi/2\mu$
$Y = \frac{\partial\psi}{\partial\theta}$	rate of change of the stress function with respect to angle of twist per unit length
ϕ	warping function in the torsion problem
s	measure of length along the lateral surface in the torsion problem
$\overline{n}$	external vector normal to a boundary

NOMENCLATURE (continued)

T, S	components of dimensionless deviatoric stress
τ	maximum shear stress
ε	deviatoric strain in the simple tension problem
c	a measure of strain in the simple shear and simple tension problems

Note - For the equations which are in tensor notation, the summation convention is implied

CHAPTER I

INTRODUCTION

The mathematical study of the stresses and strains in plastically deformed metals began a century ago. In 1864 Tresca proposed that a metal yielded plastically when the maximum shear stress attained a critical value. A system of five equations governing the stresses and strains in two dimensional flow was proposed by Saint-Venant in 1870 [23]. Saint-Venant postulated that the directions of maximum shear strain rate coincided with the directions of maximum shear stress. In 1871 Lévy proposed three-dimensional relations between stress and rate of plastic strain. In 1913 von Mises suggested a yield criterion which is probably the most widely used today. Von Mises also independently proposed equations similar to Lévy's. In 1926 Lode conducted a series of experiments showing the validity of the Lévy-Mises stress-strain relations to a first approximation. In 1930 Reuss, following an earlier suggestion by Prandtl, generalized the theory so that elastic strains were accounted for. Schmidt (1932) and Odqvist (1933) showed in different ways how work-hardening of the metal could be incorporated into the Lévy-Mises equations. Little progress was made in the next decade. However, since World War II significant advances have been made in the solution of special problems.

A large amount of the difficulty encountered during the solu-

tion of elastic-plastic problems arises because there are often two different regions separated by the elastic-plastic boundary. Hooke's Law is associated with the elastic region while the elastic-plastic constitutive equations govern the plastic region. The elastic-plastic boundary is found as part of the solution.

In 1955 Truesdell [1] proposed the theory of hypoelasticity where the constitutive equations are of the form;

$$\text{rate of stress} = f(\text{stress, rate of deformation}),$$

where the function f is a homogeneous and linear function with respect to the rate of deformation. Chapter II shows the development of the hypoelastic theory and shows how the hypoelastic equations may be used to represent an elastic-perfectly plastic solid or a work-hardening material. The advantage in using hypoelastic theory is that the entire body is governed by one constitutive equation and the problem of finding an elastic-plastic boundary disappears.

Truesdell applied hypoelastic theory to simple problems involving homogeneous deformation. A.E. Green [14,15] also applied hypoelastic theory to the problems of simple extension, simple shear and torsion of a circular bar using a particular form of the hypoelastic equations. Solutions for loading were fitted together with solutions for unloading. Green obtained solutions using a dynamically correct form of the rate of stress. The solutions were then simplified by assuming that a certain material constant (u/k) was large with respect

to unity. In 1960 Bernstein [6,7] showed that by changing the initial stresses a particular hypoelastic constitutive equation could describe two totally different materials.

Chapter III contains the solutions of some simple problems using both hypoelastic and elastic-perfectly plastic theory. Comparison of the two theories is made wherever possible. It is shown in Chapter III that under certain conditions the dynamically correct form of stress rate may be replaced by the material rate of stress and the solutions obtained with this approximation are the same as the simplified solutions obtained by Green [14,15] in a different way. This is important because the use of the material stress rate simplifies most problems considerably. This thesis applied hypoelastic theory to a non-homogeneous deformation problem (torsion of a square bar) and uses the material rate of stress.

Chapter IV describes some experimental work that was carried out using a work-hardening material. Torsion and tension tests were performed on commercially pure Aluminum specimens.

In Chapter V various work-hardening problems are solved using a particular form of the hypoelastic constitutive equation. The work-hardening function is evaluated from the results of the experimental tension test. This function is then used in the hypoelastic constitutive equation to predict the results of the torsion experiments for a square and a circular cross-section.

CHAPTER II

THE RELATION BETWEEN HYPOELASTICITY AND PLASTICITY

2.1 The General Hypoelastic Constitutive Equation

The classical linear theory of elasticity is based on the relation

$$\text{stress} = g(\text{small strain from an unstressed state}) \qquad (2.1)$$

where g is a single valued function. This relation has been generalized for the theory of finite strain as

$$\text{stress} = h(\text{finite strain}) \qquad (2.2)$$

where h is a single valued function. Truesdell [1] suggested that the basic assumption (2.1) of the classical linear theory could be regarded as a first approximation to a more general theory of finite strain different from (2.2) and proposed the relation

$$\text{stress increment} = f_1(\text{strain increment})$$

or

$$\text{rate of stress} = f_2(\text{rate of deformation})$$

where f_1 and f_2 are single valued functions.

Further, Truesdell sought to free this concept of elasticity from any connection with a natural or otherwise preferred state. It was proposed that the constitutive equation may depend on the current stress, so that

$$\text{rate of stress} = f(\text{stress, rate of deformation}) \ . \qquad (2.3)$$

This theory may be regarded as representing a material in which the stress is built up by increments which at any instant obey a linear stress increment-strain increment relation with coefficients depending upon the current stress. The response predicted by equation (2.3) is identical to that predicted by the classical theory if the strain is infinitesimal.

Equation (2.3) can be written as

$$\frac{\mathcal{D}}{\mathcal{D}t} \sigma^k_\ell = f^k_\ell \left(\sigma^m{}_n, d^r{}_s\right) , \qquad (2.4)$$

where

$$d_{ij} = \frac{1}{2} \left(v_{i;j} + v_{j;i}\right)$$

is the rate of deformation tensor, v_i are the velocity components and the semi-colon denotes covariant differentiation. The stress tensor

is denoted by σ^k_ℓ while $\mathcal{D}\sigma^k_\ell/\mathcal{D}t$ is the "rate of stress" which may take one of various forms each of which must be objective in order that the constitutive equation be dynamically correct.

The rate of stress that is used in this thesis is the co-rotational derivative,

$$\frac{\mathcal{D}\sigma^k_\ell}{\mathcal{D}t} = \frac{D\sigma^k_\ell}{Dt} + \sigma^k_m\omega^m_\ell - \sigma^m_\ell\omega^k_m \tag{2.5}$$

where

$$\omega_{ij} = \frac{1}{2}\,(v_{i;j} - v_{j;i})$$

are the components of the spin tensor and

$$\frac{D\sigma^k_\ell}{Dt} = \frac{\partial\sigma^k_\ell}{\partial t} + \sigma^k_{\ell;m}\ v^m$$

is the material derivative of the stress tensor.

Prager [2] has discussed certain other definitions of stress rate and has noted that the definition given by equation (2.5) has the property that zero stress rate implies that the stress invariants are stationary whereas the other definitions do not have this property.

The stress rate (2.5) used in this thesis was derived by Noll [3] and earlier by Jaumann [4] in a different way. The Jaumann stress rate measures the material rate of change of the stress components with respect to coordinate axes that rotate with the material and in-

stantaneously coincide with the fixed axes.

Returning now to the general form of the constitutive equation for hypoelasticity, equation (2.4) can be rewritten as

$$\frac{\mathcal{D}t^i_j}{\mathcal{D}t} = f^i_j(d^k_\ell, t^m_n) \qquad (2.6)$$

where

$$t^i_j = \frac{\sigma^i_j}{2\mu}$$

are the components of the stress tensor with twice the elastic shear modulus as the unit of stress.

All constitutive equations must satisfy certain invariance requirements.* In order that the well known principle of objectivity be satisfied, it can be shown that the function $\underset{\sim}{f}$ must be a hemitropic function of $\underset{\sim}{d}$ and $\underset{\sim}{T}$, where $\underset{\sim}{f}$, $\underset{\sim}{d}$ and $\underset{\sim}{T}$ are the matrix equivalents of f^i_j, d^k_ℓ and t^m_n respectively.

According to a theorem of Rivlin [5], a hemitropic polynomial $\underset{\sim}{f}$ of two tensor variables $\underset{\sim}{d}$ and $\underset{\sim}{T}$ can be represented in the form

$$\begin{aligned}\underset{\sim}{f}(\underset{\sim}{d},\underset{\sim}{T}) = {} & a_{00}\underset{\sim}{I} + a_{10}\underset{\sim}{d} + a_{20}\underset{\sim}{d}^2 + a_{01}\underset{\sim}{T} + a_{02}\underset{\sim}{T}^2 \qquad (2.7) \\ & + a_{11}(\underset{\sim}{T}\underset{\sim}{d} + \underset{\sim}{d}\underset{\sim}{T}) + a_{12}(\underset{\sim}{d}\underset{\sim}{T}^2 + \underset{\sim}{T}^2\underset{\sim}{d}) \\ & + a_{21}(\underset{\sim}{d}^2\underset{\sim}{T} + \underset{\sim}{T}\underset{\sim}{d}^2) + a_{22}(\underset{\sim}{T}^2\underset{\sim}{d}^2 + \underset{\sim}{d}^2\underset{\sim}{T}^2) .\end{aligned}$$

---

*For simplicity matrix notation, which is valid in general coordinates, is now used.

Use has been made here of the Cayley-Hamilton theorem which states that a square matrix satisfies its own characteristic equation. That is

$$\underset{\sim}{d}^3 = I_d \underset{\sim}{d}^2 - II_d \underset{\sim}{d} + III_d \ , \ \underset{\sim}{T}^3 = I_t \underset{\sim}{T}^2 - II_t \underset{\sim}{T} + III_t$$

where I, II and III are the first, second and third invariants respectively. The coefficients $a_{\alpha\beta}$ above are functions of the ten invariants I_d, II_d, III_d, I_t, II_t, III_t, R, N, P, Q of which the last four are the joint invariants defined as

$$R = t^k_\ell d^\ell_k \quad , \quad N = t^k_\ell t^\ell_m d^m_k$$

$$P = t^k_\ell d^\ell_m d^m_k \quad , \quad Q = t^k_\ell t^\ell_m d^m_n d^n_k \ .$$

By using the principle of material objectivity, the function $\underset{\sim}{f}$ has been put in the form of equation (2.7). This equation can be refined further by applying dimensional invariance.

One of the hypoelastic hypotheses is that no constitutive coefficient of a hypoelastic material can have a dimension independent of stress. Since there is no modulus with dimension "time", there is no relaxation effect.

Since $\mathcal{D}t^i_j/\mathcal{D}t$ and d^i_j are of dimension t^{-1}, where t is time, equation (2.6) must reduce to the form*

---

*The more general bodies which do not have the restriction of linearity in d^i_j are called hygrosteric by Noll [3].

$$\frac{\mathcal{D}t^i_j}{\mathcal{D}t} = A^{ik}_{j\ell}\, d^\ell_k \tag{2.8}$$

where $A^{ik}_{j\ell}$ is a dimensionless function of t^i_j. It may be deduced from equation (2.7) that $a_{20} = a_{21} = a_{22} = 0$, a_{00}, a_{01} and a_{02} are of degree one in d^k_ℓ and a_{10}, a_{11} and a_{12} are independent of d^k_ℓ . The joint invariants

$$P \equiv t^k_\ell d^\ell_m d^m_k \quad \text{and} \quad Q \equiv t^k_\ell t^\ell_m d^m_n d^n_k$$

do not appear since they are of degree two in d^k_ℓ .

Since $a_{\alpha\beta}$ are power series in $\underset{\sim}{T}$, equations (2.6) and (2.7) reduce to

$$\begin{aligned} \frac{\mathcal{D}\underset{\sim}{T}}{\mathcal{D}t} &= \delta\, \alpha_0 \underset{\sim}{I} + \alpha_1 \underset{\sim}{d} + \delta\, \alpha_2 \underset{\sim}{T} + R\alpha_3 \underset{\sim}{I} \\ &+ \frac{1}{2}\alpha_4(\underset{\sim}{d}\underset{\sim}{T} + \underset{\sim}{T}\underset{\sim}{d}) + \delta\, \alpha_5 \underset{\sim}{T}^2 + R\alpha_6 \underset{\sim}{T} \\ &+ N\alpha_7 \underset{\sim}{I} + \frac{1}{2}\alpha_8(\underset{\sim}{d}\underset{\sim}{T}^2 + \underset{\sim}{T}^2\underset{\sim}{d}) + R\alpha_9 \underset{\sim}{T}^2 \\ &+ N\alpha_{10}\underset{\sim}{T} + N\alpha_{11}\underset{\sim}{T}^2 \end{aligned} \tag{2.9}$$

for a compressible solid, where α_γ $(\gamma = 0,1,2,\ldots,11)$ are dimensionless analytic functions of the three principle invariants of $\underset{\sim}{T}$:

$$\alpha_\gamma = \alpha_\gamma(I_t, II_t, III_t)$$

and

$$\delta = I_d = d^k_k \ .$$

For an incompressible medium it can be shown that

$$\frac{\mathcal{D}\underset{\sim}{T}}{\mathcal{D}t} = - \frac{\dot{p}}{2\mu}\underset{\sim}{I} + (\alpha_1 + \frac{p}{\mu})\underset{\sim}{d} + \frac{1}{2}\,\alpha_4(\underset{\sim}{d}\underset{\sim}{T} + \underset{\sim}{T}\underset{\sim}{d}) +$$

$$(\alpha_3 R + \alpha_7 N)\underset{\sim}{I} + (\alpha_6 R + \alpha_{10} N)\underset{\sim}{T} + \qquad (2.10)$$

$$(\alpha_9 R + \alpha_{11} N)\underset{\sim}{T}^2 + \frac{1}{2}\,\alpha_8(\underset{\sim}{d}\underset{\sim}{T}^2 + \underset{\sim}{T}^2\underset{\sim}{d}) \ .$$

If

$$\alpha_1(0,0,0) = 1 \quad \text{and} \quad \alpha_0(0,0,0) = \frac{\lambda}{2\mu} = \frac{\nu}{1-\nu}$$

where λ and μ are Lamé constants and ν is Poisson's ratio, the constitutive equations of hypoelasticity reduce to those of the classical theory of elasticity as a first approximation.

However, the constitutive differential equations (2.9, 2.10) and the initial conditions are not enough to define uniquely the hypoelastic material behavior. A hypoelastic material is defined by the assignment of a set of constitutive differential equations (2.8) and a

corresponding equivalence class of stress configurations. Bernstein [6,7] has shown that by changing the initial stress, a particular constitutive equation may define totally different materials.

2.2 An Elastic-Perfectly Plastic Constitutive Equation

The following discussion assumes that the elastic part of the strain is small and can be regarded as infinitesimal. The rate of deformation tensor d_{ij} may then be written as the sum of an elastic part d^e_{ij} and a plastic part d^p_{ij} [31]

$$d_{ij} = d^e_{ij} + d^p_{ij} \quad .$$

At this stage it is convenient to consider strain increments rather than rates of deformation so that the total strain increment de_{ij} can be written as the sum of an elastic and a plastic part.

$$de_{ij} = de^e_{ij} + de^p_{ij} \tag{2.11}$$

The strain increment de_{ij} [9] is defined by the equation

$$de_{ij} = \frac{1}{2} \left(\frac{\partial}{\partial x_j} (du_i) + \frac{\partial}{\partial x_i} (du_j)\right)$$

where du_i is the incremental displacement of a point whose current position-vector is x_i referred to fixed Cartesian axes $\{Ox_i\}$. It should be noted that du_i does not denote $u_i(\overline{x} + d\overline{x}) - u_i(\overline{x})$.

If the total strain is small the total strain rate is identical to the rate of deformation and can be written as

$$\dot{e}_{ij} = d_{ij} = \frac{1}{2}(v_{i,j} + v_{j,i})$$

where v_i are the velocity components referred to rectangular Cartesian axes $\{0x_i\}$ and a comma preceding a subscript denotes partial differentiation with respect to the appropriate spatial variable.

An assumption of classical plasticity is that there exists a yield condition described by the equation

$$f(\sigma_{ij}) = 0$$

where σ_{ij} is the symmetric stress tensor and the sign of the yield function f is chosen so that $f < 0$ corresponds to the elastic regime. The function f also depends on the temperature and prior history of work-hardening and heat treatment.

The flow rule [8] for perfectly plastic materials associated with the yield function $f(\sigma_{ij})$ is given by

$$d^p_{ij} = \dot{\lambda} \frac{\partial f}{\partial \sigma_{ij}} \tag{2.12}$$

where it is assumed that the yield function f is regular at the stress point considered and d^p_{ij} are the plastic rates of deformation. $\dot{\lambda}$ is a

non-negative scalar factor of proportionality and is not a material constant, but varies during the deformation and

$$\dot{\lambda} = 0 \quad \text{if} \quad f < 0 \quad \text{or} \quad \text{if } f = 0 \quad \text{and } \dot{f} \equiv \frac{\partial f}{\partial \sigma_{ij}} \dot{\sigma}_{ij} < 0$$

$$\dot{\lambda} \geq 0 \quad \text{if} \quad f = 0 \quad \text{and } \dot{f} = 0 \ .$$

The function f is often called the plastic potential. An example of such a function is the von Mises yield function, which is considered later.

For a perfectly plastic solid with a constant state of stress at the yield point non-vanishing strain rates may occur. However, for a work-hardening material, an increase of stress beyond the yield limit is required to produce non-vanishing strain rates. The flow rule for a work-hardening material with a regular yield surface is

$$d^p_{ij} = 0 \quad \text{if} \quad f < 0 \quad \text{or if} \quad f = 0 \text{ and } \dot{f} \equiv \frac{\partial f}{\partial \sigma_{ij}} \dot{\sigma}_{ij} \leq 0$$

$$d^p_{ij} = g \frac{\partial f}{\partial \sigma_{ij}} \dot{f} \quad \text{if} \quad f = 0 \quad \text{and} \quad \dot{f} \geq 0$$

where the positive work-hardening function g may depend on the stress and strain histories, but is independent of stress rates. Therefore the plastic rates of deformation for loading ($\dot{f} > 0$) are assumed to be linear functions of the stress rates.

It is assumed that metals are plastically incompressible. Consequently

$$d^p_{kk} = 0 \ .$$

With the assumptions of isotropy and absence of Bauschinger effect, along with the experimental fact that yielding is to a first approximation unaffected by moderate hydrostatic tension or pressure, it can be shown [9] that the yield function can be put in the form

$$f(II_S, III_S) = 0$$

where

$$II_s = \frac{1}{2} S_{ij} S_{ij} \qquad III_S = \frac{1}{3} S_{ij} S_{jk} S_{ki}$$

and f is an even function of III_S. S_{ij} is the deviatoric stress tensor.

Von Mises suggested the following yield function for a non-work-hardening material;

$$S_{ij} S_{ij} = 2k^2 \quad \text{or} \quad II_S = k^2 \ ,$$

where k is a constant. That is

$$f \equiv \frac{1}{2} S_{ij} S_{ij} - k^2 \ .$$

Equation (2.12) then yields

$$d^p_{ij} = \dot{\lambda}\, S_{ij} \ .$$

In terms of strain increments this can be written as

$$de^p_{ij} = d\lambda\, S_{ij} \ . \tag{2.13}$$

From Hooke's Law

$$de^e_{ij} = \frac{dS_{ij}}{2\mu} + \frac{d\sigma}{3\lambda + 2\mu}\ \delta_{ij}$$

where $d\sigma = d\sigma_{kk}/3$. Equation (2.11) then implies that

$$de_{ij} = \frac{dS_{ij}}{2\mu} + d\lambda S_{ij} + \frac{d\sigma}{3\lambda + 2\mu}\ \delta_{ij} \ .$$

These equations, which are known as the Prandtl-Reuss equations, may be rewritten as

(a)

$$d\varepsilon_{ij} = \frac{dS_{ij}}{2\mu} + S_{ij}\, d\lambda$$

(b)

$$de = de^e = \frac{d\sigma}{3\lambda + 2\mu} \tag{2.14}$$

(c)

$$S_{ij}\, S_{ij} = 2k^2$$

where

$$de_{ij} = d\varepsilon_{ij} + de\,\delta_{ij}\ .$$

Equation (2.14b) is the compressibility condition. The external work dW per unit volume done on the element during the strain increment de_{ij} is

$$dW = dW_e + dW_p$$

where

$$dW_e = \sigma_{ij}\ de_{ij}^{e}\quad ,\quad dW_p = S_{ij}\ d\varepsilon_{ij}^{p}\quad . \qquad (2.15)$$

dW_e is the elastic recoverable energy while dW_p is the plastic work per unit volume. Now since plastic distortion is irreversible in the thermodynamic sense,

$$dW_p > 0$$

during plastic deformation.* From equations (2.13) and (2.15) it follows that

---

*Yield surfaces in stress space which do not enclose the origin are not considered.

$$dW_p = 2k^2 \, d\lambda > 0 \; .$$

Now during loading in the plastic region

$$de^p_{ij} = d\varepsilon^p_{ij} = d\lambda \; S_{ij} \; .$$

The trace of the product of both sides with S_{ij} is

$$S_{ij} \; d\varepsilon^p_{ij} = d\lambda \; S_{ij} \; S_{ij} = 2k^2 \; d\lambda$$

or

$$d\lambda = \frac{S_{ij} \; de^p_{ij}}{2k^2} \equiv \frac{S_{ij} \; d\varepsilon^p_{ij}}{2k^2} \; .$$

Therefore during loading in the plastic regime

$$d\varepsilon_{ij} = \frac{dS_{ij}}{2\mu} + \frac{S_{k\ell} \; d\varepsilon^p_{k\ell}}{2k^2} \; S_{ij}$$

$$de = \frac{d\sigma}{3\lambda + 2\mu} \tag{2.16}$$

$$S_{ij} \; S_{ij} = 2k^2 \; .$$

For unloading or during loading when $S_{ij} \; S_{ij} < 2k^2$

$$d\varepsilon_{ij} = \frac{dS_{ij}}{2\mu}$$

$$de = \frac{d\sigma}{3\lambda + 2\mu} \quad .$$

The above is one example of the constitutive equations used in the solution of elastic-perfectly plastic problems. It should be noted that the stress increments in the above equations are referred to fixed axes and are not objective. However, if the rotations are small these equations are valid.

2.3 A Hypoelastic Constitutive Equation Similar to the Prandtl-Reuss Equation

In this section, it will be shown that under the proper assumptions the constitutive equation for a hypoelastic body can be reduced to a form resembling that of the elastic-perfectly plastic body described in Section 2.2.

From Section 2.1 it is clear that in developing the theory of hypoelasticity, no assumptions are made as to the magnitudes of the deformations. The theory is completely general and applies to large as well as small deformations. If the dynamically correct form of the Prandtl-Reuss equations is used, the only assumption concerning magnitudes of deformations is that the elastic strain is infinitesimal.

The constitutive equation (2.16) for the elastic-perfectly plastic body obeying the von Mises yield criterion is a combination of classical linear elasticity and pure plastic flow in which the components

of deviatoric strain rate are proportional to the components of deviatoric stress.

The constitutive equations (2.9) and (2.10) for the compressible and incompressible hypoelastic body are general in that they may describe many different materials depending on what values are given for the coefficients in the equations.

Hypoelastic and plastic constitutive equations are rate independent. Consequently the hypoelastic theory can not, for example, describe a viscous fluid. Also in both the hypoelastic theory and the plastic theory as described in Section 2.2 it is assumed that the materials are isotropic.

Thomas [10] has obtained the dynamically correct form of the Prandtl-Reuss equations in terms of stress rates rather than stress increments. These equations, referred to a fixed system of curvilinear coordinates $\{Oy^i\}$, are

$$d'_{ij} = \frac{1}{2\mu}\frac{\mathcal{D}S_{ij}}{\mathcal{D}t} + \dot{\lambda}\, S_{ij} \quad . \tag{2.17}$$

The symbols used in the equation are defined above.

Now for loading in the plastic domain

$$\dot{\lambda} = \frac{S_{ij}\; d'^{p}_{ij}}{2k^2} \quad .$$

Substitution into equation (2.17) yields

$$\frac{1}{2\mu}\,\frac{\mathcal{D}S_{ij}}{\mathcal{D}t} = d'_{ij} - \frac{S_{mn}\;d'^{\,p}_{mn}}{2k^2}\;S_{ij} \tag{2.18}$$

where the second term on the right is present only for loading in the plastic zone. For an elastically compressible material

$$\frac{1}{2\mu}\,\frac{D\sigma}{Dt} = \left(1 + \frac{3\lambda}{2\mu}\right)\frac{d^{e}_{kk}}{3} \quad . \tag{2.19}$$

Consider, now, the general constitutive equation (2.9) for a compressible hypoelastic material.

$$\begin{aligned}\frac{\mathcal{D}t_{ij}}{\mathcal{D}t} &= \alpha_0\, d_{kk}\delta_{ij} + \alpha_1 d_{ij} + \alpha_2\, d_{kk}t_{ij} + \alpha_3\, t_{k\ell}d_{k\ell}\delta_{ij}\\ &+ \frac{1}{2}\,\alpha_4(d_{ik}t_{kj}+t_{ik}d_{kj}) + \alpha_5\, d_{\ell\ell}t_{ik}t_{kj} + \alpha_6\, t_{k\ell}d_{k\ell}t_{ij}\\ &+ \alpha_7\, t_{k\ell}t_{\ell m}d_{mk}\delta_{ij} + \frac{1}{2}\,\alpha_8(d_{ik}t_{km}t_{mj}+t_{ik}t_{km}d_{mj})\\ &+ \alpha_9\, t_{k\ell}d_{\ell k}t_{im}t_{mj} + \alpha_{10}\, t_{k\ell}t_{\ell m}d_{mk}t_{ij} + \alpha_{11}\, t_{k\ell}t_{\ell m}d_{mk}t_{in}t_{nj} \;.\end{aligned} \tag{2.20}$$

If [11]

$$\alpha_0 = \frac{\lambda}{2\mu} + \frac{h}{9}\,(t_{kk})^2$$

$$\alpha_1 = 1$$

$$\alpha_2 = -\frac{h}{3} t_{kk}$$

$$\alpha_3 = -\frac{h}{3} t_{kk}$$

$$\alpha_6 = h$$

all other $\alpha_i = 0$,

then equation (2.20) becomes

$$\frac{\mathcal{D}t_{ij}}{\mathcal{D}t} = d_{ij} + \frac{\lambda}{2\mu} d_{kk}\delta_{ij} + h\{t_{ij} - \frac{t_{kk}}{3}\delta_{ij}\}\{t_{k\ell}d_{k\ell} - \frac{t_{kk}d_{\ell\ell}}{3}\} \quad .(2.21)$$

Let

$$t_{ij} = \frac{\sigma_{ij}}{2\mu} \quad \text{and} \quad h = -\frac{2\mu^2}{k^2} \quad .$$

Then equation (2.21) can be rewritten as

$$\frac{1}{2\mu}\frac{\mathcal{D}\sigma_{ij}}{\mathcal{D}t} = d_{ij} + \frac{\lambda}{2\mu} d_{kk}\delta_{ij} - \frac{1}{2k^2}\{\sigma_{ij} - \frac{\sigma_{kk}}{3}\delta_{ij}\}$$
$$\{\sigma_{k\ell}d_{k\ell} - \frac{\sigma_{kk}d_{\ell\ell}}{3}\} \quad . \qquad (2.22)$$

Equation (2.22) can be written in terms of the deviatoric and hydro-

static components;

$$\frac{1}{2\mu}\frac{\mathcal{D}S_{ij}}{\mathcal{D}t} = d'_{ij} - \frac{S_{k\ell}d'_{k\ell}}{2k^2} S_{ij} \tag{2.23}$$

$$\frac{1}{2\mu}\frac{D\sigma}{Dt} = (1 + \frac{3\lambda}{2\mu})\ d\ . \tag{2.24}$$

Equation (2.23) is similar to the Prandtl-Reuss equation (2.18) except that the second term on the right hand side of equation (2.18) is present only for loading in the plastic zone while the corresponding term in equation (2.23) is present for all "loading" deformations. Also in the elastic-perfectly plastic theory, d'_{ij} is divided into elastic and plastic components whereas this is not true in hypoelasticity. Thus the second term on the right hand side of (2.18) is not quite the same as the corresponding term in equation (2.23) even though we may be loading in the plastic region.

Upon comparing equations (2.19) and (2.24) it is noticed that in equation (2.24) "d" is the total rate of dilatation while in the elastic-perfectly plastic theory it is assumed that the body is plastically incompressible.

Truesdell [12] has shown that for certain incompressible hypoelastic solids, the constitutive equation can be written as

$$\frac{1}{2\mu}\frac{\mathcal{D}S_{ij}}{\mathcal{D}t} = d_{ij} - \frac{S_{mn}d_{mn}}{2k^2} S_{ij}\ .$$

The differences between this equation and the corresponding one in classical plasticity are identical to those stated above for the compressible body.

Further comparison between the two theories may be made in regard to the notion of a yield criterion. In the theory of plasticity a yield criterion is assumed. Truesdell [13] on the other hand has shown that by using the equations of hypoelasticity one can obtain what is called a hypoelastic yield as one of the results in the solution of the simple shear problem. In the paper referred to above, Truesdell solves the problem of simple shear using equation (2.23) and compares the hypoelastic yield to the von Mises yield for various values of (μ/k).

2.4 A Hypoelastic Constitutive Equation Suitable for Some Work-Hardening Materials

The hypoelastic constitutive equation derived earlier in this chapter can be written as

$$\frac{\mathcal{D}T_{ij}}{\mathcal{D}t} = d'_{ij} + h\, T_{k\ell} d'_{k\ell} T_{ij} \tag{2.25}$$

where $T_{ij} = S_{ij}/2\mu$ and $h = -\,2\mu^2/k^2$. However, in general h is a dimensionless function of J and K where

$$J = \frac{1}{2} T_{k\ell} T_{k\ell}$$

$$K = \frac{1}{3} T_{k\ell} T_{\ell m} T_{mk} \ .$$

In Chapter V, this thesis considers the application of equation (2.25) to problems involving work-hardening solids. The assumption is made that h is a function of J only. The functional relationship for commercially pure aluminum is approximated from the results of a simple tension experiment. The constitutive equation (2.25) is then used to solve the torsion problem for this material for both square and circular cross-sections, and the solutions are compared to experimental results.

CHAPTER III

SOLUTIONS TO SOME HYPOELASTIC PROBLEMS AND COMPARISON TO CORRESPONDING ELASTIC-PERFECTLY PLASTIC SOLUTIONS

This chapter contains the solutions of some problems using the hypoelastic constitutive equation

$$\frac{\mathcal{D}T_{ij}}{\mathcal{D}t} = d'_{ij} - \alpha^2 M'T_{ij}$$

where $\alpha^2 = 2\mu^2/k^2$ and $M' = T_{k\ell}d'_{k\ell}$. Comparisons are made to the classical elastic-plastic solutions in which the Prandtl-Reuss equations and the von Mises yield criterion are used.

3.1 Simple Extension

Consider the velocity field

$$v_1 = \dot{c}(t)\, x_1 \qquad v_2 = -\frac{\dot{c}(t)}{2}\, x_2 \qquad v_3 = -\frac{\dot{c}(t)}{2}\, x_3$$

for an incompressible material where the components of velocity are referred to a Cartesian coordinate system. Then

$$d'_{ij} = d_{ij} = \begin{bmatrix} \dot{c} & 0 & 0 \\ 0 & -\frac{\dot{c}}{2} & 0 \\ 0 & 0 & -\frac{\dot{c}}{2} \end{bmatrix}$$

and the rate of spin tensor is zero. Assume

$$T_{ij} \equiv \frac{S_{ij}}{2\mu} = \begin{bmatrix} T & 0 & 0 \\ 0 & -\frac{T}{2} & 0 \\ 0 & 0 & -\frac{T}{2} \end{bmatrix} .$$

The constitutive equation can be written as

$$\frac{DT_{ij}}{Dt} + T_{ik}\omega_{kj} + T_{jk}\omega_{ki} = d'_{ij} - \alpha^2 T_{k\ell}d'_{k\ell}T_{ij} . \qquad (3.1)$$

Now since $\omega_{ij} = 0$ and the stresses are assumed to be homogeneous, equation (3.1) becomes

$$\frac{dT}{dt} = \dot{c} - \frac{3}{2}\alpha^2 T^2\dot{c} ,$$

or since c is assumed to be a monotonically increasing parameter

$$\frac{dT}{dc} = 1 - \frac{3}{2}\alpha^2 T^2 . \qquad (3.2)$$

Equation (3.2) and the initial condition that $T = 0$ when $c = 0$ implies [14] that

$$T = \frac{\sqrt{2}}{\sqrt{3}\alpha} \tanh\left(\sqrt{\frac{3}{2}}\alpha c\right)$$

or

$$T = \frac{1}{\sqrt{3}} \left(\frac{k}{\mu}\right) \tanh \left(\sqrt{3}\, \frac{\mu}{k}\, c\right) .$$

The classical elastic-plastic theory predicts that

$$T = c \quad \text{if} \quad c \leq \frac{1}{\sqrt{3}} \left(\frac{k}{\mu}\right)$$

and

$$T = \frac{1}{\sqrt{3}} \left(\frac{k}{\mu}\right) \quad \text{if } c \geq \frac{1}{\sqrt{3}} \left(\frac{k}{\mu}\right)$$

where "c" is the logarithmic strain.

Figure 3.1 shows the relationship graphically between dimensionless deviatoric stress and logarithmic strain for both the elastic-plastic theory and the hypoelastic theory when $\mu/k = 1000$.

3.2 Simple Shear

In this section the problem of simple shear is considered for both the elastic-plastic solid and the hypoelastic solid. The problem is solved for both cases using the objective stress rate $\frac{\mathcal{D}}{\mathcal{D}t}$ and the non-objective stress rate $\frac{\partial}{\partial t}$.

The velocity field, referred to fixed Cartesian axes Ox_i, is

$$v_1 = 2\dot{c}(t)\, x_2 \ , \ v_2 = v_3 = 0$$

and $2c = \tan \xi$ where ξ is the angle of shear as shown in Figure 3.2.

The equations of motion are satisfied if body forces are zero and $\ddot{c} = 0$.

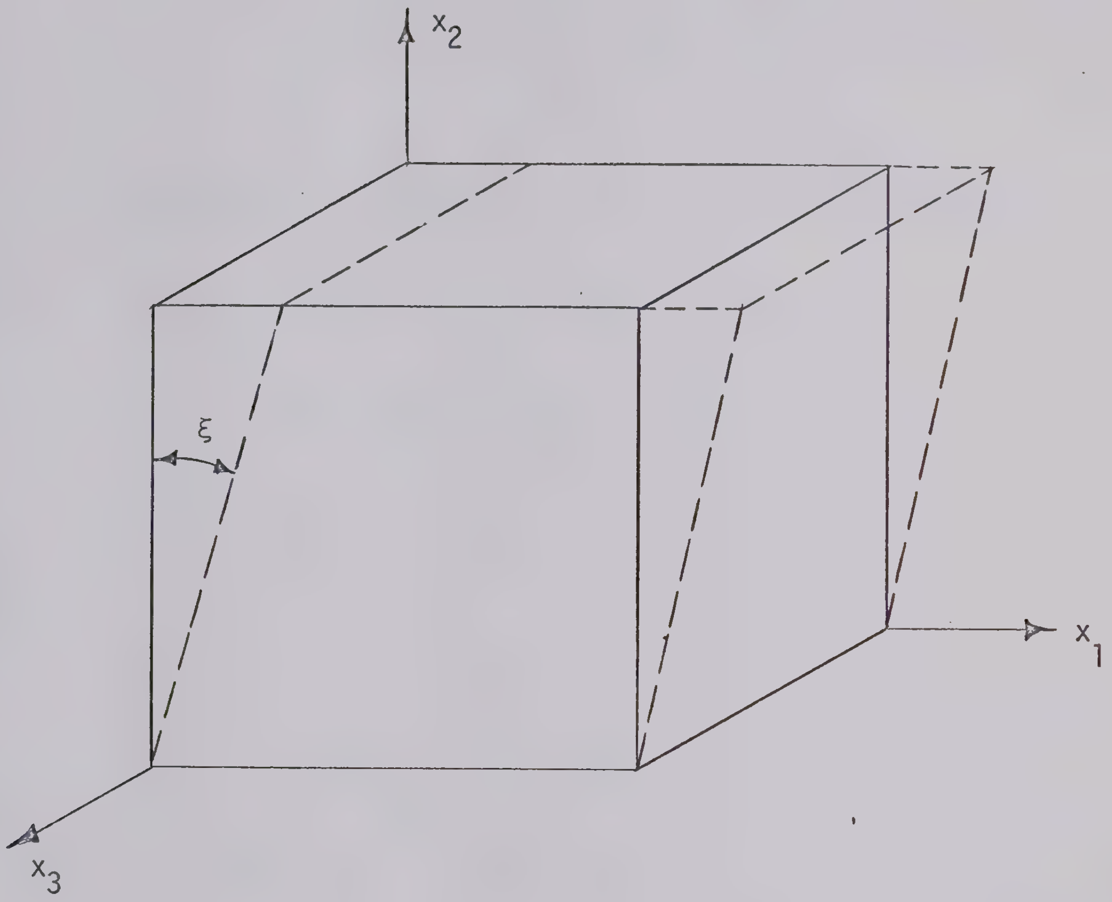

Fig. 3.2 Typical Rectangular Element in Simple Shear

The rate of deformation tensor is

$$d_{ij} \equiv d'_{ij} = \begin{bmatrix} 0 & \dot{c} & 0 \\ \dot{c} & 0 & 0 \\ 0 & 0 & 0 \end{bmatrix}$$

while the spin tensor is given by

$$\omega_{ij} = \begin{bmatrix} 0 & \dot{c} & 0 \\ -\dot{c} & 0 & 0 \\ 0 & 0 & 0 \end{bmatrix} \quad .$$

Assume

$$S_{ij} = \begin{bmatrix} T & S & 0 \\ S & -T & 0 \\ 0 & 0 & 0 \end{bmatrix} \quad ,$$

where S_{ij} is the deviatoric stress tensor and

$$T = T(t) \quad S = S(t) \quad .$$

That is, it is assumed that a state of homogeneous stress exists. The deviatoric stress is used rather than the non-dimensional deviatoric

stress in the simple shear problem.

The elastic-perfectly plastic solutions are now obtained using both the dynamically correct form of the Prandtl-Reuss equations (i.e. with the Jaumann stress rate) and the approximate form with the material derivative of stress. The hypoelastic shear problem is then solved using both the Jaumann and the material stress rate.

If the Jaumann stress rate is used, the elastic-plastic theory predicts that

$$\frac{DS_{ij}}{Dt} + S_{ik}\omega_{kj} + S_{jk}\omega_{ki} = 2\mu\, d'_{ij}$$

during elastic deformation. It follows that

$$\frac{dT}{dc} = 2S \tag{3.3}$$

and

$$\frac{dS}{dc} = - 2T + 2\mu \quad . \tag{3.4}$$

Integration of equations (3.3) and (3.4) subject to the initial conditions that T = 0 and S = 0 when c = 0 leads to

$$T = \mu(1 - \cos 2c)$$

and

$$S = \mu \sin 2c \ .$$

The yield criteria predicts that the material yields when

$$\cos 2c = 1 - \frac{k^2}{2\mu^2} \ . \qquad (3.5)$$

Then

$$T = \frac{k^2}{2\mu}$$

and

$$S = k\sqrt{1 - \frac{k^2}{4\mu^2}} \ .$$

For the yield point to exist equation (3.5) implies that

$$\frac{\mu}{k} \geq \frac{1}{2} \ .$$

The Prandtl-Reuss equation

$$\frac{DS_{ij}}{Dt} + S_{ik}\omega_{kj} + S_{jk}\omega_{ki} = 2\mu d'_{ij} - \frac{\mu}{k^2} S_{k\ell} d_{k\ell} S_{ij}$$

implies that for $2c \geq \cos^{-1}\left(1 - \frac{k^2}{2\mu^2}\right)$

$$\frac{dT}{dc} = 2S - \frac{2\mu}{k^2} ST \tag{3.6}$$

and

$$\frac{dS}{dc} = -2T - \frac{2\mu}{k^2} S^2 + 2\mu \quad . \tag{3.7}$$

Equations (3.6) and (3.7) imply that

$$T^2 + S^2 = k^2$$

during plastic deformation. In other words the maximum shear stress remains constant. This is merely a statement of the yield criterion.

To find the individual components of stress during plastic flow, the equations

$$\frac{dT}{dc} = 2\left(1 - \frac{\mu}{k^2} T\right) (k^2 - T^2)^{1/2}$$

and

$$S = (k^2 - T^2)^{1/2}$$

are solved subject to the condition

$$T = \frac{k^2}{2\mu} \quad \text{when} \quad \cos 2c = 1 - \frac{k^2}{2\mu^2} \quad .$$

If the material stress rate is used in place of the Jaumann derivative then

$$\left.\begin{array}{l} T = 0 \\ \\ S = 2\mu c \end{array}\right] \quad 2c \leq \frac{k}{\mu}$$

and

$$\left.\begin{array}{l} T = 0 \\ \\ S = k \end{array}\right] \quad 2c \geq \frac{k}{\mu}$$

For most metals $k/\mu << 1$. Consequently these two solutions are almost identical.

The hypoelastic constitutive equation

$$\frac{DS_{ij}}{Dt} + S_{ik}\omega_{kj} + S_{jk}\omega_{ki} = 2\mu d'_{ij} - \frac{\mu}{k^2} S_{k\ell} d_{k\ell} S_{ij} \tag{3.8}$$

in which the Jaumann stress rate is used, reduces to

$$\frac{dT}{dc} = 2S - \frac{2\mu}{k^2} ST$$

and

$$\frac{dS}{dc} = -2T - \frac{2\mu}{k^2} S^2 + 2\mu$$

for simple shear. Again the initial conditions are

$$(S)_{c=0} = 0$$

and

$$(T)_{c=0} = 0 \ .$$

For S to remain real it can be shown that

$$\frac{\mu}{k} \geq 1 \ .$$

If the material rate of stress is used, equation (3.8) reduces to

$$\frac{DS_{ij}}{Dt} = 2\mu \, d'_{ij} - \frac{\mu}{k^2} S_{k\ell} d_{k\ell} S_{ij} \ .$$

The resulting differential equations are

$$\frac{dT}{dc} = - \frac{2\mu}{k^2} ST$$

and

$$\frac{dS}{dc} = - \frac{2\mu}{k^2} S^2 + 2\mu$$

subject to the initial conditions

$$(S)_{c=0} = 0$$

and

$$(T)_{c=0} = 0 \ .$$

Therefore

$$T = 0$$

and

$$S = k \tanh \left(\frac{2\mu c}{k}\right) .$$

The results of the four solutions are shown graphically in Figures 3.3 to 3.6. Figure 3.3 shows a plot of τ/k vs. tan ξ for various

values of μ/k where

$$\tau = \sqrt{T^2 + S^2}$$

and

$$\tan \xi = 2c \ .$$

For the values of μ/k used in Figure 3.3 the results obtained using the material derivative are the same as those obtained when using the Jaumann derivative. It can be seen that in the hypoelastic solution, τ/k rapidly approaches unity from below.

Figure 3.4 indicates however that for $\mu/k = 1$ the same results are not obtained when the material stress rate is used in place of the Jaumann stress rate. In fact a different yield point is obtained when the material derivative replaces the Jaumann derivative in the elastic-plastic theory. Figures 3.5 and 3.6 show the values of T/k and S/k for $\mu/k = 1$ when the Jaumann stress rate is used.

It can be shown that if the Jaumann stress rate is used, T/k approaches k/μ asymptotically from below for both the elastic-plastic and the hypoelastic solutions. At the same time S/k rises above $\sqrt{1 - k^2/\mu^2}$ and then approaches $\sqrt{1 - k^2/\mu^2}$ asymptotically from above. The only difference between the elastic-plastic and the hypoelastic solutions is that $\tau/k = 1$ in the plastic solution whereas τ/k

approaches 1 from below in the hypoelastic solution.

Two conclusions can be drawn from the above exercise. It appears reasonable to conclude that hypoelastic theory can be used as an approximation for elastic-plastic theory in certain problems. This is beneficial since in some cases the hypoelastic constitutive equations are easier to solve. Also since μ/k is approximately 10^3 for most metals, the Jaumann stress rate can be replaced by the material stress rate if the components of the rate of spin tensor are of the same order of magnitude as those of the rate of deformation tensor.

3.3 Torsion

3.3.a Statement of the Problem

Consider a prismatic bar of any cross section twisted by couples applied at the ends. The lateral surface of the bar is to be free from external forces while the ends are allowed to warp in the axial direction.

The x_3 axis is chosen parallel to the generators with the origin at one end as shown in Figure 3.7.

3.3.b Classical Elastic Torsion

Saint-Venant [17] solved the classical elastic torsion problem by the semi-inverse method. That is certain assumptions were made concerning the deformations of the twisted bar and it was shown that a solution could then be found that would satisfy the governing equations and the boundary conditions. Then from the uniqueness of elastic solutions it is known that this is the exact solution.

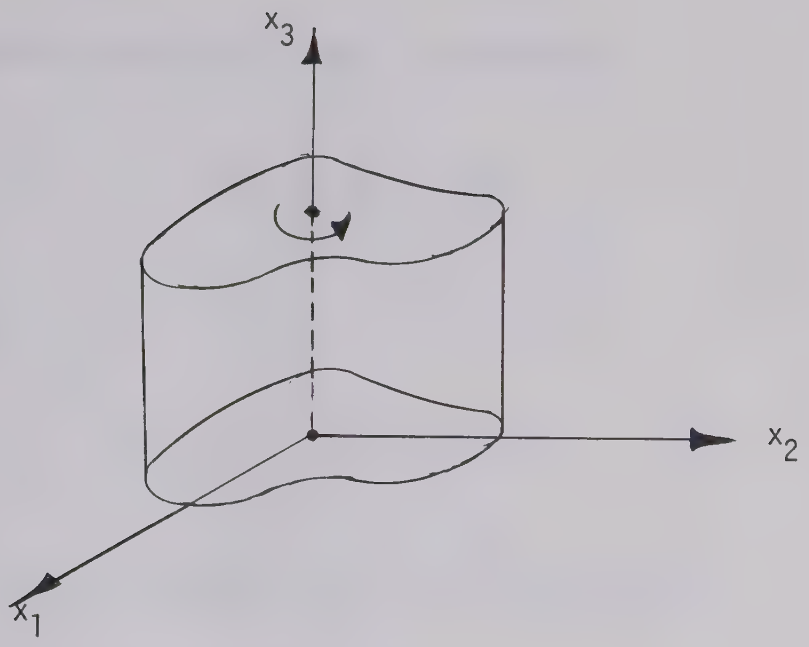

Fig. 3.7 Right Prismatic Bar Under Pure Torsion

The displacements are assumed to be

$$u_1 = -\theta x_2 x_3$$

$$u_2 = \theta x_1 x_3$$

$$u_3 = \theta\phi(x_1, x_2)$$

where θ is the angle of twist per unit length and $\phi(x_1, x_2)$ is called the warping function. Displacements and rotations are assumed to be small so that the boundary conditions may be referred to the undeformed configuration.

Now since the strain tensor is defined as

$$e_{ij} = \frac{1}{2} \left(\frac{\partial u_i}{\partial x_j} + \frac{\partial u_j}{\partial x_i}\right)$$

it follows that

$$e_{11} = e_{22} = e_{33} = e_{12} = 0$$

$$e_{13} = \frac{\theta}{2} \left(\frac{\partial \phi}{\partial x_1} - x_2\right) \quad e_{23} = \frac{\theta}{2} \left(\frac{\partial \phi}{\partial x_2} + x_1\right) .$$

From Hooke's law it follows that

$$\sigma_{11} = \sigma_{22} = \sigma_{33} = \sigma_{12} = 0$$

$$\sigma_{13} = \mu\theta\left(\frac{\partial \phi}{\partial x_1} - x_2\right) \quad \sigma_{23} = \mu\theta\left(\frac{\partial \phi}{\partial x_2} + x_1\right)$$

where μ is the modulus of rigidity. If the stresses are to satisfy the equilibrium equations and the boundary conditions then it can be shown that

$$\frac{\partial^2 \phi}{\partial x_1^2} + \frac{\partial^2 \phi}{\partial x_2^2} = 0$$

subject to the condition

$$(\frac{\partial\phi}{\partial x_1} - x_2)\frac{dx_2}{dS} - (\frac{\partial\phi}{\partial x_2} + x_1)\frac{dx_1}{dS} = 0$$

on the boundary, where S is a measure of length along the lateral surface in the x_1x_2 plane. Body forces are neglected in the equilibrium equations.

The problem can also be formulated in terms of the Prandtl stress function [18]. If

$$\sigma_{13} = \frac{\partial\Psi}{\partial x_2}(x_1,x_2)$$

$$\sigma_{23} = -\frac{\partial\Psi}{\partial x_1}(x_1,x_2)$$

where Ψ is the stress function, the governing equation is

$$\frac{\partial^2\Psi}{\partial x_1^2} + \frac{\partial^2\Psi}{\partial x_2^2} = -2\mu\theta$$

subject to

$$\Psi = \text{constant}$$

on the boundary. For a simply connected region Ψ will be chosen to be zero along the boundary.

It can also be shown that

$$M = 2\iint_A \Psi\, dx_1\, dx_2$$

where M represents the torque applied at the ends of the bar and the integral is taken over the area of the cross section.

3.3.c Hypoelastic Torsion

Consider a hypoelastic material that obeys a constitutive equation of the type

$$\frac{1}{2\mu}\frac{\mathcal{D}S_{ij}}{\mathcal{D}t} = d'_{ij} - \frac{S_{k\ell}d'_{k\ell}}{2k^2}S_{ij} . \tag{3.9}$$

This equation was developed in Section 2.3 for both compressible and incompressible bodies.

Throughout this discussion Cartesian coordinates are used and a suffix preceded by a comma denotes partial differentiation with respect to the appropriate spatial variable.

Displacements and rotations are assumed small so that the boundary conditions may be referred to the initial configuration.

The velocity field is assumed to be

$$v_1 = -\dot{\theta}\, x_2\, x_3$$

$$v_2 = \dot{\theta}\, x_1\, x_3$$

$$v_3 = \dot{\theta}\phi(x_1,x_2,\theta)$$

where $\dot{\theta}$ is the rate of change of angle of twist per unit length. Then

$$d'_{ij} = d_{ij} = \frac{\dot{\theta}}{2} \begin{bmatrix} 0 & 0 & (\frac{\partial\phi}{\partial x_1} - x_2) \\ 0 & 0 & (\frac{\partial\phi}{\partial x_2} + x_1) \\ (\frac{\partial\phi}{\partial x_1} - x_2) & (\frac{\partial\phi}{\partial x_2} + x_1) & 0 \end{bmatrix}$$

and

$$\omega_{ij} = \frac{\dot{\theta}}{2} \begin{bmatrix} 0 & -2x_3 & -(\frac{\partial\phi}{\partial x_1} + x_2) \\ 2x_3 & 0 & -(\frac{\partial\phi}{\partial x_2} - x_1) \\ (\frac{\partial\phi}{\partial x_1} + x_2) & (\frac{\partial\phi}{\partial x_2} - x_1) & 0 \end{bmatrix} .$$

Upon replacing the Jaumann stress rate by the material stress rate, equation (3.9) becomes

$$\frac{DT_{ij}}{Dt} = d'_{ij} - \dot{\theta}\alpha^2 W'T_{ij} \tag{3.10}$$

where

$$\alpha^2 = \frac{2\mu^2}{k^2}$$

and

$$T_{ij} = \frac{S_{ij}}{2\mu} .$$

Also

$$T_{k\ell}d_{k\ell} = \dot{\theta}[T_{13}(\frac{\partial\phi}{\partial x_1} - x_2) + T_{23}(\frac{\partial\phi}{\partial x_2} + x_1)] = \dot{\theta}W' \quad .$$

Now the material rate of stress is defined as

$$\frac{DT_{ij}}{Dt} = \frac{\partial T_{ij}}{\partial t} + v_k \frac{\partial T_{ij}}{\partial x_k} \quad . \qquad (3.11)$$

Since

$$\frac{\partial T_{ij}}{\partial x_3} = 0 \ ,$$

equation (3.11) reduces to

$$\frac{DT_{ij}}{Dt} = \frac{\partial T_{ij}}{\partial t} - \dot{\theta}\ x_3 x_2 \frac{\partial T_{ij}}{\partial x_1} + \dot{\theta}\ x_3 x_1 \frac{\partial T_{ij}}{\partial x_2} \ .$$

Since stresses and stress rates are assumed to be independent of x_3 the last two terms in the above expression are omitted and the material derivative can be replaced by the partial derivative with respect to time. The constitutive equation (3.10) can then be written as

$$\frac{\partial T_{ij}}{\partial t} = d'_{ij} - \dot{\theta}\ \alpha^2\ W'T_{ij} \ .$$

Since $\theta(t)$ is a monotically increasing function of time one can write

$$\frac{\partial}{\partial t} \equiv \dot{\theta} \frac{\partial}{\partial \theta} .$$

Then

$$\dot{\theta} \frac{\partial T_{ij}}{\partial \theta} = d'_{ij} - \dot{\theta} \alpha^2 W' T_{ij} .$$

The six constitutive equations become

(a)

$$\frac{\partial T_{11}}{\partial \theta} = - \alpha^2 W' T_{11}$$

(b)

$$\frac{\partial T_{22}}{\partial \theta} = - \alpha^2 W' T_{22}$$

(c)

$$\frac{\partial T_{33}}{\partial \theta} = - \alpha^2 W' T_{33} \qquad (3.12)$$

(d)

$$\frac{\partial T_{12}}{\partial \theta} = - \alpha^2 W' T_{12}$$

(e)

$$\frac{\partial T_{13}}{\partial \theta} = \frac{1}{2} \left(\frac{\partial \phi}{\partial x_1} - x_2\right) - \alpha^2 W' T_{13}$$

(f)

$$\frac{\partial T_{23}}{\partial \theta} = \frac{1}{2} \left(\frac{\partial \phi}{\partial x_2} + x_1\right) - \alpha^2 W' T_{23} .$$

The initial conditions are

$$T_{ij} = 0 \quad \text{when} \quad \theta = 0 \ .$$

From the initial conditions and the first four of equations (3.12) it can be shown that

$$T_{11} = T_{22} = T_{33} = T_{12} = 0$$

for all θ .

If body forces and acceleration effects are neglected, the only non-trivial equation of motion reduces to

$$\frac{\partial T_{13}}{\partial x_1} + \frac{\partial T_{23}}{\partial x_2} = 0 \ .$$

Consequently the stresses are derivable from a stress function ψ where

$$T_{13} = \frac{\partial \psi}{\partial x_2} \quad \text{and} \quad T_{23} = -\frac{\partial \psi}{\partial x_1} \ .$$

The boundary conditions require that ψ be constant on the boundary and since the section is simply connected the constant can be taken as zero. The hypoelastic torsion problem reduces then to solving the equations

$$\frac{\partial T_{13}}{\partial \theta} = (\tfrac{1}{2} - \alpha^2 T_{13}^2)(\frac{\partial \phi}{\partial x_1} - x_2) - \alpha^2 T_{13} T_{23} (\frac{\partial \phi}{\partial x_2} + x_1) \qquad (3.14a)$$

$$\frac{\partial T_{23}}{\partial \theta} = (\tfrac{1}{2} - \alpha^2 T_{23}^2)(\frac{\partial \phi}{\partial x_2} + x_1) - \alpha^2 T_{13} T_{23} (\frac{\partial \phi}{\partial x_1} - x_2) \qquad (3.14b)$$

where

$$T_{13} = \frac{\partial\psi}{\partial x_2} \qquad T_{23} = -\frac{\partial\psi}{\partial x_1} ,$$

and

$$\psi = 0$$

on the boundary of the cross-section. Multiply equation (3.14a) by $\alpha^2 T_{13} T_{23}$ and equation (3.14b) by $(\frac{1}{2} - \alpha^2 T_{13}^2)$ and add the two equations. The result is

$$\frac{\partial\phi}{\partial x_2} + x_1 = \frac{(\frac{1}{2} - \alpha^2 T_{13}^2)\,\frac{\partial T_{23}}{\partial\theta} + \alpha^2 T_{13} T_{23}\,\frac{\partial T_{13}}{\partial\theta}}{[\frac{1}{4} - \frac{1}{2}\,\alpha^2(T_{13}^2 + T_{23}^2)]} . \qquad (3.15)$$

Multiply equation (3.14a) by $(\frac{1}{2} - \alpha^2 T_{23}^2)$ and equation (3.14b) by $\alpha^2 T_{13} T_{23}$ and add. The result is

$$\frac{\partial\phi}{\partial x_1} - x_2 = \frac{(\frac{1}{2} - \alpha^2 T_{23}^2)\,\frac{\partial T_{13}}{\partial\theta} + \alpha^2 T_{13} T_{23}\,\frac{\partial T_{23}}{\partial\theta}}{[\frac{1}{4} - \frac{1}{2}\,\alpha^2(T_{13}^2 + T_{23}^2)]} . \qquad (3.16)$$

The above operations are valid provided

(a)

$$\alpha^2 T_{13} T_{23} \neq 0$$

(b)

$$\frac{1}{2} - \alpha^2 T_{13}^2 \neq 0$$

(3.17)

(c)

$$\frac{1}{2} - \alpha^2 T_{23}^2 \neq 0$$

(d)

$$\frac{1}{2} - \alpha^2 (T_{13}^2 + T_{23}^2) \neq 0 \quad .$$

Multiplying equation (3.12e) by T_{13} and equation (3.12f) by T_{23} and adding gives

$$\frac{1}{2} \frac{\partial}{\partial \theta} (T_{13}^2 + T_{23}^2) = W'[\frac{1}{2} - \alpha^2 (T_{13}^2 + T_{23}^2)] \ .$$

Since W' is always positive it follows that

$$\frac{1}{2} - \alpha^2 (T_{13}^2 + T_{23}^2) > 0 \qquad (3.18)$$

and $\alpha^2 (T_{13}^2 + T_{23}^2)$ approaches $\frac{1}{2}$ asymptotically from below. It is interesting to note that the von Mises yield criteria is

$$\frac{1}{2} - \alpha^2 (T_{13}^2 + T_{23}^2) = 0 \quad .$$

Assumption (3.17d) is therefore valid and since

$$\frac{1}{2} - \alpha^2(T_{13}^2 + T_{23}^2) > 0$$

then

$$\frac{1}{2} - \alpha^2 T_{13}^2 > 0$$

and

$$\frac{1}{2} - \alpha^2 T_{23}^2 > 0$$

showing the validity of assumptions (3.17b) and (3.17c). It is necessary that $T_{13} \neq 0$ and $T_{23} \neq 0$ for assumption (3.17a) to be true. The assumption that $T_{13} \neq 0$ and $T_{23} \neq 0$ was also used in obtaining equation (3.18).

Differentiating equation (3.15) with respect to x_1 yields

$$\frac{\partial^2\phi}{\partial x_1 \partial x_2} = -1 + \frac{(\frac{1}{2} - \alpha^2 T_{13}^2)\frac{\partial}{\partial\theta}(\frac{\partial T_{23}}{\partial x_1}) - 2\alpha^2 T_{13}\frac{\partial T_{13}}{\partial x_1}\frac{\partial T_{23}}{\partial\theta}}{[\frac{1}{4} - \frac{1}{2}\alpha^2(T_{13}^2 + T_{23}^2)]}$$
$$+ \frac{\alpha^2 \frac{\partial T_{13}}{\partial x_1} T_{23}\frac{\partial T_{13}}{\partial\theta} + \alpha^2 T_{13}\frac{\partial T_{23}}{\partial x_1}\frac{\partial T_{13}}{\partial\theta} + \alpha^2 T_{13}T_{23}\frac{\partial}{\partial\theta}(\frac{\partial T_{13}}{\partial x_1})}{[\frac{1}{4} - \frac{1}{2}\alpha^2(T_{13}^2 + T_{23}^2)]} \qquad (3.19)$$
$$+ \frac{[(\frac{1}{2} - \alpha^2 T_{13}^2)\frac{\partial T_{23}}{\partial\theta} + \alpha^2 T_{13}T_{23}\frac{\partial T_{13}}{\partial\theta}]\,\alpha^2\,(T_{13}\frac{\partial T_{13}}{\partial x_1} + T_{23}\frac{\partial T_{23}}{\partial x_1})}{[\frac{1}{4} - \frac{1}{2}\alpha^2(T_{13}^2 + T_{23}^2)]^2} .$$

Differentiating equation (3.16) with respect to x_2 yields

$$\frac{\partial^2\phi}{\partial x_2 \partial x_1} = 1 + \frac{(\frac{1}{2} - \alpha^2 T_{23}) \frac{\partial}{\partial\theta} (\frac{\partial T_{13}}{\partial x_2}) - 2\alpha^2 T_{23} \frac{\partial T_{23}}{\partial x_2} \frac{\partial T_{13}}{\partial\theta}}{[\frac{1}{4} - \frac{1}{2} \alpha^2 (T_{13}^2 + T_{23}^2)]}$$

$$+ \frac{\alpha^2 \frac{\partial T_{13}}{\partial x_2} T_{23} \frac{\partial T_{23}}{\partial\theta} + \alpha^2 T_{13} \frac{\partial T_{23}}{\partial x_2} \frac{\partial T_{23}}{\partial\theta} + \alpha^2 T_{13} T_{23} \frac{\partial}{\partial\theta} (\frac{\partial T_{23}}{\partial x_2})}{[\frac{1}{4} - \frac{1}{2} \alpha^2 (T_{13}^2 + T_{23}^2)]} \quad (3.20)$$

$$+ \frac{[(\frac{1}{2} - \alpha^2 T_{23}^2) \frac{\partial T_{13}}{\partial\theta} + \alpha^2 T_{13} T_{23} \frac{\partial T_{23}}{\partial\theta}] \alpha^2 (T_{13} \frac{\partial T_{13}}{\partial x_2} + T_{23} \frac{\partial T_{23}}{\partial x_2})}{[\frac{1}{4} - \alpha^2 (T_{13}^2 + T_{23}^2)]^2} .$$

Let

$$\frac{1}{4} - \frac{1}{2} \alpha^2 (T_{13}^2 + T_{23}^2) = \beta^2, \ \frac{1}{2} - \alpha^2 T_{13}^2 = \gamma^2 \ , \ \frac{1}{2} - \alpha^2 T_{23}^2 = \eta^2 \ .$$

Now since

$$\frac{\partial^2\phi}{\partial x_1 \partial x_2} = \frac{\partial^2\phi}{\partial x_2 \partial x_1}$$

ϕ can be eliminated from equations (3.19) and (3.20) to obtain

$$\frac{2 + \eta^2 \frac{\partial}{\partial x_2} (\frac{\partial T_{13}}{\partial\theta}) - 2\alpha^2 T_{23} \frac{\partial T_{23}}{\partial x_2} \frac{\partial T_{13}}{\partial\theta} + \alpha^2 \frac{\partial T_{13}}{\partial x_2} T_{23} \frac{\partial T_{23}}{\partial\theta}}{\beta^2}$$

$$+ \frac{\alpha^2 T_{13} \frac{\partial T_{23}}{\partial x_2} \frac{\partial T_{23}}{\partial \theta} + \alpha^2 T_{13} T_{23} \frac{\partial}{\partial x_2} (\frac{\partial T_{23}}{\partial \theta}) - \gamma^2 \frac{\partial}{\partial x_1} (\frac{\partial T_{23}}{\partial \theta})}{\beta^2}$$

$$+ \frac{2\, \alpha^2 T_{13} \frac{\partial T_{13}}{\partial x_1} \frac{\partial T_{23}}{\partial \theta} - \alpha^2 \frac{\partial T_{13}}{\partial x_1} T_{23} \frac{\partial T_{13}}{\partial \theta} - \alpha^2 T_{13} \frac{\partial T_{23}}{\partial x_1} \frac{\partial T_{13}}{\partial \theta}}{\beta^2}$$

$$- \frac{\alpha^2 T_{13} T_{23} \frac{\partial}{\partial x_1} (\frac{\partial T_{13}}{\partial \theta})}{\beta^2} + \frac{[\eta^2 \frac{\partial T_{13}}{\partial \theta} + \alpha^2 T_{13} T_{23} \frac{\partial T_{23}}{\partial \theta}] \alpha^2 (T_{13} \frac{\partial T_{13}}{\partial x_2} + T_{23} \frac{\partial T_{23}}{\partial x_2})}{\beta^4}$$

$$- \frac{[\gamma^2 \frac{\partial T_{23}}{\partial \theta} + \alpha^2 T_{13} T_{23} \frac{\partial T_{13}}{\partial \theta}]\, \alpha^2 (T_{13} \frac{\partial T_{13}}{\partial x_1} + T_{23} \frac{\partial T_{23}}{\partial x_1})}{\beta^4} = 0 \ ,$$

or

$$\begin{aligned}
&2\beta^4 + \eta^2 \beta^2 \frac{\partial}{\partial x_2} (\frac{\partial T_{13}}{\partial \theta}) - \gamma^2 \beta^2 \frac{\partial}{\partial x_1} (\frac{\partial T_{23}}{\partial \theta}) + 2\alpha^2 \beta^2 T_{13} T_{23} \frac{\partial}{\partial x_2} (\frac{\partial T_{23}}{\partial \theta}) \\
&- \alpha^2 \beta^2 (\frac{\partial T_{13}}{\partial \theta}) (T_{23} \frac{\partial T_{23}}{\partial x_2} + T_{13} \frac{\partial T_{23}}{\partial x_1}) + \alpha^2 \beta^2 (\frac{\partial T_{23}}{\partial \theta}) (T_{13} \frac{\partial T_{13}}{\partial x_1} + T_{23} \frac{\partial T_{13}}{\partial x_2}) \\
&+ (\frac{\partial T_{13}}{\partial \theta}) [\eta^2 \alpha^2 (T_{13} \frac{\partial T_{13}}{\partial x_2} + T_{23} \frac{\partial T_{23}}{\partial x_2}) - \alpha^4 T_{13} T_{23} (T_{13} \frac{\partial T_{13}}{\partial x_1} + T_{23} \frac{\partial T_{23}}{\partial x_1})] \\
&+ (\frac{\partial T_{23}}{\partial \theta}) [\alpha^4 T_{13} T_{23} \,(T_{13} \frac{\partial T_{13}}{\partial x_2} + T_{23} \frac{\partial T_{23}}{\partial x_2}) \\
&- \gamma^2 \alpha^2 (T_{13} \frac{\partial T_{13}}{\partial x_1} + T_{23} \frac{\partial T_{23}}{\partial x_1})] = 0 \ .
\end{aligned} \tag{3.21}$$

Let

$$A = \gamma^2\beta^2$$

$$B = -\alpha^2\beta^2 T_{13}T_{23}$$

$$C = \eta^2\beta^2$$

$$D = -\alpha^2\beta^2(T_{13}\frac{\partial T_{13}}{\partial x_1} + T_{23}\frac{\partial T_{13}}{\partial x_2}) + \gamma^2\alpha^2(T_{13}\frac{\partial T_{13}}{\partial x_1} + T_{23}\frac{\partial T_{23}}{\partial x_1})$$

$$-\alpha^4 T_{13}T_{23}(T_{13}\frac{\partial T_{13}}{\partial x_2} + T_{23}\frac{\partial T_{23}}{\partial x_2})$$

$$E = -\alpha^2\beta^2(T_{23}\frac{\partial T_{23}}{\partial x_2} + T_{13}\frac{\partial T_{23}}{\partial x_1}) + \eta^2\alpha^2(T_{13}\frac{\partial T_{13}}{\partial x_2} + T_{23}\frac{\partial T_{23}}{\partial x_2})$$

$$-\alpha^4 T_{13}T_{23}(T_{13}\frac{\partial T_{13}}{\partial x_1} + T_{23}\frac{\partial T_{23}}{\partial x_1})$$

$$F = 2\beta^4 \quad .$$

Equations (3.13) and (3.21) then become

$$A\frac{\partial^2}{\partial x_1^{\,2}}(\frac{\partial\psi}{\partial\theta}) + 2B\frac{\partial^2}{\partial x_1\partial x_2}(\frac{\partial\psi}{\partial\theta}) + C\frac{\partial^2}{\partial x_2^{\,2}}(\frac{\partial\psi}{\partial\theta}) \tag{3.22}$$

$$+ D\frac{\partial}{\partial x_1}(\frac{\partial\psi}{\partial\theta}) + E\frac{\partial}{\partial x_2}(\frac{\partial\psi}{\partial\theta}) + F = 0 \ .$$

It can be shown that

$$B^2 - AC = - [\frac{1}{4} - \frac{1}{2} \alpha^2(T_{13}^2 + T_{23}^2)]^3 < 0 .$$

Therefore equation (3.22) is elliptic until infinite deformation at which time it becomes parabolic.

The boundary condition associated with equation (3.22) becomes

$$\frac{\partial\psi}{\partial\theta} = 0 \qquad (3.23)$$

on the boundary.

The hypoelastic torsion problem could also have been formulated in terms of the warping function ϕ, however it was found that problems arose when trying to satisfy the boundary conditions in the numerical procedure.

3.3.d Numerical Procedure for a Square Cross-Section

The governing equation (3.22) for hypoelastic torsion and the associated boundary condition (3.23) will now be applied to a square cross-section. Since the classical elastic and plastic solutions possess eight fold symmetry, it is reasonable to assume that the hypoelastic solution will behave similarly. Referring to Figure 3.8, only the shaded area OMN in the first quadrant will be considered.

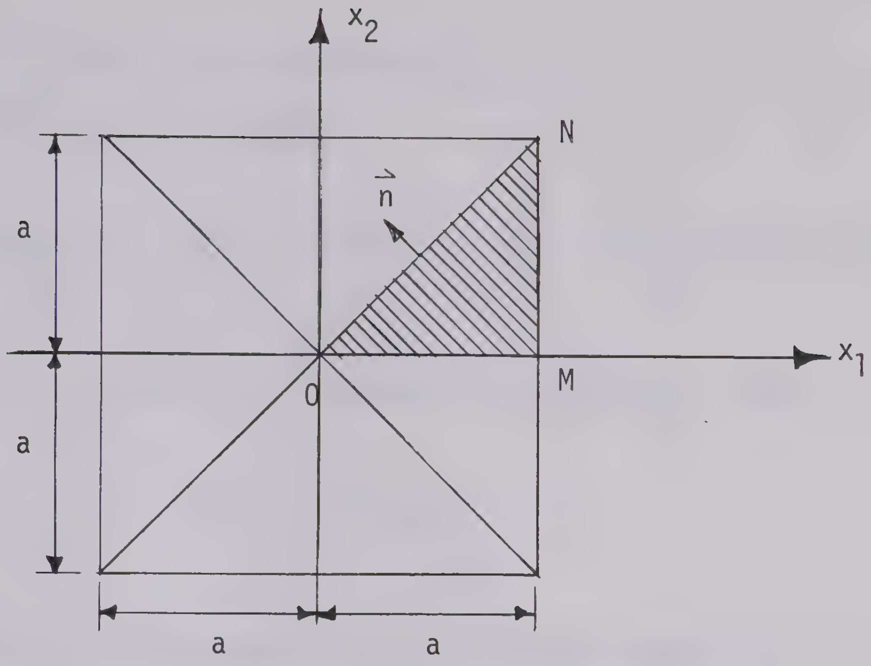

Fig. 3.8 Square Cross-Section of the Bar

In applying the boundary condition (3.23) to the triangle OMN it is clear that

$$\frac{\partial\psi}{\partial\theta} = 0 \quad \text{at} \quad x_1 = a \ .$$

Due to the symmetry of the stress function

$$\frac{\partial}{\partial x_2}\left(\frac{\partial\psi}{\partial\theta}\right) = 0 \quad \text{at} \quad x_2 = 0$$

and

$$\frac{\partial}{\partial n}\left(\frac{\partial\psi}{\partial\theta}\right) = 0 \quad \text{at} \quad x_1 = x_2$$

where $\bar{n}$ is the normal to the boundary ON.

Equation (3.22) becomes

$$A \frac{\partial^2 Y}{\partial x_1^2} + 2B \frac{\partial^2 Y}{\partial x_1 \partial x_2} + C \frac{\partial^2 Y}{\partial x_2^2} + D \frac{\partial Y}{\partial x_1} + E \frac{\partial Y}{\partial x_2} + F = 0 \qquad (3.24)$$

where A, B, C, D, E and F are functions of T_{13} and T_{23} , and

$$Y \equiv \frac{\partial \psi}{\partial \theta} \quad .$$

Since T_{13} and T_{23} are zero when $\theta = 0$, the coefficients A, B, C, D, E and F can be evaluated at any point in the region OMN. Equation (3.24) is solved for $\partial\psi/\partial\theta$ using a finite difference procedure. The stress function ψ is known to be zero initially and by using a forward integration of the type

$$\psi(\theta+\Delta\theta) = \psi(\theta-\Delta\theta) + 2\Delta\theta \frac{\partial \psi(\theta)}{\partial \theta} + O((\Delta\theta)^3) \ ,$$

or neglecting higher order terms

$$\psi(\theta+\Delta\theta) = \psi(\theta-\Delta\theta) + 2\Delta\theta \cdot \frac{\partial \psi(\theta)}{\partial \theta} \quad ,$$

$\psi(\theta+\Delta\theta)$ can be found at each point of the finite difference mesh. New stresses can be found from the new stress function $\psi(\theta+\Delta\theta)$ which are then used to calculate new coefficients A, B, C, D, E and F. This pro-

cedure is repeated until the total angle of twist per unit length reaches the desired amount.

An 11 x 11 finite difference mesh was set up in the octant OMN as in Figure 3.9.

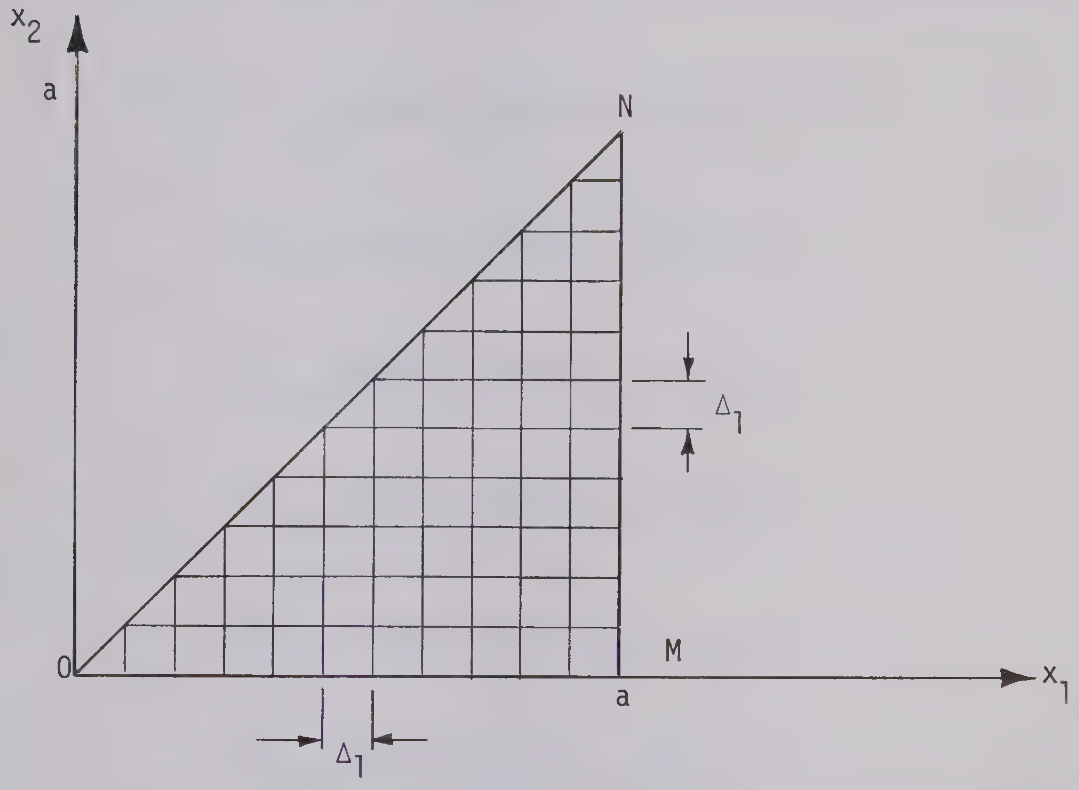

Fig. 3.9 Typical Gridded Region for Numerical Calculation

Now

$$\Delta_1 = \frac{a}{10} = a\Delta$$

where

$$\Delta = \frac{1}{10} .$$

Since $Y = Y(x_1, x_2)$, let $Y_{m,n}$ denote $Y((m-1)\Delta_1, (n-1)\Delta_1)$ where $n = 1, 2, 3 \ldots 11$ and $m = n, n+1, \ldots, 11$. Similarly for the coefficients,

$A_{m,n}$ denotes $A((m-1)\Delta_1,(n-1)\Delta_1)$

$B_{m,n}$ denotes $B((m-1)\Delta_1,(n-1)\Delta_1)$

$C_{m,n}$ denotes $C((m-1)\Delta_1,(n-1)\Delta_1)$

$D_{m,n}$ denotes $D((m-1)\Delta_1,(n-1)\Delta_1)$

$E_{m,n}$ denotes $E((m-1)\Delta_1,(n-1)\Delta_1)$

$F_{m,n}$ denotes $F((m-1)\Delta_1,(n-1)\Delta_1)$.

Let the derivatives of $Y_{m,n}$ be replaced by the following difference equations

$$\frac{\partial Y_{m,n}}{\partial x_1} = \frac{Y_{m+1,n} - Y_{m-1,n}}{2a\Delta}$$

$$\frac{\partial Y_{m,n}}{\partial x_2} = \frac{Y_{m,n+1} - Y_{m,n-1}}{2a\Delta}$$

$$\frac{\partial^2 Y_{m,n}}{\partial x_1^2} = \frac{Y_{m+1,n} - 2Y_{m,n} + Y_{m-1,n}}{a^2\Delta^2}$$

$$\frac{\partial^2 Y_{m,n}}{\partial x_2^2} = \frac{Y_{m,n+1} - 2Y_{m,n} + Y_{m,n-1}}{a^2\Delta^2}$$

$$\frac{\partial^2 Y_{m,n}}{\partial x_1 \partial x_2} = \frac{Y_{m+1,n+1} - Y_{m-1,n+1} - Y_{m+1,n-1} + Y_{m-1,n-1}}{4a^2\Delta^2}$$

The truncation error in each of the above approximations is $O(a^2\Delta^2)$. Substituting the above expressions for the derivatives of Y into equation (3.24) results in fifty-five linear equations for fifty-five unknowns. The fifty-five unknowns are the values of Y for the fifty-five points in the octant OMN excluding the eleven points along the boundary MN where Y is known to be zero from the boundary conditions. The equations are of the form

$$P_{m,n}\frac{Y_{m,n}}{a^2} + Q_{m,n}\frac{Y_{m+1,n}}{a^2} + R_{m,n}\frac{Y_{m,n+1}}{a^2}$$

$$+ S_{m,n}\frac{Y_{m,n-1}}{a^2} + T_{m,n}\frac{Y_{m-1,n}}{a^2} + U_{m,n}\frac{Y_{m-1,n-1}}{a^2}$$

$$+ U_{m,n}\frac{Y_{m+1,n+1}}{a^2} - U_{m,n}\frac{Y_{m-1,n+1}}{a^2} - U_{m,n}\frac{Y_{m+1,n-1}}{a^2}$$

$$= - F_{m,n}$$

$$n = 1,2,\ldots, 10$$

$$m = n,n+1,\ldots, 10$$

where

$$P_{m,n} = -\frac{2A_{m,n}}{\Delta^2} - \frac{2C_{m,n}}{\Delta^2}$$

$$Q_{m,n} = \frac{A_{m,n}}{\Delta^2} + a\frac{D_{m,n}}{2\Delta}$$

$$R_{m,n} = \frac{C_{m,n}}{\Delta^2} + a\frac{E_{m,n}}{2\Delta}$$

$$S_{m,n} = \frac{C_{m,n}}{\Delta^2} - a\frac{E_{m,n}}{2\Delta}$$

$$T_{m,n} = \frac{A_{m,n}}{\Delta^2} - a\frac{D_{m,n}}{2\Delta}$$

$$U_{m,n} = \frac{B_{m,n}}{2\Delta^2} \quad .$$

Each time that the above equations were solved for the dimensionless quantities $Y_{m,n}/a^2$ new stresses and the corresponding moment were calculated by the following equations. Since

$$Y = \frac{\partial\psi}{\partial\theta}$$

and

$$\psi(\theta+\Delta\theta) = \psi(\theta-\Delta\theta) + 2\Delta\theta\left(\frac{\partial\psi}{\partial\theta}\right)$$

it follows that

$$\frac{\psi}{a}\,(\theta a+\Delta(\theta a)) = \frac{\psi}{a}\,(\theta a-\Delta(\theta a)) + 2\Delta(\theta a)\,\left(\frac{Y}{a^2}\right) .$$

From equations (3.13) it is known that

$$T_{13} = \frac{\partial\psi}{\partial x_2}\ , \quad T_{23} = -\frac{\partial\psi}{\partial x_1} .$$

These stresses can be found approximately as

$$\left(\frac{S_{13}}{2\mu}\right)_{m,n} = (T_{13})_{m,n} = \frac{\psi_{m,n+1} - \psi_{m,n-1}}{2a\Delta}$$

and

$$\left(\frac{S_{23}}{2\mu}\right)_{m,n} = (T_{23})_{m,n} = \frac{\psi_{m-1,n} - \psi_{m+1,n}}{2a\Delta} .$$

Also

$$\frac{M}{2\mu a^3} = \frac{2}{a^2}\int_{-a}^{a}\int_{-a}^{a} \left(\frac{\psi}{a}\right) dx_1\ dx_2$$

or

$$\frac{M}{2\mu a^3} = 8\int_{0}^{1}\int_{0}^{1} \left(\frac{\psi}{a}\right) dX_1\ dX_2 \tag{3.25}$$

where

$$dX_1 = \frac{dx_1}{a} \qquad dX_2 = \frac{dx_2}{a} \quad .$$

The double integral in equation (3.25) was evaluated by Simpson's Rule.

The above numerical procedure was carried out using a model 360/67 IBM computer. The results are tabulated and the corresponding graphs are given in Section 3.3.e.

3.3.e Results for Torsion of Square Bar

The classical elastic theory for torsion of a square bar [19] predicts that

$$\frac{M_e}{2\mu a^3} = 1.125\ (\theta a)$$

and the bar begins to yield when

$$\theta a = \frac{1}{1.352}\ (\frac{k}{\mu}) \quad .$$

It can also be shown that the perfectly-plastic moment M_p is given by

$$\frac{M_p}{2\mu a^3} = \frac{4}{3}\ (\frac{k}{\mu}) \ .$$

For the numerical calculations it is assumed that

$$\frac{\mu}{k} = 1000$$

so that

$$\frac{M_p}{2\mu a^3} = \frac{4}{3} \times 10^{-3}$$

and the classical elastic-plastic theory predicts initial plastic flow when

$$(\theta a)_y = \frac{1}{1352} \quad .$$

The numerical procedure described in Section 3.3.d calculates $M/2\mu a^3$, $\Psi/2\mu a$,* $S_{13}/2\mu$, $S_{23}/2\mu$ and $\tau/2\mu$** for values of (θa) up to $3(\theta a)_y$. Some of these results are shown in Table 3.1 for an increment size of $\Delta(\theta a) = \frac{1}{450}\left(\frac{1}{1352}\right)$. The computer printed out results for the first increment, which is merely the classical elastic problem, and for every twenty-fifth increment thereafter.

Graphs of $M/2\mu a^3$ Vs θa, $\Psi_{max}/2\mu a$ Vs θa and $\tau_{max}/2\mu$ Vs θa for $\mu/k = 1000$ and $\Delta(\theta a) = \left(\frac{1}{450}\right)\left(\frac{1}{1352}\right)$ are shown in Figures 3.10, 3.11, and 3.12 respectively.

3.3.f Hypoelastic Torsion of a Circular Bar

For the case of a bar with a circular cross-section it can be shown [14] that integration of equation (3.9) yields

---

* $\frac{\Psi}{2\mu} = \psi$

** $\tau^2 = S_{13}^2 + S_{23}^2$

$$\frac{S_{\theta z}}{2\mu} = \frac{1}{2}\left(\frac{k}{\mu}\right) \tanh\left(\frac{\mu}{k} r\theta\right) \tag{3.26}$$

where θ is the angle of twist per unit length and r is a measure of radial distance. The Jaumann derivative in equation (3.9) was replaced by the material derivative in obtaining equation (3.26).

The torque is

$$M = 2\pi k \int_0^a r^2 \tanh\left(\frac{\mu}{k} r\theta\right) dr$$

or in dimensionless form

$$\frac{M}{2\mu a^3} = \pi\left(\frac{k}{\mu}\right) \int_0^1 \left(\frac{r}{a}\right)^2 \tanh\left(\frac{\mu}{k}\frac{r}{a}\theta a\right) d\left(\frac{r}{a}\right)$$

where "a" is the radius of the circular bar.

Simpson's Rule is used to evaluate the torque for various values of θa. For the computations, $\mu/k = 1000$ and $n = 20$. The results are plotted in Figure 3.13 and compared with the elastic-plastic and perfectly plastic solutions.

For the elastic-plastic solution,

$$\frac{M}{2\mu a^3} = \frac{\pi}{4}\theta a \qquad \left(0 \leq \theta a \leq \frac{k}{\mu}\right)$$

and

$$\frac{M}{2\mu a^3} = \frac{\pi}{3}\frac{k}{\mu} - \frac{\pi}{12}\left(\frac{k}{\mu}\right)^4 \frac{1}{(\theta a)^3} \qquad \left(\theta a \geq \frac{k}{\mu}\right) .$$

Perfectly plastic theory predicts

$$\frac{M}{2\mu a^3} = \frac{\pi}{3}\left(\frac{k}{\mu}\right) \qquad (\theta a > 0) .$$

TABLE 3.1

Results for Elastic-Plastic Torsion of a Square Bar

(θa) $(\mathrm{x}10^{+3})$	$\frac{M}{2\mu a^3}$ $(\mathrm{x}10^{+3})$	$\frac{\psi_{max}}{2\mu a}$ $(\mathrm{x}10^{+3})$	$\frac{\tau_{max}}{2\mu}$ $(\mathrm{x}10^{+3})$
0.0000	0.0000	0.0000	0.0000
0.001644	0.001844	0.0004834	0.001028
0.1233	0.1378	0.03614	0.07663
0.2465	0.2722	0.07162	0.1504
0.3698	0.4004	0.1058	0.2188
0.4931	0.5198	0.1383	0.2798
0.6164	0.6288	0.1686	0.3324
0.7396	0.7264	0.1965	0.3759
0.8629	0.8123	0.2220	0.4108
0.9862	0.8870	0.2449	0.4376
1.1095	0.9511	0.2655	0.4577
1.2327	1.0056	0.2839	0.4721
1.3560	1.0516	0.3003	0.4821
1.4793	1.0903	0.3148	0.4888
1.6026	1.1228	0.3276	0.4932
1.7258	1.1501	0.3391	0.4960
1.8491	1.1731	0.3493	0.4978
1.9724	1.1924	0.3584	0.4989
2.0957	1.2088	0.3665	0.4996
2.2189	1.2227	0.3739	0.5000

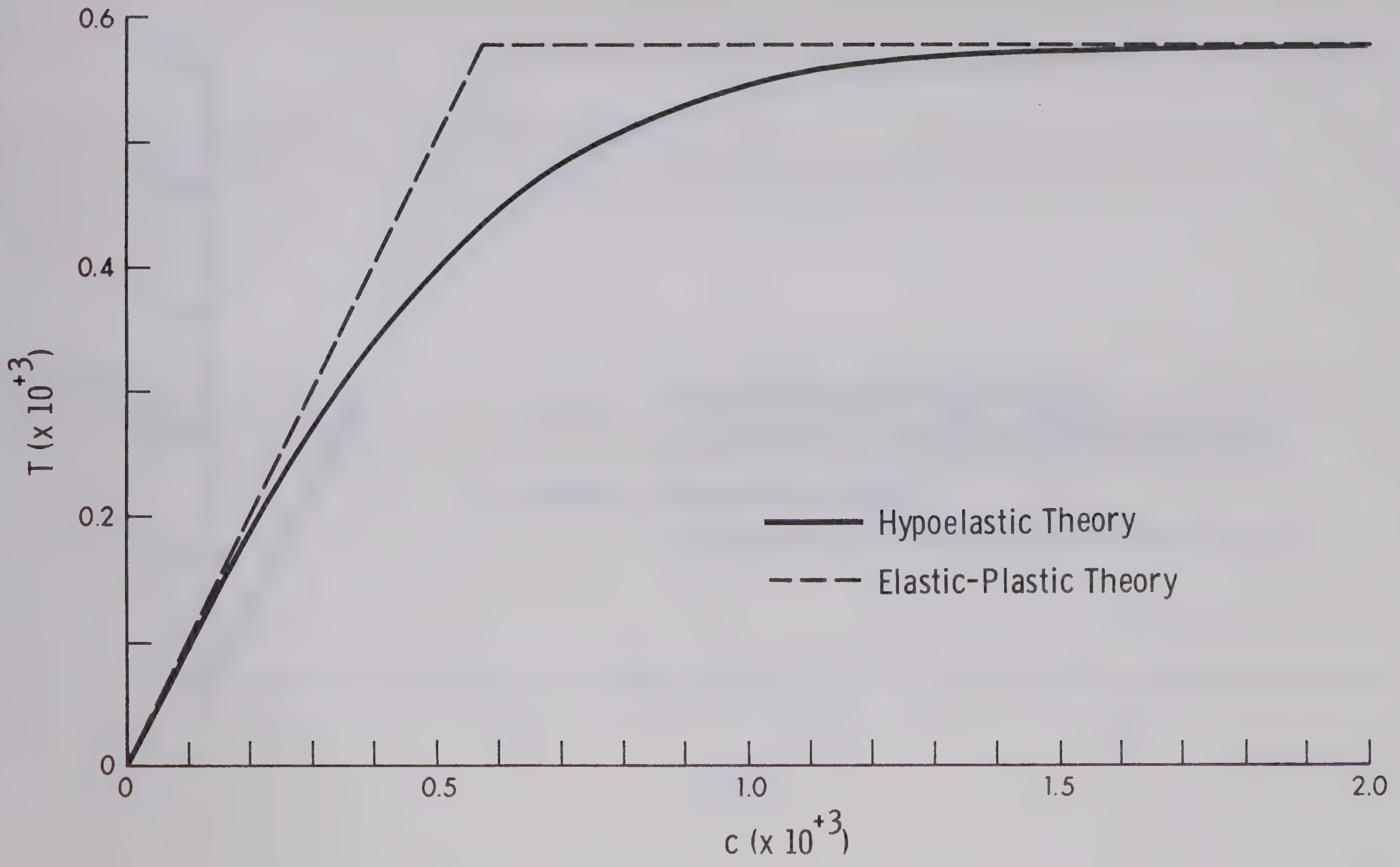

Fig. 3.1 Simple Extension ($\frac{\mu}{k}$ = 1000)

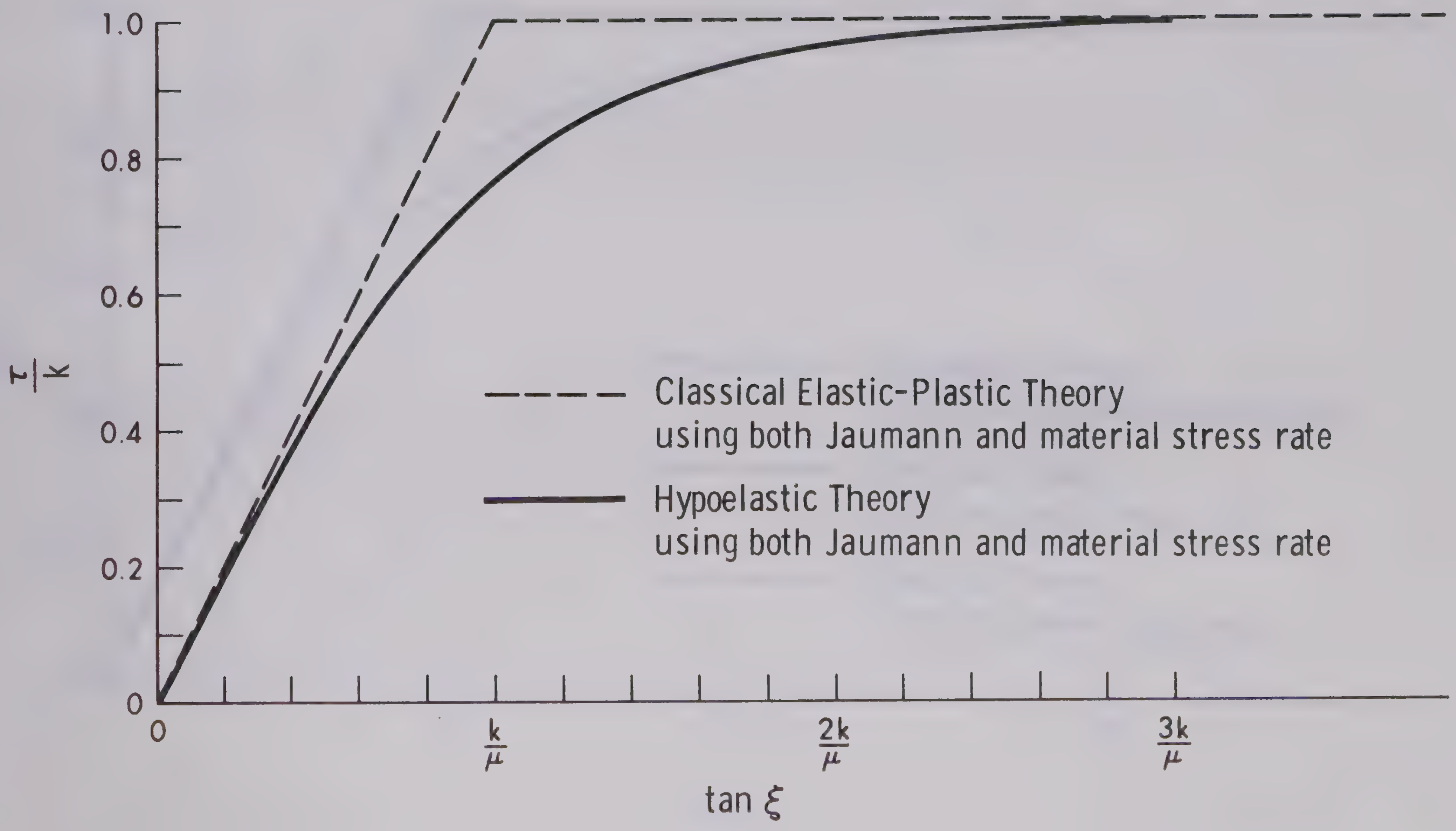

Fig. 3.3 Simple Shear ($\frac{\mu}{k}$ = 1000, 100, 10)

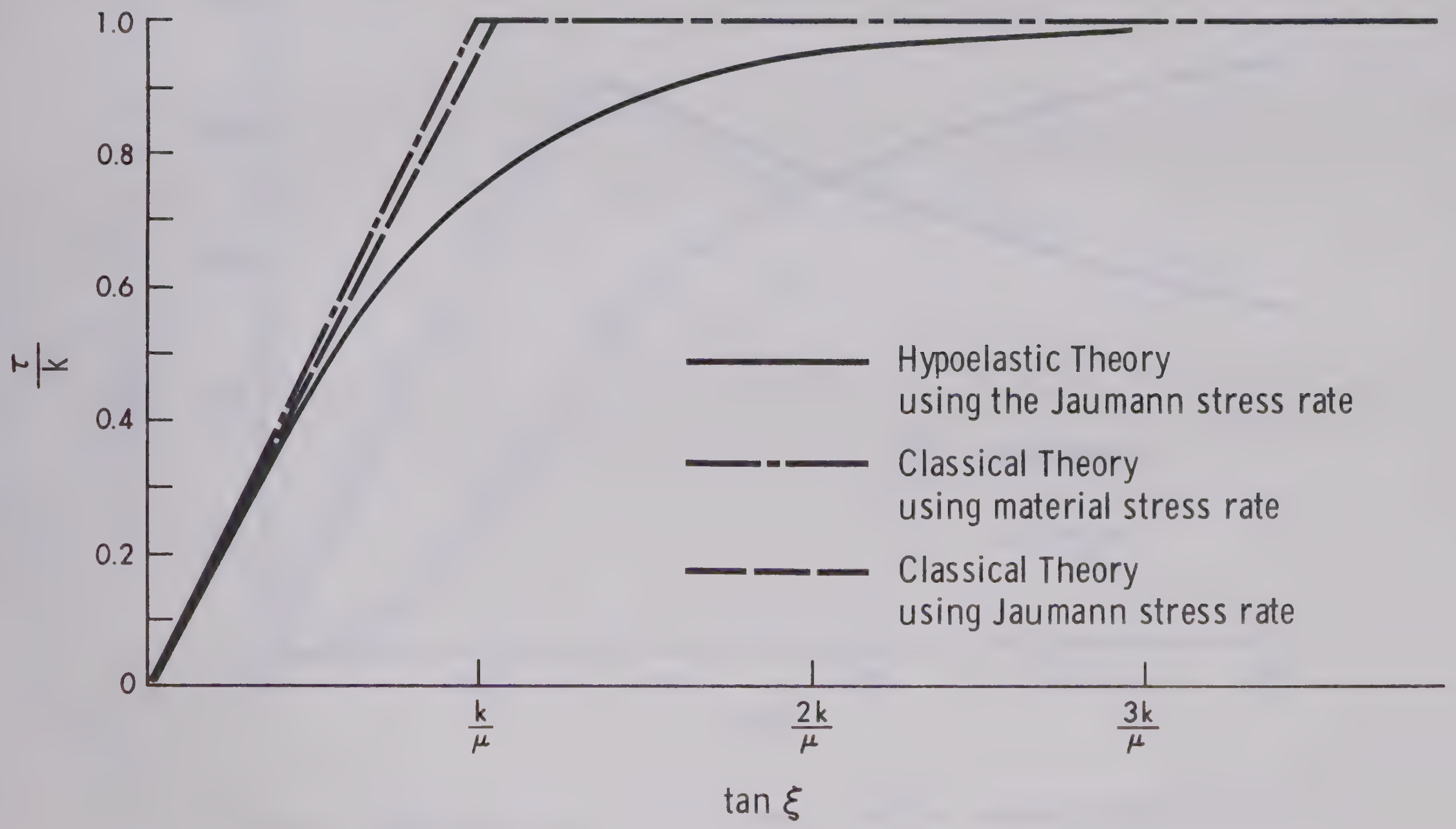

Fig. 3.4 Simple Shear ($\frac{\mu}{k} = 1$)

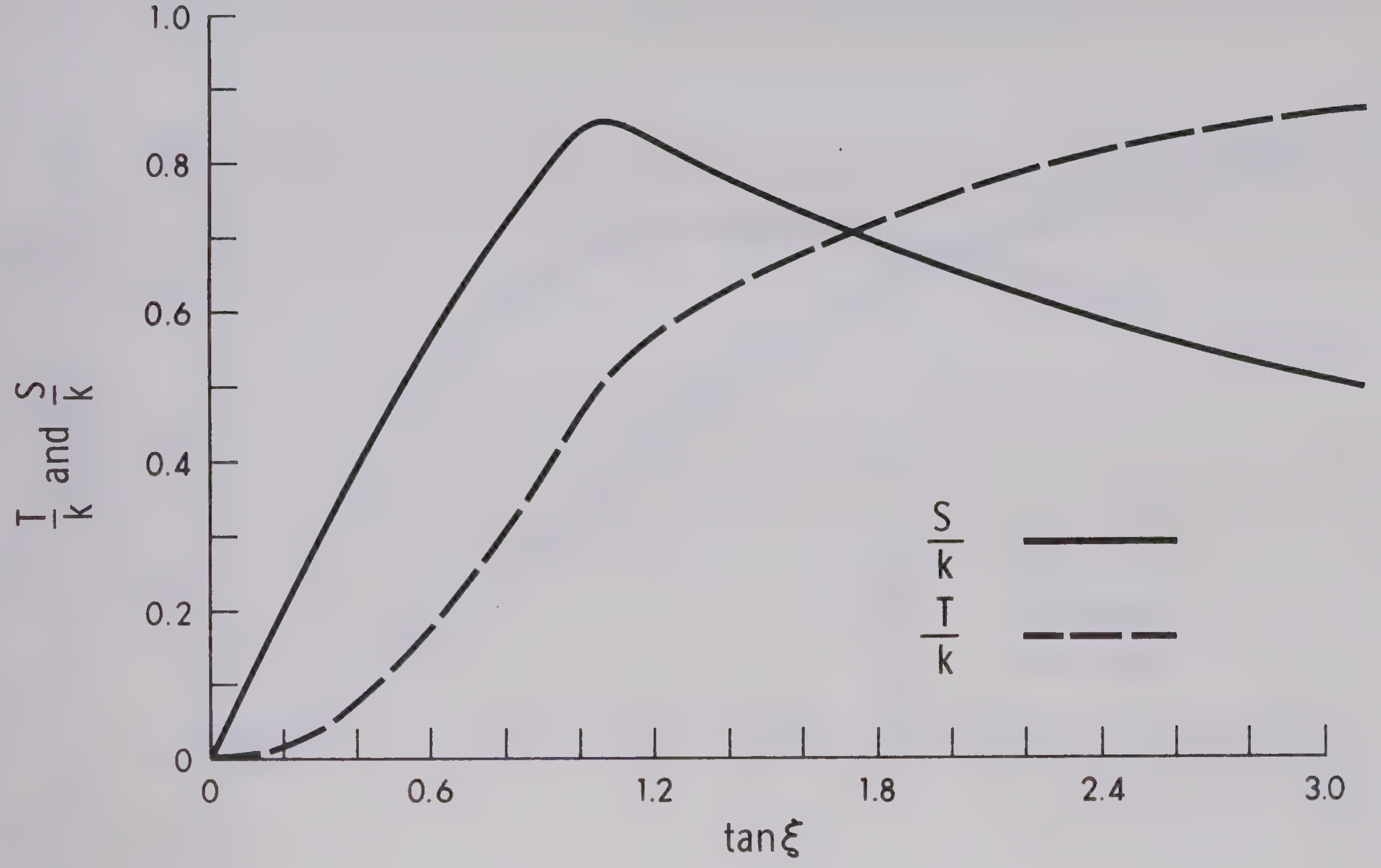

Fig. 3.5 Classical Elastic-Plastic Theory Using the Jaumann Stress Rate ($\frac{\mu}{k} = 1$)

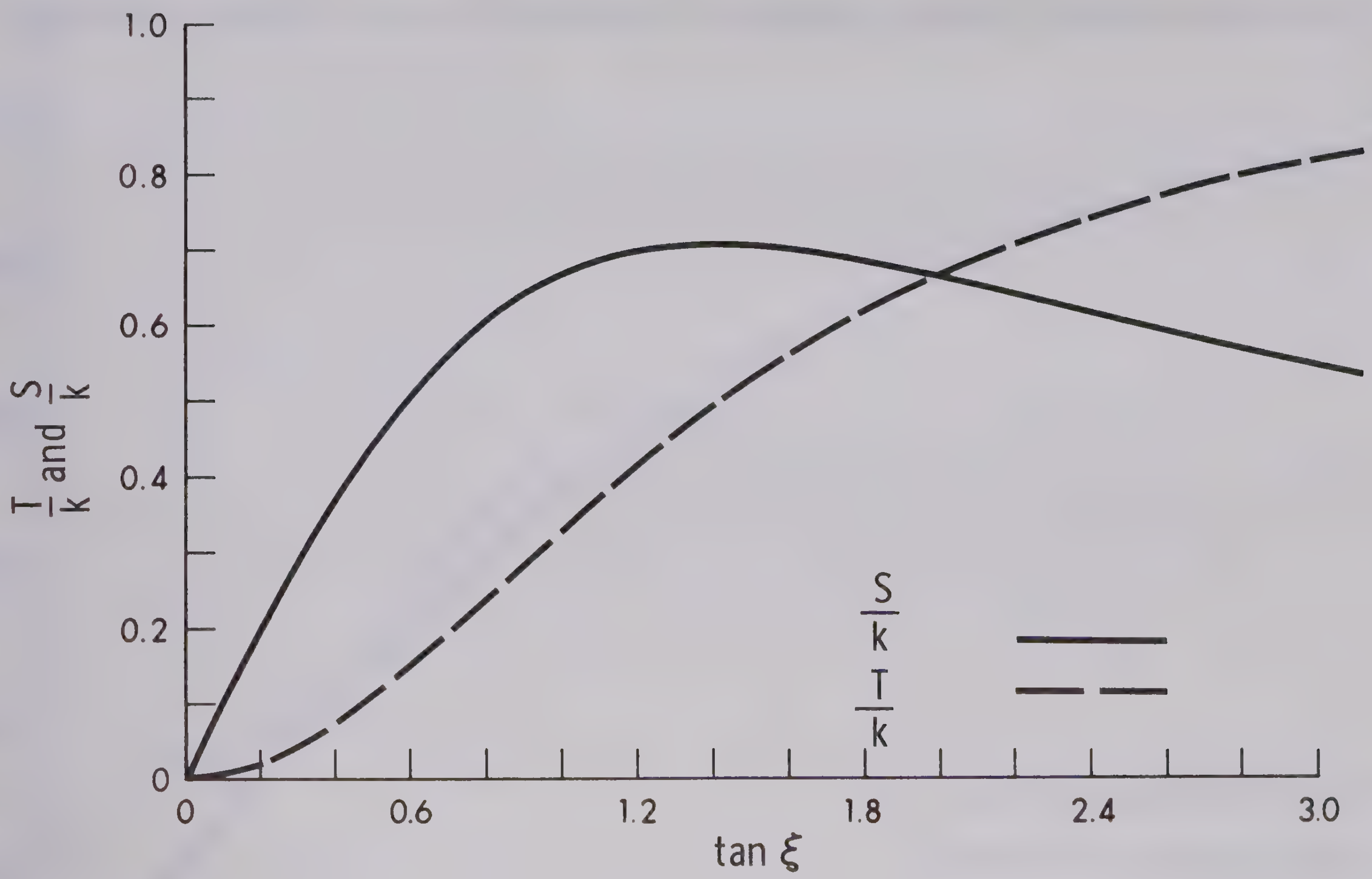

Fig. 3.6 Hypoelastic Theory Using the Jaumann Stress Rate ($\frac{\mu}{k}$ = 1)

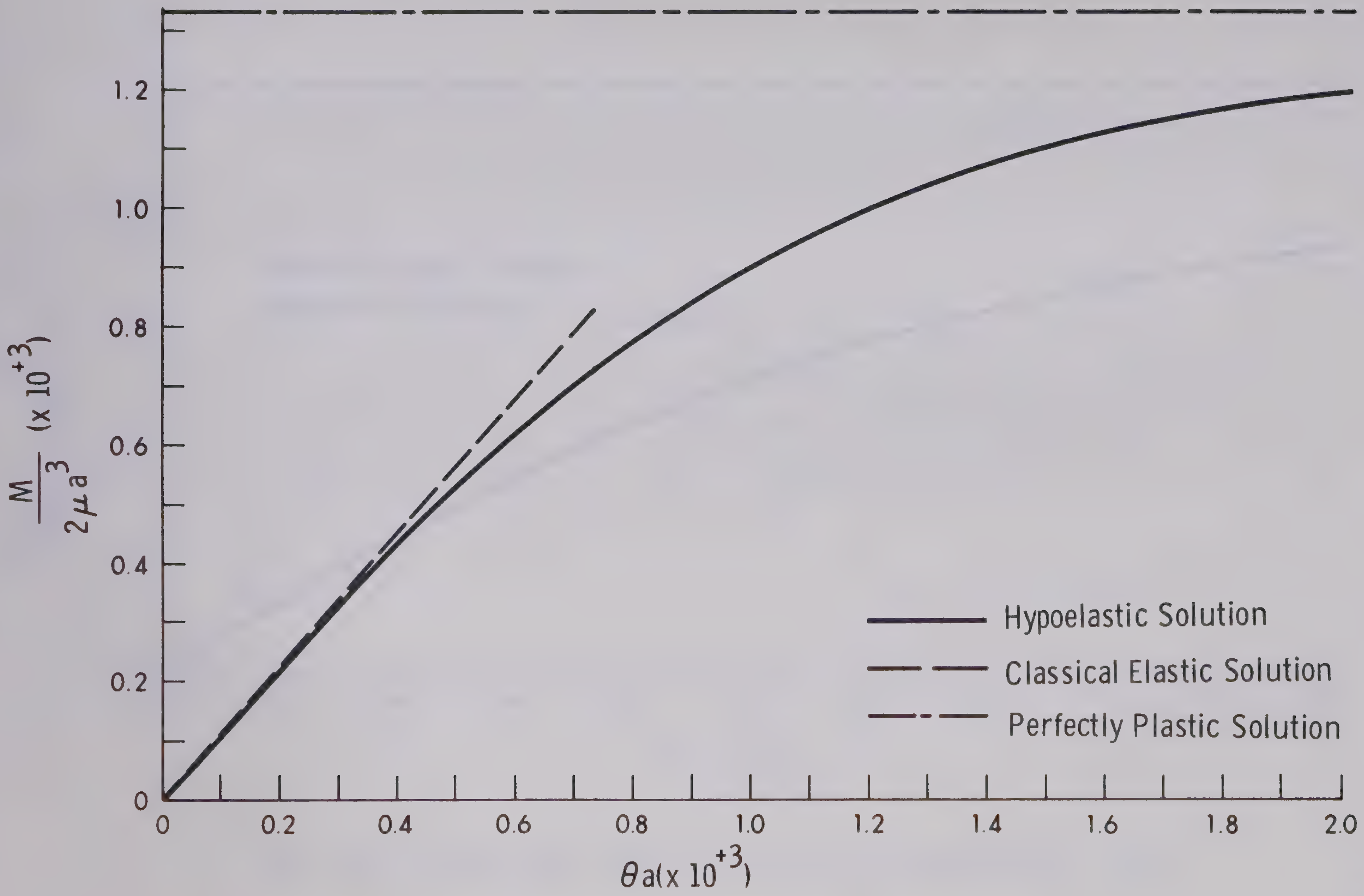

Fig. 3.10 Moment for Torsion of a Square Bar ($\frac{\mu}{k}$ = 1000)

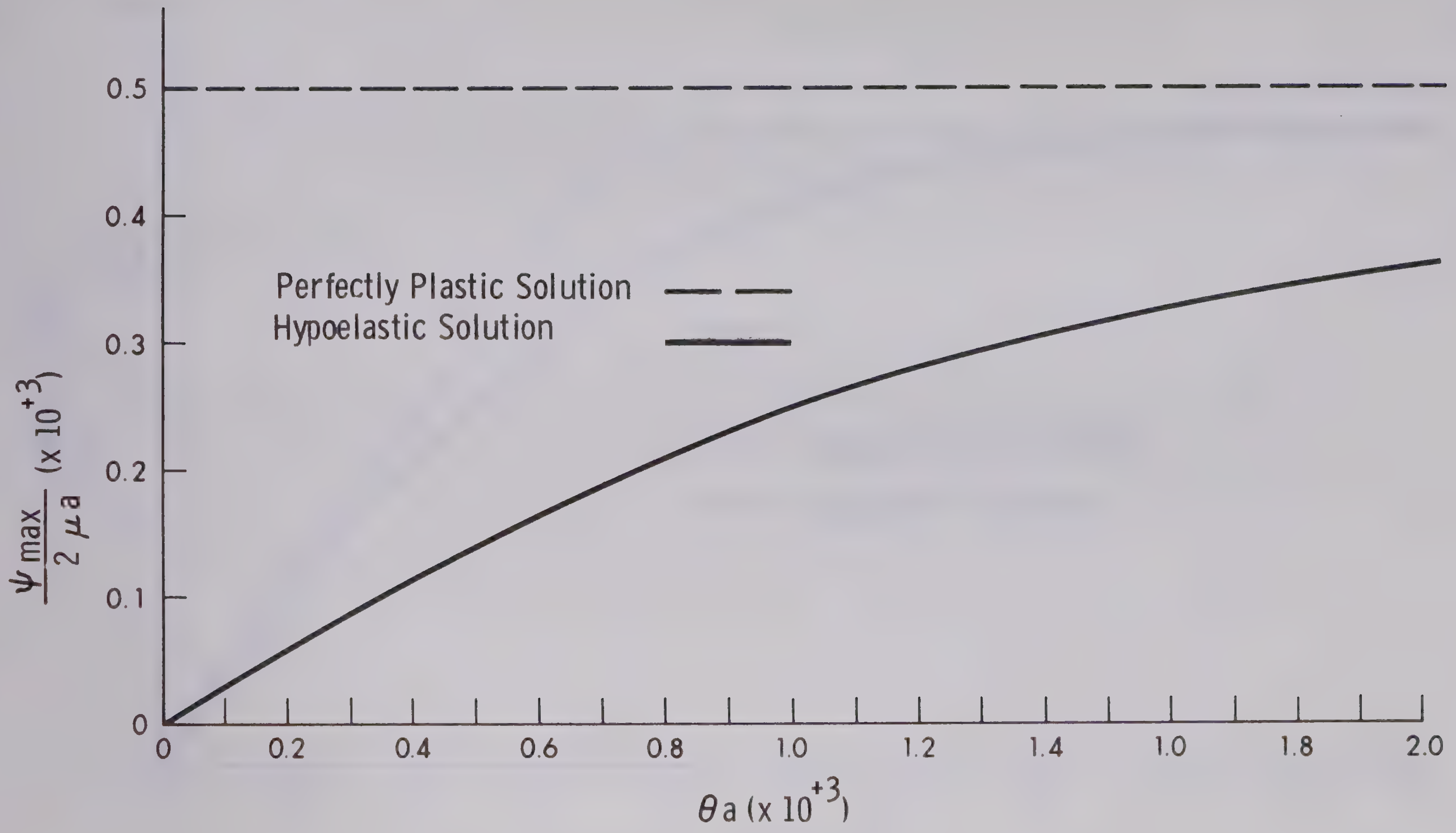

Fig. 3.11 Maximum Stress Function for Torsion of a Square Bar ($\frac{\mu}{k}$ = 1000)

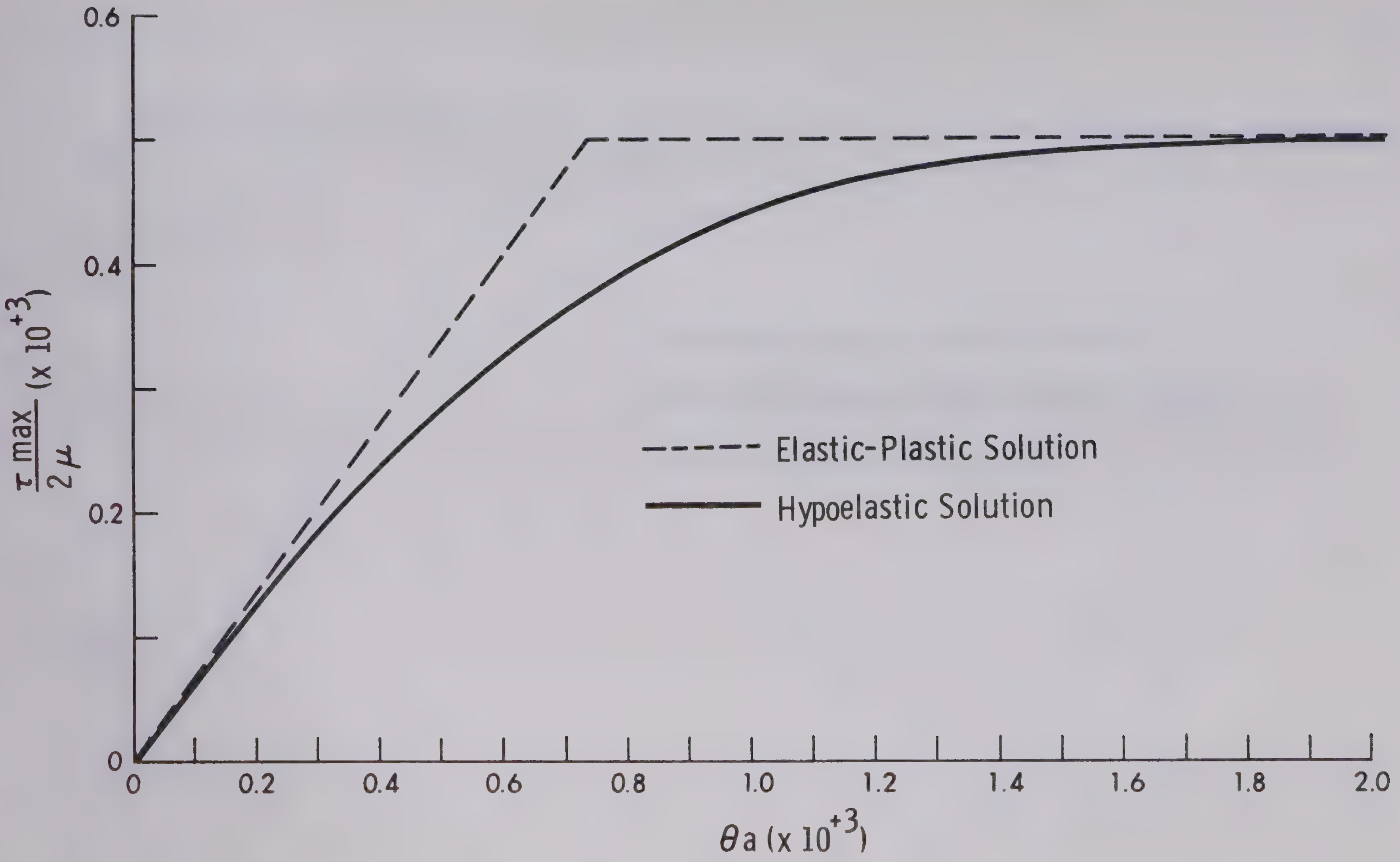

Fig. 3.12 Maximum Shear Stress for Torsion of a Square Bar ($\frac{\mu}{k}$ = 1000)

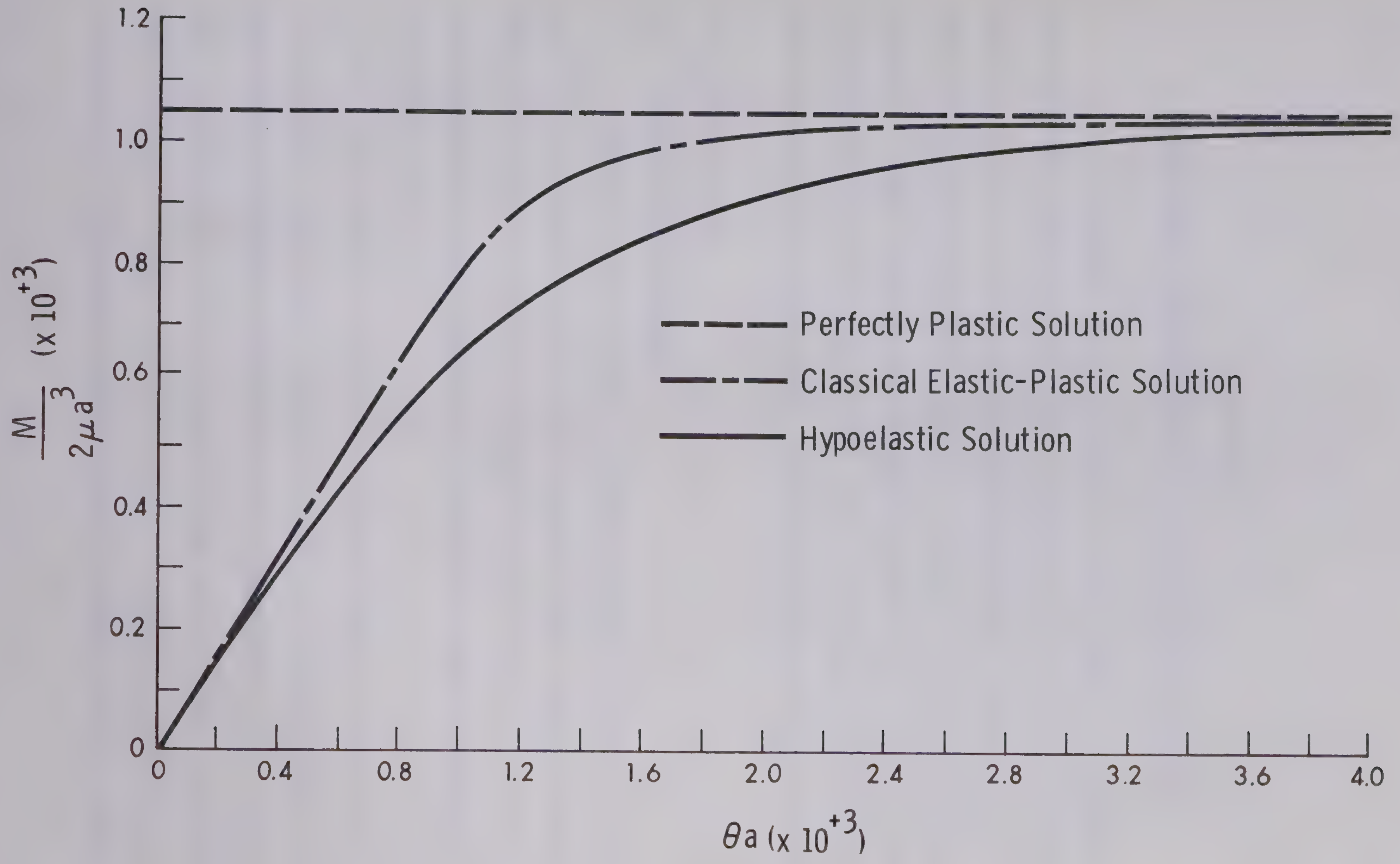

Fig. 3.13 Moment for Torsion of a Circular Bar ($\frac{\mu}{k} = 1000$)

CHAPTER IV

EXPERIMENTAL CONSIDERATION OF A WORK-HARDENING MATERIAL

Two separate tests, torsion and simple extension, are carried out on commercially-pure Aluminum. The purpose of the torsion experiments is to obtain a curve of moment versus angle of twist per unit length for a work-hardening material. The tension test is performed in order to obtain the work-hardening function which is used in calculating a moment versus angle of twist per unit length curve theoretically. The theoretical and experimental results for torsion are then compared.

4.1 Torsion Tests

4.1.1 Experimental Apparatus

Since it was necessary to measure angles of twist as small as 10^{-3} rad. an apparatus which would measure small angles of twist was designed. The device measures tangential displacements by a linear transducer and the displacements are converted to angles of twist by a calibration curve.

As is shown in Figure 4.1, circular mounts are attached to the specimen at each end of the gauge length by means of screws. Four indentations are made at each end of the gauge length at 90° from each other and the points of the screws fit into these. This is to ensure that the planes of the "spiders" (circular mounts) are perpendicular to the axis of the specimen and also that the outer circular edges of

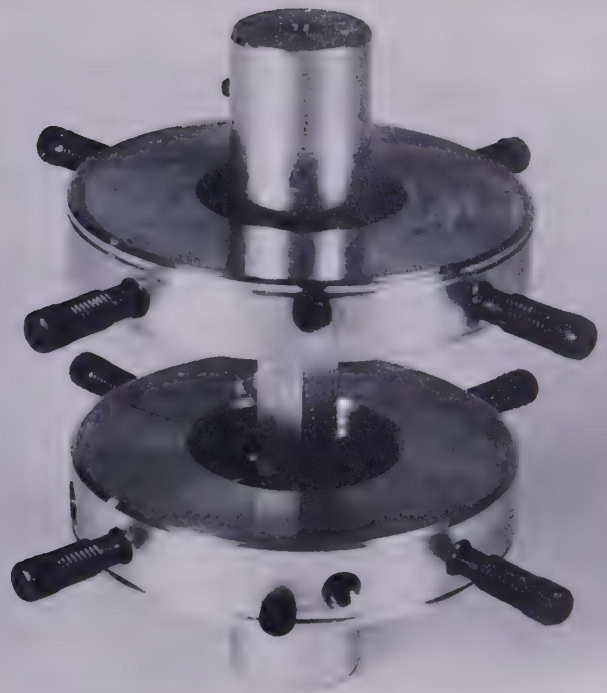

Fig. 4.1 Spider Apparatus Mounted on Specimen

the spiders are concentric about the axis of the specimen. To the outer edge of each spider is attached a very fine wire which is used to measure tangential displacement. The displacement is amplified by a lever mechanism with a mechanical advantage of about ten before being attached to the core of the transducer. Figure 4.2 shows the lever arms and the transducers. A displacement of the transducer cores causes a change in voltage which is measured by voltmeters connected to the transducers.

Torques are measured by means of a set of four strain gauges mounted at 45° on the shaft leading to the upper set of jaws on the torsion machine. The dynamometer is explained in more detail in Section 4.1.3a.

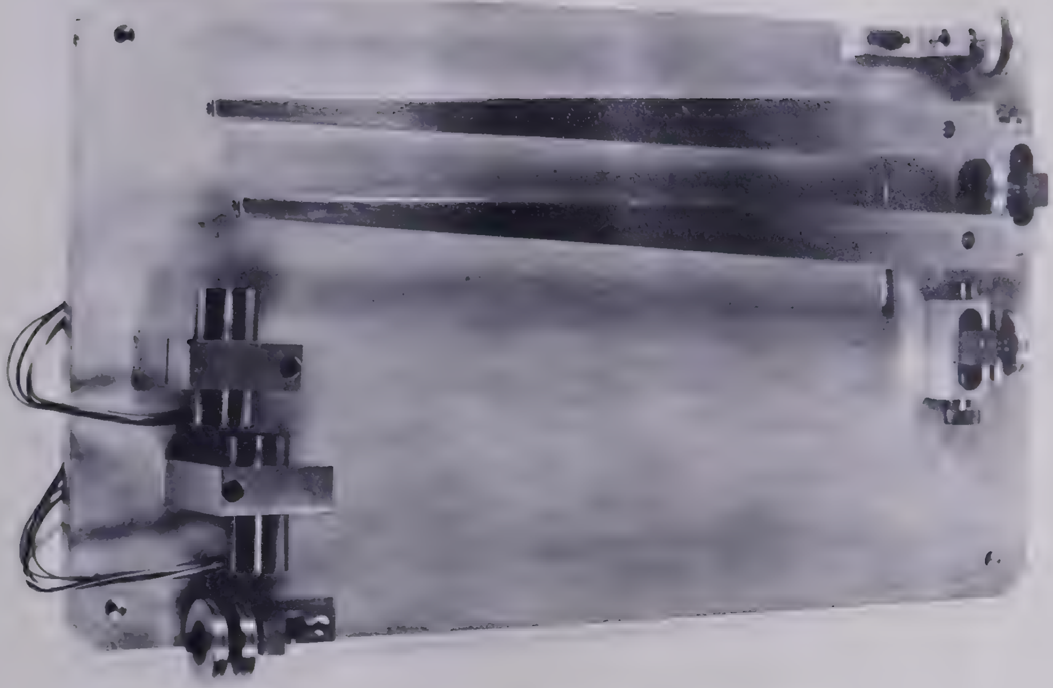

Fig. 4.2 Lever Arms and Transducers

4.1.2 The Test Specimens

The material used was commercially-pure Aluminum which was annealed by the following procedure. The machined specimens were heated gradually in an oven from room temperature to 700°F over a period of forty-five minutes. The temperature was controlled at 700°F for thirty minutes and the specimens were then allowed to cool to room temperature overnight.

Two different cross-sections were used in the torsion tests. The specifications are shown in Figure 4.18. The taper was kept to within ± 0.001".

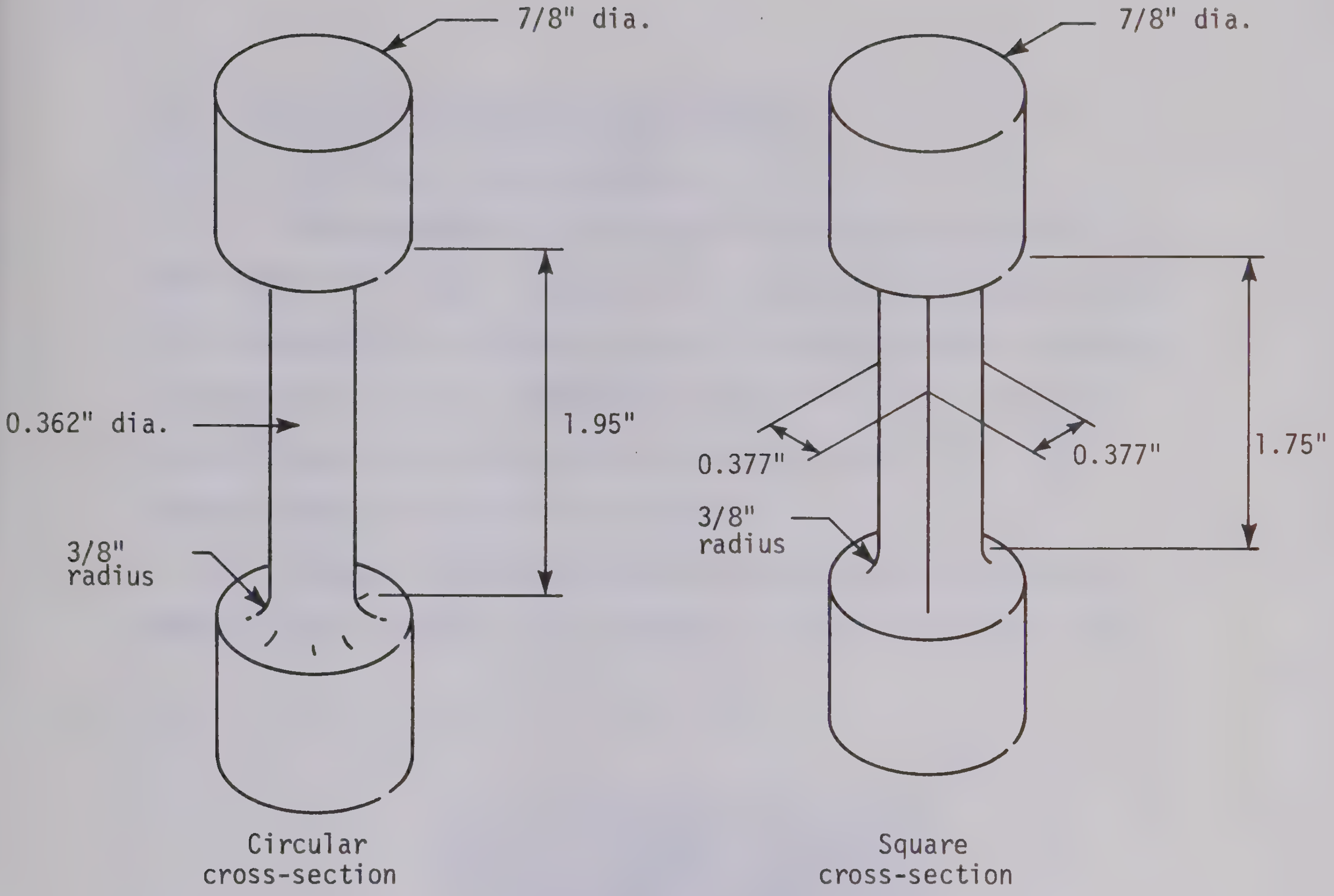
7/8" dia.
7/8" dia.
0.362" dia.
1.95"
3/8"
radius
0.377"
0.377"
1.75"
3/8"
radius
Circular
cross-section
Square
cross-section

Fig. 4.18 The Torsion Specimens

4.1.3 Calibration and Experimental Procedure

4.1.3.a Calibration of the Dynamometer

The dynamometer was calibrated by mounting a lever arm on the upper jaws of the torsion apparatus and applying known moments by means of pulleys and various weights as shown in Figure 4.3. As was mentioned in Section 4.1.1, strain gauges were mounted on the shaft leading to the upper jaws and the moments were correlated to the strain gauge readings which were taken from a voltmeter.

Care was taken to minimize bending or axial loading during the calibration. However, the arrangement of the strain gauges com-

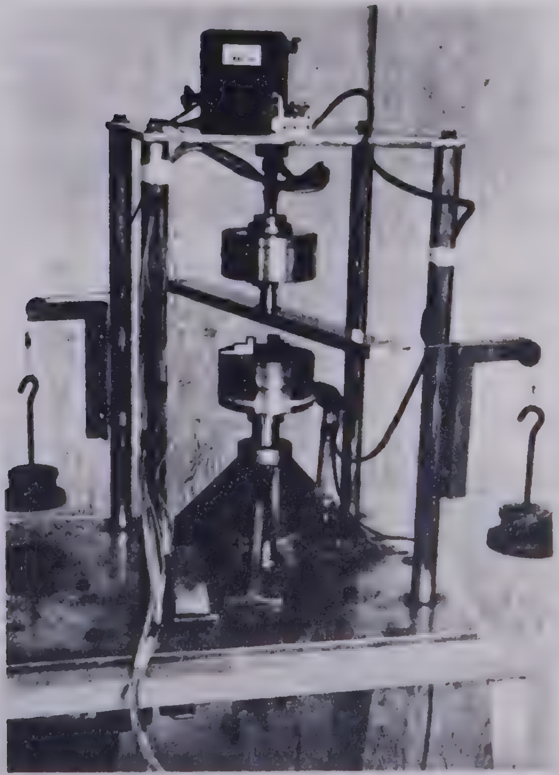

Fig. 4.3 Calibration of the Dynamometer

pensated for any bending or longitudinal straining. Two of the strain gauges were in tension and were diametrically opposite while the other two gauges were in compression and were also diametrically opposite. Bending was compensated for since the gauges were opposite one another. Axial stretching was compensated for since two of the gauges were in tension and two were in compression.

Results of the calibration can be seen in Table 4.1 and Figure 4.4. The calibration curve is linear and the conversion factor from gauge readings to torque, as calculated by the ratio $(\sum_i M_i V_i)/(\sum V_i^2)$, is 179 in-lb/mv.

4.1.3.b Calibration of Twist Measurement

The lower jaws on the torsion machine were rotated by a "dividing head" which was connected by a chain-sprocket mechanism. It was found that 5970 revolutions of the handle of the dividing head were required to make one complete revolution of the lower jaws.

The specimen was then gripped in the lower jaws and the spiders were attached. The wires from the transducer-lever arm apparatus were secured to the outer edges of the spiders and the slack was taken up by means of an adjustment in the apparatus. The voltage output readings from the linear transducers could then be correlated with true angles turned by the upper and lower spiders. Assuming that each revolution of the dividing head handle turned the lower jaws through the same angle, a calibration curve was plotted which converted voltage output from the transducer to angle of twist for each spider. The calibration

readings for the circular specimen and the square specimen are shown in Tables 4.2 and 4.3 respectively. The corresponding curves are shown in Figures 4.5 to 4.8.

There was some slack in the system prior to the calibrations. This shows up in the best-fit curves shown in Figures 4.5 to 4.8. It took approximately 1/8 of a revolution on the handle of the dividing head to take up the slack.

A curve of the type

$$N = cV + \frac{1}{8}$$

where N is the number of revolutions of the dividing head and V is the voltage reading in volts was fitted to the calibration data so that the quantity $\sum_i (N_i - cV_i - \frac{1}{8})^2$ is minimized with respect to c. Therefore

$$c = \frac{\Sigma N_i V_i - \frac{1}{8} \Sigma V_i}{\Sigma V_i^2} .$$

The angle of twist is then given by

$$\theta = \frac{2\pi}{5970} (cV + \frac{1}{8}) . \tag{4.1}$$

Equation (4.1) for the circular specimen became

$$\theta = 9.15 \times 10^{-3} V + 0.132 \times 10^{-3} \text{ rad} .$$

for the upper spider and

$$\theta = 8.18 \times 10^{-3}\ V + 0.132 \times 10^{-3}\ \text{rad.}$$

for the lower. The corresponding equations for the square specimen are

$$\theta = 9.19 \times 10^{-3}\ V + 0.132 \times 10^{-3}\ \text{rad.}$$

for the upper spider and

$$\theta = 8.22 \times 10^{-3}\ V + 0.132 \times 10^{-3}\ \text{rad.}$$

for the lower spider. Since the difference of the upper and lower angles of twist is required, the term 0.132×10^{-3} rad. has no effect on the results.

It was observed that when the transducer cores moved approximately one-tenth of an inch, the output voltage increased by about 0.6 volts. Voltage readings were taken on the one volt scale and the voltages ran from 0.200 volts to 0.800 volts. When the voltage reached 0.800 volts the transducer core was reset to its initial position by an adjustment in the lever arm apparatus, thus in effect resetting the voltage reading to 0.200 volts. By using this procedure more sensitive voltage increments could be read from the voltmeters. Another reason for this procedure was that the final displacements were larger than

the allowable displacements of the transducer cores.

4.1.3.c Experimental Procedure

As soon as each particular specimen was calibrated the upper jaws of the torsion machine were tightened and the experiments were performed.

A constant tension was maintained in the wires by attaching some "dead weights" to the cores of the transducers by means of wires and pulleys. The tension in the wires caused a negative moment of magnitude 1.79 in.-lb. in the specimen.

It was also noticed that the angle measuring apparatus was not reversible due to friction and possibly some slack in the gears. For this reason, readings were taken for loading only.

Pins were inserted in each end of the specimens to help ensure that there would be no slip in the jaws of the torsion machine. If there was slip however, it had no bearing on the results because the moment measured would still be the true moment and the difference in the readings given by the two spiders would still give angle of twist per unit length.

4.1.4 Results of the Torsion Tests

The output voltage readings for the circular cross-section and the square cross-section are listed in Tables 4.4 and 4.6 respectively. These readings are then converted to moments and corresponding angles of twist per unit length by the calibration equations shown in Sections 4.1.3.a and 4.1.3.b. The results are shown in Tables

4.5 and 4.7. The angles of twist per unit length for Tables 4.5 and 4.7 are calculated by dividing the difference in angles turned by the upper and lower spiders by the respective gauge lengths. As was mentioned in Section 4.1.2 the gauge length for the circular specimen is 1.95 in. whereas the square specimen has a gauge length of 1.75 in.

Figure 4.9 shows a plot of moment M versus angle of twist per unit length θ for the specimen of circular cross-section.

The classical elastic theory for torsion of a circular bar of radius "a" predicts that

$$\frac{M}{2\mu a^3} = \frac{\pi}{4} (\theta a) \ .$$

The slope of the M Vs θ curve in the elastic region then is

$$\frac{M}{\theta} = \frac{\pi a^4}{2} \mu \ .$$

Since the radius of the circular specimen is 0.181 in., the initial slope of the curve in Figure 4.9 should be

$$\frac{\pi(0.181)^4}{2} (3.76 \times 10^6) = 6.34 \times 10^3 \ .$$

This slope is in good agreement with the experimental data. In calculating the dimensionless moments $M/2\mu a^3$, which are shown in Tables 4.8 and 4.9, the shear modulus μ is taken as 3.76×10^6 psi [20]. The re-

lation between $M/2\mu a^3$ and θa is shown graphically for the circular cross-section in Figure 4.10 and for the square cross-section in Figure 4.11. The initial slope for the circular specimen is approximately 0.825 whereas for the square specimen the initial slope is approximately 1.15. The classical theory predicts an elastic slope of $\pi/4$ or 0.785 for the circular specimen and 1.125 for the square specimen [19].

The angles of twist were corrected so that the curves in Figures 4.10 and 4.11 extrapolated through the origin. For the circular cross-section, 0.02×10^{-3} was subtracted from the angles of twist (θa) while 0.03×10^{-3} was added for the square bar.

4.1.5 Comparison Test

The purpose of the next test was to compare the angle of twist per unit length obtained by the spider apparatus with that determined by strain gauges. Since strain gauges can be used to find angle of twist per unit length for circular specimens, a commercially pure Aluminum specimen was machined and annealed as described in Section 4.1.2.

The test diameter of the circular specimen was 0.371 in. and the gauge length was 1.942 in. Four strain gauges were attached at approximately the center of the test section of the specimen. The strain gauges were mounted at 45° to the axis of the specimen so that two of the gauges acted in tension and two in compression when the specimen was twisted. The gauges were located at 90° to each other

such that each similar pair were diametrically opposite. This arrangement compensated for any bending or axial stretching.

The calibration curves for angle of twist determined by the spider apparatus are shown in Figures 4.12 and 4.13 for the lower and upper spiders respectively. The calibration readings are tabulated in Table 4.10. The equations for converting voltage readings to angles of twist are

$$\theta = 9.33 \times 10^{-3} V + 0.526 \times 10^{-3} \text{ rad.}$$

and

$$\theta = 8.48 \times 10^{-3} V + 0.526 \times 10^{-3} \text{ rad.}$$

for the upper and lower spiders respectively. These equations were obtained by a least squares approximation.

Table 4.11 shows the strain gauge readings and the spider voltage readings that were taken during the test. The strain gauge readings are converted to angles of twist per unit length in Table 4.11 and the spider voltage readings are converted to their corresponding angles of twist per unit length in Table 4.12. Figure 4.14 compares the two graphically.

4.2 Tension Test

A commercially pure Aluminum tension specimen with a circular cross-section was prepared as in Section 4.1.2. Figure 4.15 shows the specifications.

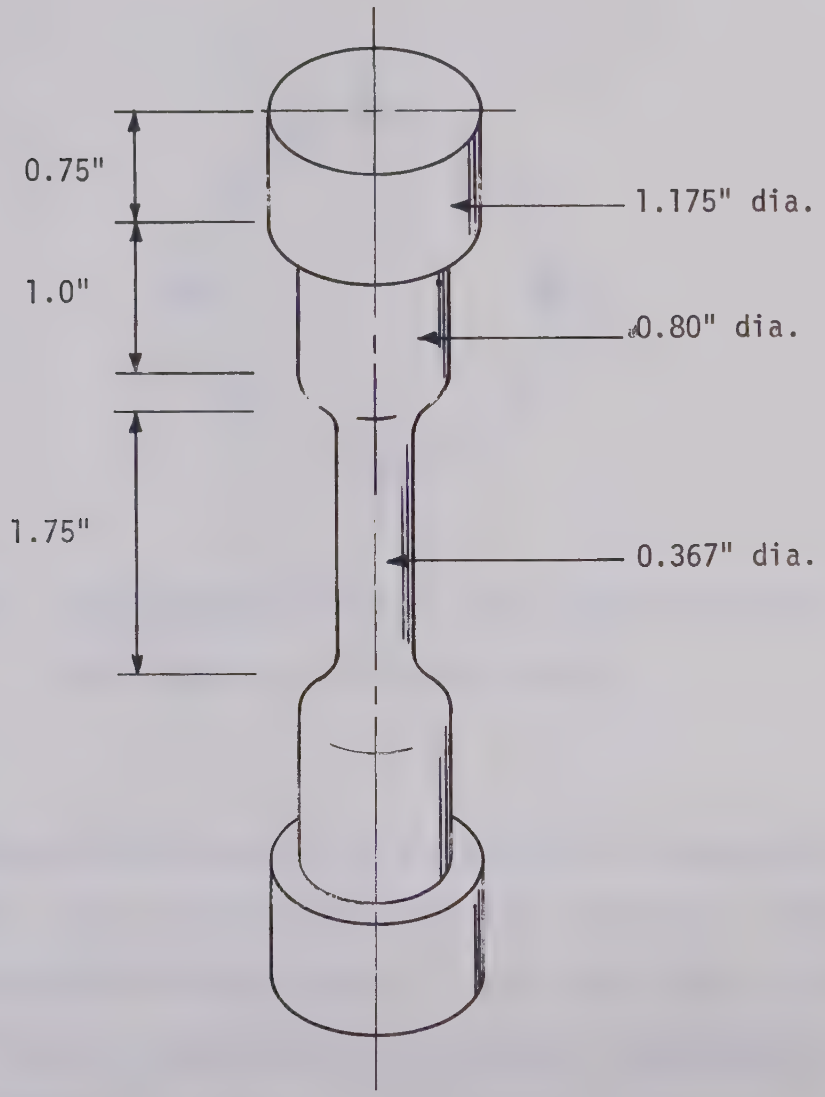
0.75"
1.0"
1.75"
1.175" dia.
0.80" dia.
0.367" dia.

Fig. 4.15 The Tensile Test Specimen

Four strain gauges were attached longitudinally at the center of the specimen and were located at diametrically opposite positions as in Figure 4.16.

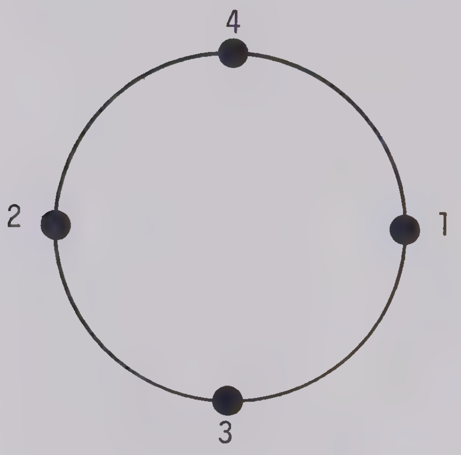

Fig. 4.16 Cross-Sectional View of Tensile Specimen Showing the Location of the Strain Gauges

The load and corresponding average strain readings are listed in Table 4.13. Since the diameter of the test section was 0.367 in., the cross-sectional area was 0.106 in.^{2}. Also since [20] $\nu = 0.33$ and $E = 10 \times 10^6$ psi for commercially pure Aluminum, the deviatoric strain can be found from

$$\varepsilon = e_{11} - \frac{(1-2\nu)}{3E}\sigma_{11} = e_{11} - 1.13 \times 10^{-8}\sigma_{11}$$

where σ_{11} is given in units of psi. The corresponding deviatoric stresses and strains are shown in Table 4.14 and plotted in Figure 4.17. In finding the non-dimensional deviatoric stress, μ was taken to be 3.76×10^6 psi [20].

TABLE 4.1

Torque Calibration

Moment (in.lb)	Voltage (mv)
0	0
2.20	0.013
6.61	0.038
11.02	0.062
15.43	0.087
19.84	0.111
24.25	0.135
28.66	0.160
33.07	0.184
37.48	0.208
41.89	0.232
46.30	0.256

TABLE 4.2

Calibration of Angle of Twist for Circular Specimen

No. of Revs. of Dividing Head	Voltage Reading (volts)		Voltage Increase (volts)	
	Upper Spider	Lower Spider	Upper Spider	Lower Spider
0	0.200	0.200	0.000	0.000
1	0.287	0.312	0.087	0.112
2	0.394	0.432	0.194	0.232
3	0.525	0.565	0.325	0.365
4	0.620	0.689	0.420	0.489
5	0.775	0.217	0.575	0.617
6	0.271	0.351	0.671	0.751
7	0.377	0.473	0.777	0.873
8	0.509	0.610	0.909	1.010
9	0.600	0.732	1.000	1.132
10	0.753	0.270	1.153	1.270
11	0.260	0.402	1.260	1.402
12	0.371	0.531	1.371	1.531
13	0.480	0.658	1.480	1.658
14	0.597	0.795	1.597	1.795

TABLE 4.3

Calibration of Angle of Twist for Square Specimen

No. of Revs. of Dividing Head	Voltage Reading (volts)		Voltage Increase (volts)	
	Upper Spider	Lower Spider	Upper Spider	Lower Spider
0	0.200	0.200	0.000	0.000
1	0.310	0.328	0.110	0.128
2	0.410	0.439	0.210	0.239
3	0.520	0.562	0.320	0.362
4	0.635	0.690	0.435	0.490
5	0.780	0.220	0.580	0.620
6	0.268	0.332	0.668	0.732
7	0.375	0.460	0.775	0.860
8	0.510	0.600	0.910	1.000
9	0.620	0.730	1.020	1.130
10	0.750	0.268	1.150	1.268
11	0.250	0.400	1.250	1.400
12	0.350	0.520	1.350	1.520
13	0.465	0.659	1.465	1.659
14	0.580	0.780	1.580	1.780
15	0.700	0.300	1.700	1.900
16	0.230	0.440	1.830	2.040
17	0.329	0.566	1.929	2.166
18	0.440	0.690	2.040	2.290
19	0.560	0.220	2.160	2.420
20	0.680	0.348	2.280	2.548
21	0.800	0.464	2.400	2.664

TABLE 4.4

Experimental Data for Torsion of Circular Bar

No. of Revs. of Dividing Head	Upper Spider (volts)	Lower Spider (volts)	Moment Output (mv)
0	0.200	0.200	0.000
2	0.205	0.328	0.014
4	0.241	0.512	0.039
6	0.267	0.701	0.061
8	0.294	0.298	0.084
10	0.314	0.482	0.104
12	0.329	0.684	0.119
14	0.340	0.300	0.129
16	0.345	0.522	0.135
18	0.350	0.750	0.140
20	0.360	0.406	0.145
22	0.360	0.625	0.149
24	0.368	0.290	0.152
26	0.368	0.530	0.153
28	0.368	0.748	0.158
30	0.369	0.399	0.160
32	0.369	0.639	0.161
34	0.370	0.280	0.163
36	0.379	0.540	0.165
38	0.380	0.790	0.168
40	0.389	0.440	0.169
42	0.400	0.656	0.171
44	0.402	0.331	0.172
46	0.402	0.582	0.174
48	0.417	0.213	0.177
50	0.420	0.451	0.179
52	0.420	0.703	0.180
54	0.431	0.320	0.181

TABLE 4.5

Results for Circular Cross-Section

Moment (in.lb)	Angle of Twist Upper Spider ($\times 10^{+3}$ rad)	Angle of Twist Lower Spider ($\times 10^{+3}$ rad)	Difference in angle ($\times 10^{+3}$ rad)	Angle of Twist per unit length ($\times 10^{+3}$ rad/in)
0.00	0.000	0.000	0.000	0.00
2.51	0.046	1.047	1.00	0.51
6.98	0.375	2.552	2.18	1.12
10.92	0.613	4.098	3.49	1.79
15.0	0.860	5.710	4.85	2.49
18.6	1.04	7.21	6.17	3.16
21.3	1.18	8.87	7.69	3.94
23.1	1.28	10.6	9.3	4.77
24.2	1.33	12.4	11.1	5.69
25.1	1.37	14.3	12.9	6.62
26.0	1.46	16.4	14.9	7.64
26.7	1.46	18.2	16.7	8.56
27.2	1.54	20.4	18.9	9.69
27.4	1.54	22.3	20.8	10.7
28.3	1.54	24.1	22.6	11.6
28.6	1.55	26.2	24.7	12.7
28.8	1.55	28.1	26.5	13.6
29.2	1.56	30.1	28.5	14.6
29.5	1.64	32.2	30.6	15.7
30.1	1.65	34.3	32.6	16.7
30.3	1.73	36.3	34.6	17.7
30.6	1.83	38.1	36.3	18.6
30.8	1.85	40.3	38.4	19.7
31.1	1.85	42.4	40.5	20.8
31.7	1.99	44.3	42.3	21.7
32.0	2.01	46.2	44.2	22.7
32.2	2.01	48.3	46.3	23.7
32.4	2.11	50.1	48.0	24.6

TABLE 4.6

Experimental Data for Torsion of Square Bar

No. of Revs. of Dividing Head	Upper Spider (volts)	Lower Spider (volts)	Moment Output (mv)
0	0.200	0.200	0.011
2	0.220	0.330	0.041
4	0.240	0.474	0.074
6	0.265	0.635	0.110
8	0.305	0.207	0.143
10	0.320	0.409	0.162
12	0.333	0.620	0.176
14	0.353	0.259	0.188
16	0.369	0.478	0.194
18	0.380	0.715	0.200
20	0.400	0.352	0.207
22	0.411	0.601	0.210
24	0.435	0.230	0.220
26	0.440	0.473	0.220
28	0.441	0.721	0.223
30	0.468	0.350	0.230
32	0.468	0.600	0.231
34	0.488	0.220	0.240
36	0.490	0.460	0.240
38	0.492	0.710	0.241
40	0.516	0.300	0.247
42	0.517	0.550	0.248
44	0.518	0.800	0.250
46	0.538	0.390	0.252
48	0.537	0.650	0.253
50	0.541	0.278	0.259
52	0.543	0.519	0.260
54	0.544	0.748	0.260

TABLE 4.7

Results for Square Cross-Section

Moment (in.lb)	Angle of Twist		Difference in Angle (x10^{+3} rad)	Angle of Twist per unit Length (x10^{+3} rad/in)
	Upper Spider (x10^{+3} rad)	Lower Spider (x10^{+3} rad)		
1.97	0.000	0.000	0.000	0.00
7.34	0.184	1.07	0.89	0.51
13.2	0.368	2.25	1.88	1.07
19.7	0.597	3.58	2.98	1.70
25.6	0.965	4.99	4.02	2.30
29.0	1.10	6.65	5.55	3.17
31.5	1.22	8.38	7.16	4.09
33.7	1.41	10.0	8.6	4.91
34.7	1.55	12.1	10.5	6.00
35.8	1.65	14.1	12.4	7.09
37.1	1.84	16.0	14.2	8.11
37.6	1.94	18.1	16.2	9.26
39.4	2.16	20.0	17.8	10.2
39.4	2.21	22.0	19.8	11.3
39.9	2.21	24.0	21.8	12.5
41.2	2.46	25.9	23.4	13.4
41.3	2.46	27.9	25.4	14.5
43.0	2.65	29.8	27.1	15.5
43.0	2.67	31.7	29.0	16.6
43.1	2.68	33.8	31.1	17.8
44.2	2.90	35.3	32.4	18.5
44.4	2.91	37.4	34.5	19.7
44.8	2.92	39.5	36.6	20.9
45.1	3.11	41.0	37.9	21.7
45.3	3.10	43.2	40.1	22.9
46.4	3.13	45.0	41.9	23.9
46.5	3.15	47.0	43.8	25.0
46.5	3.16	48.9	45.7	26.1

TABLE 4.8

Summary of Results for Circular Bar

No. of Revs. of Dividing Head	$\frac{M}{2\mu a^3}$ $(\times 10^{+3})$	$\theta a (\times 10^{+3})$	$\theta a - 0.02 \times 10^{-3}$ $(\times 10^{+3})$
0	0.000	0.000	0.000
2	0.056	0.093	0.073
4	0.157	0.202	0.182
6	0.245	0.324	0.304
8	0.337	0.450	0.430
10	0.417	0.573	0.553
12	0.478	0.714	0.694
14	0.518	0.863	0.843
16	0.542	1.03	1.01
18	0.562	1.20	1.18
20	0.582	1.38	1.36
22	0.598	1.55	1.53
24	0.610	1.75	1.73
26	0.614	1.93	1.91
28	0.634	2.10	2.08
30	0.642	2.29	2.27
32	0.646	2.46	2.44
34	0.654	2.65	2.63
36	0.662	2.84	2.82
38	0.674	3.03	3.01
40	0.678	3.21	3.19
42	0.686	3.37	3.35
44	0.690	3.56	3.54
46	0.698	3.76	3.74
48	0.711	3.93	3.91
50	0.719	4.10	4.08
52	0.723	4.30	4.28
54	0.727	4.46	4.44

TABLE 4.9

Summary of Results for Square Bar

No. of Revs. of Dividing Head	$\frac{M}{2\mu a^3}$ $(\times 10^{+3})$	$\theta a(\times 10^{+3})$	$\theta a + 0.03 \times 10^{-3}$ $(\times 10^{+3})$
0	0.039	0.00	0.03
2	0.146	0.096	0.126
4	0.263	0.203	0.233
6	0.391	0.321	0.351
8	0.508	0.433	0.463
10	0.576	0.598	0.628
12	0.625	0.771	0.801
14	0.668	0.926	0.956
16	0.689	1.13	1.16
18	0.711	1.34	1.37
20	0.736	1.53	1.56
22	0.746	1.74	1.77
24	0.782	1.92	1.95
26	0.782	2.13	2.16
28	0.793	2.35	2.38
30	0.817	2.52	2.55
32	0.821	2.74	2.77
34	0.853	2.92	2.95
36	0.853	3.12	3.15
38	0.856	3.35	3.38
40	0.878	3.49	3.52
42	0.881	3.72	3.75
44	0.888	3.94	3.97
46	0.896	4.08	4.11
48	0.899	4.32	4.35
50	0.920	4.51	4.54
52	0.924	4.72	4.75
54	0.924	4.92	4.95

TABLE 4.10

Calibration of Angle of Twist for Comparison Specimen

No. of Revs. of Dividing Head	Voltage Reading (volts)		Voltage Increase (volts)	
	Upper Spider	Lower Spider	Upper Spider	Lower Spider
0	0.200	0.200	0.000	0.000
1	0.277	0.282	0.077	0.082
2	0.379	0.382	0.179	0.182
3	0.490	0.500	0.290	0.300
4	0.606	0.630	0.406	0.430
5	0.717	0.740	0.517	0.540
6	0.230	0.265	0.630	0.665
7	0.356	0.395	0.756	0.795
8	0.460	0.510	0.860	0.910
9	0.570	0.632	0.970	1.032
10	0.679	0.769	1.079	1.169
11	0.800	0.290	1.200	1.290
12	0.300	0.420	1.300	1.420
13	0.420	0.545	1.420	1.545
14	0.519	0.670	1.519	1.670
15	0.630	0.212	1.630	1.812
16	0.744	0.340	1.744	1.940
17	0.250	0.461	1.850	2.061
18	0.360	0.590	1.960	2.190
19	0.470	0.723	2.070	2.323

TABLE 4.11

Experimental Data for Comparison Test

No. of Revs. of Dividing Head	Average Strain Gauge Reading ($\times 10^{+6}$)	Angle of Twist Per Unit Length ($\times 10^{+3}$ rad/in)	Spider Voltage Readings (volts)	
			Upper Spider	Lower Spider
0	0	0	0.200	0.200
2	43	0.46	0.203	0.280
4	103	1.11	0.227	0.443
6	169	1.82	0.250	0.621
8	231	2.49	0.278	0.203
10	297	3.20	0.308	0.388
12	358	3.86	0.350	0.569
14	422	4.55	0.378	0.769
16	478	5.15	0.425	0.350
18	546	5.89	0.460	0.540
20	607	6.54	0.486	0.744
22	672	7.24	0.537	0.346
24	737	7.94	0.557	0.540
26	812	8.75	0.580	0.754
28	880	9.49	0.610	0.362
30	955	10.3	0.620	0.576

TABLE 4.12

Calculation of Angle of Twist from Spider Voltage Readings

No. of Revs. of Dividing Head	Voltage Increase (volts)		Angle of Twist (x10^{+3} rad)		Difference in Angle (x10^{+3} rad)	Angle of Twist per unit Length, θ (x10^{+3} rad/in)
	Upper	Lower	Upper	Lower		
0	0.000	0.000	0.000	0.000	0.000	0.00
2	0.003	0.080	0.028	0.678	0.650	0.33
4	0.027	0.243	0.252	2.06	1.81	0.93
6	0.050	0.421	0.467	3.57	3.10	1.60
8	0.078	0.603	0.728	5.11	4.38	2.26
10	0.108	0.788	1.01	6.68	5.67	2.92
12	0.150	0.969	1.40	8.22	6.82	3.51
14	0.178	1.169	1.66	9.91	8.25	4.25
16	0.225	1.350	2.10	11.45	9.35	4.81
18	0.260	1.540	2.43	13.1	10.7	5.51
20	0.286	1.744	2.67	14.8	12.1	6.23
22	0.337	1.946	3.14	16.5	13.4	6.90
24	0.357	2.140	3.33	18.1	14.8	7.62
26	0.380	2.354	3.55	20.0	16.4	8.44
28	0.410	2.562	3.83	21.7	17.9	9.22
30	0.420	2.776	3.92	23.5	19.6	10.1

TABLE 4.13

Experimental Data for Tensile Test

Load (lb.)	Average Strain (e_{11}) ($\times 10^{+6}$)	$\sigma_{11} = \frac{\text{Load}}{0.106}$ (psi)	$1.13 \times 10^{-8}\ \sigma_{11}$ ($\times 10^{+6}$)
0	0	0	0
50	48	472	5.3
100	98	943	10.7
150	149	1420	16.0
200	203	1890	21.3
250	264	2360	26.6
300	361	2830	32.0
350	532	3300	37.3
400	918	3770	42.6
450	1822	4250	48.0
500	3335	4720	53.3
550	5349	5190	58.6
600	7713	5660	64.0
650	10130	6130	69.3
700	12060	6600	74.6
750	16610	7080	79.9
800	20860	7550	85.3

TABLE 4.14

Summary of Results for Tensile Test

$T \equiv \frac{\sigma_{11}}{3\mu}$ $(\times 10^{+6})$	$\varepsilon \equiv e_{11} - 1.13 \times 10^{-8}\, \sigma_{11}$ $(\times 10^{+6})$
0	0
41.8	42.7
83.6	87.3
125	133
167	182
209	237
251	329
293	495
335	875
377	1770
419	3280
461	5290
502	7650
544	10100
586	13000
628	16500
670	20800

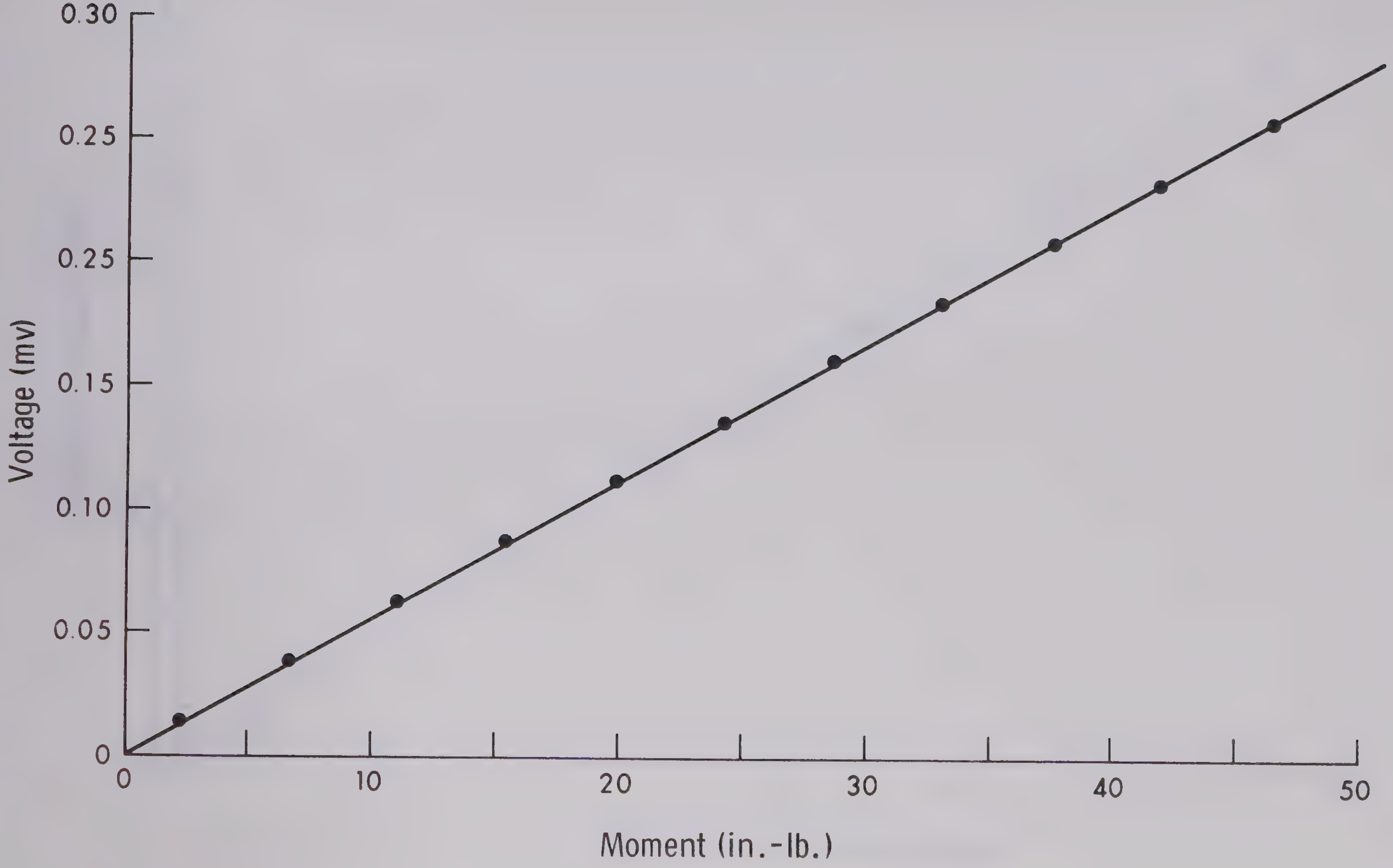

Fig. 4.4 Moment Calibration Curve

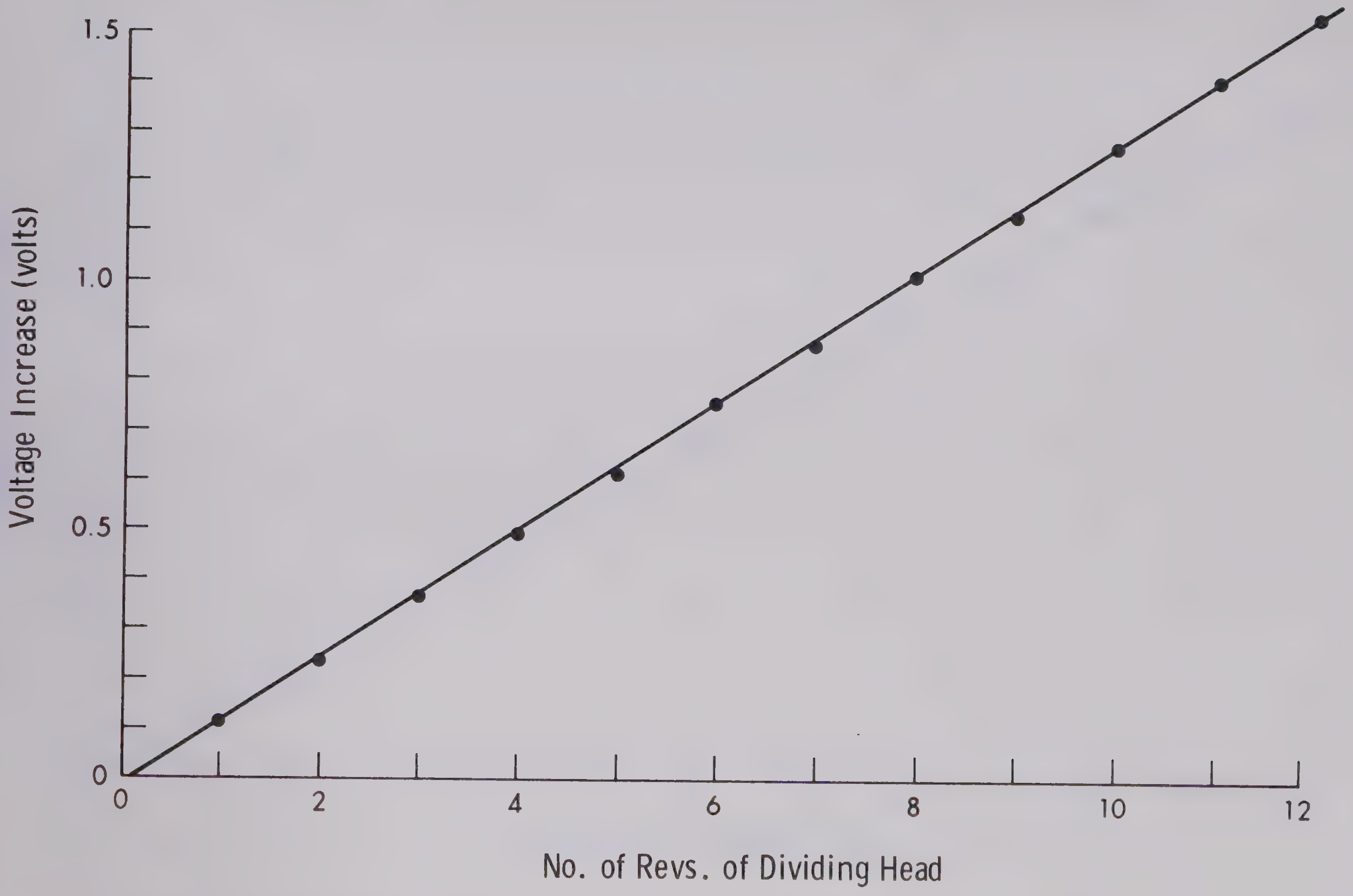

Fig. 4.5 Calibration of Angle of Twist for Lower Spider of Circular Specimen

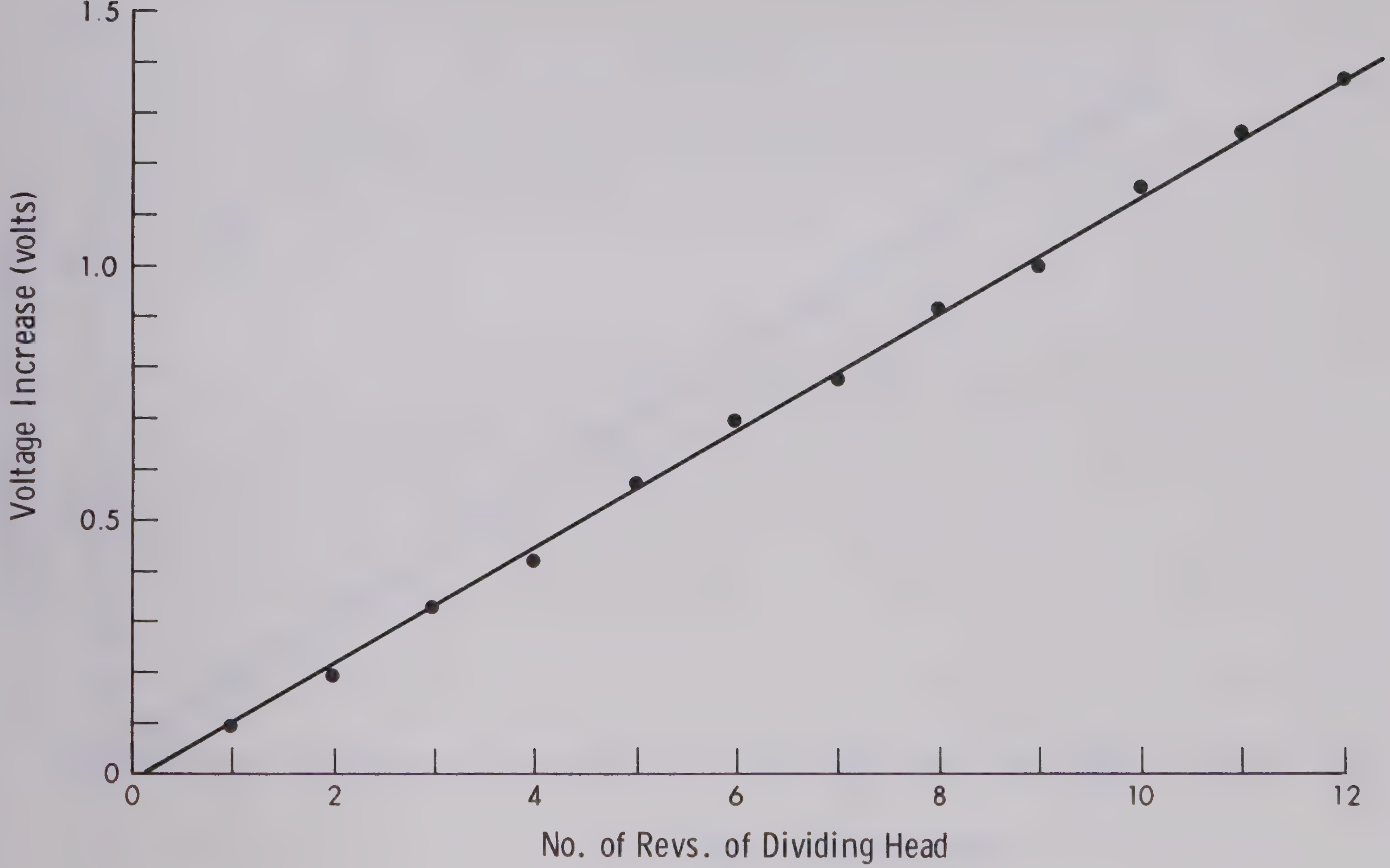

Fig. 4.6 Calibration of Angle of Twist for Upper Spider of Circular Specimen

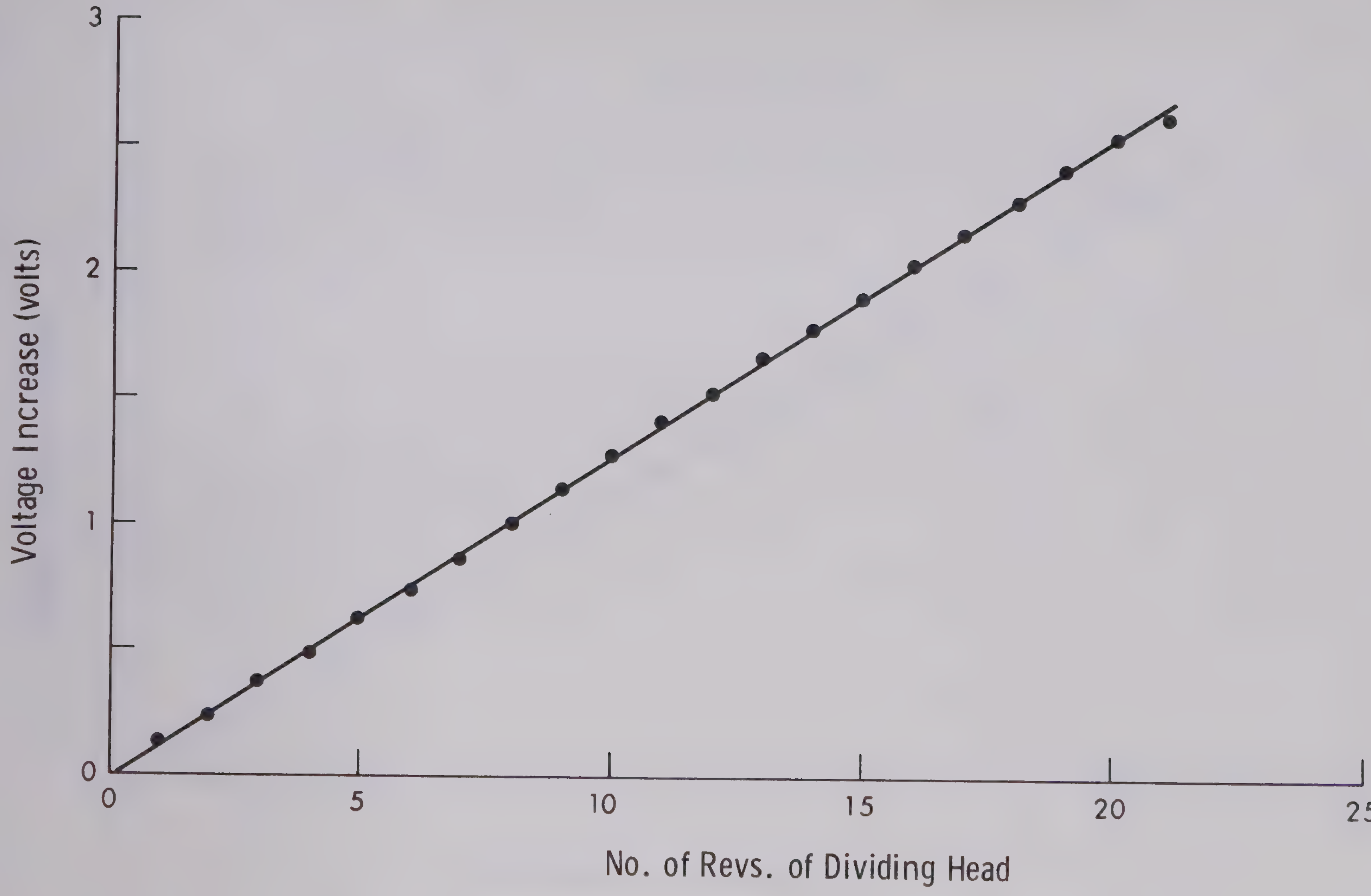

Fig. 4.7 Calibration of Angle of Twist for Lower Spider of Square Specimen

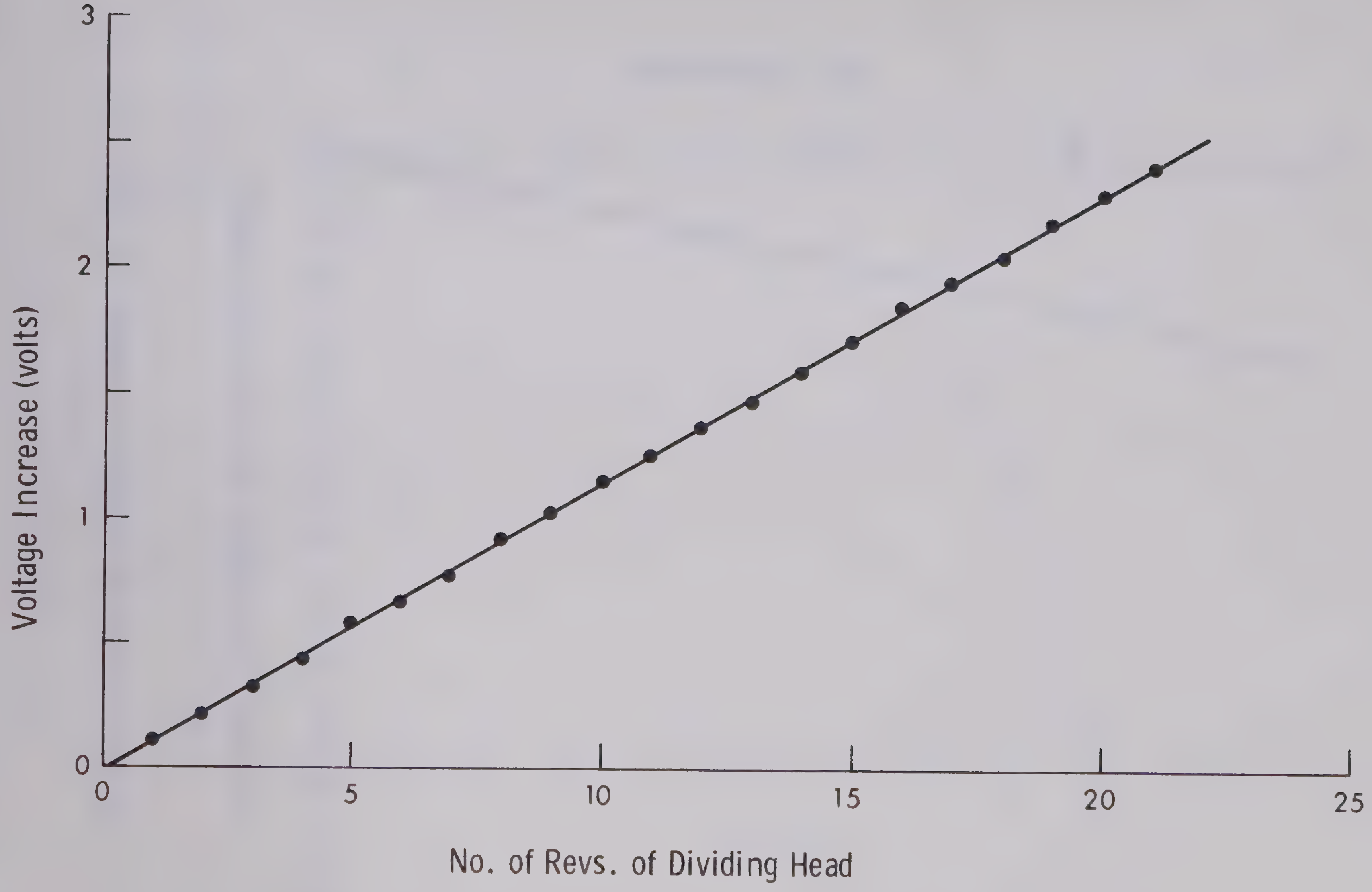

Fig. 4.8 Calibration of Angle of Twist for Upper Spider of Square Specimen

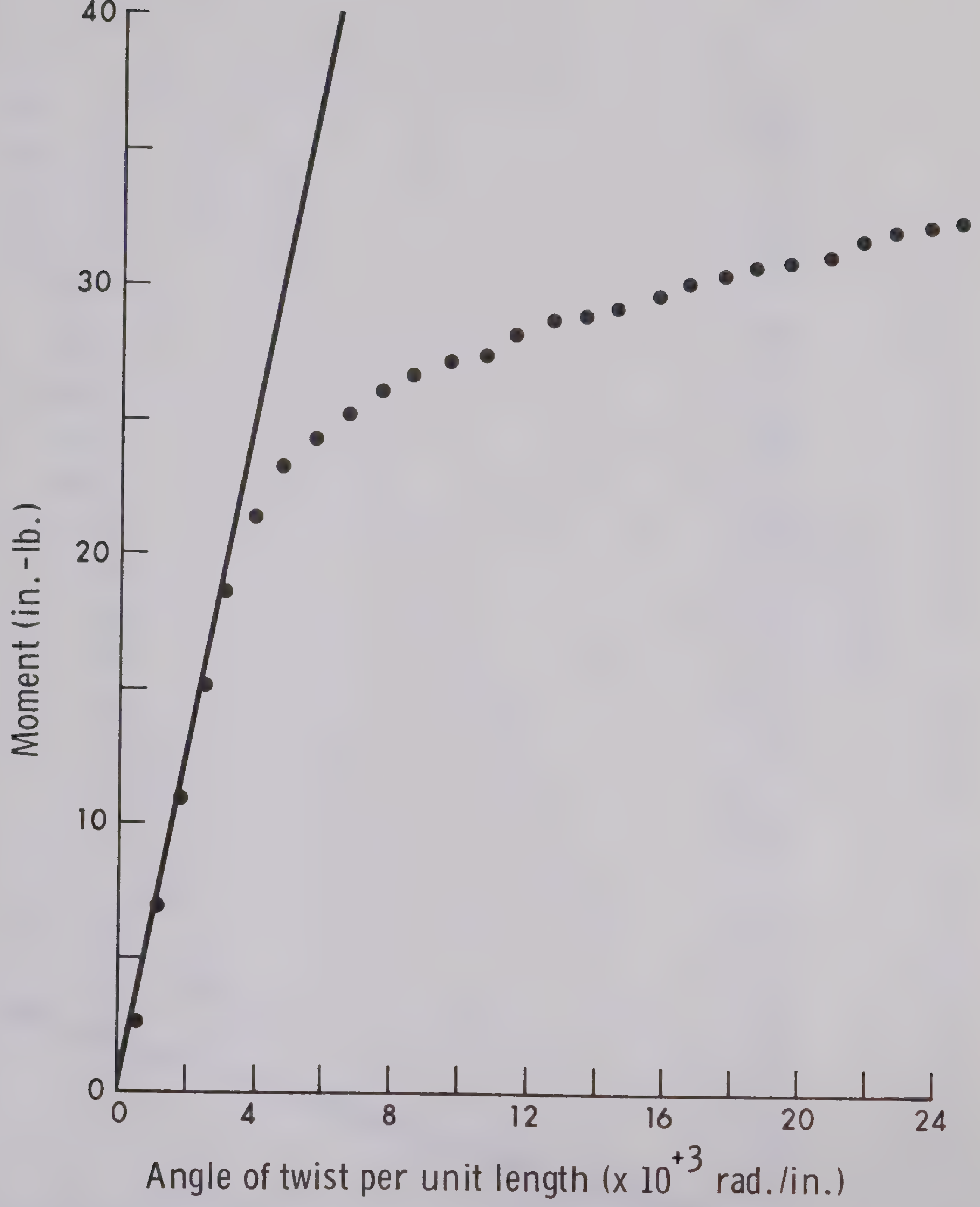

Fig. 4.9 Moment for Torsion of Circular Specimen

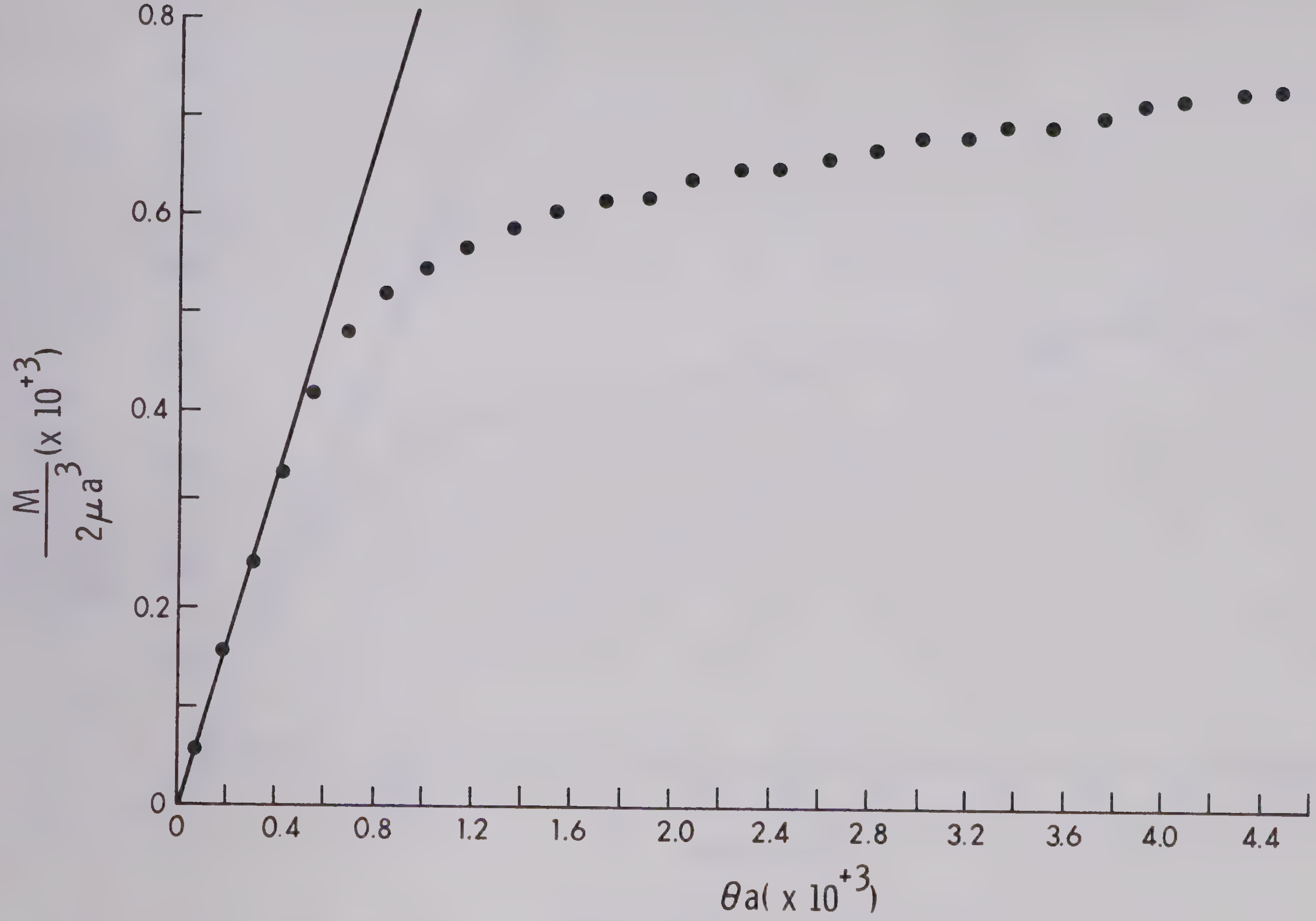

Fig. 4.10 Experimental Moment for Torsion of Circular Specimen

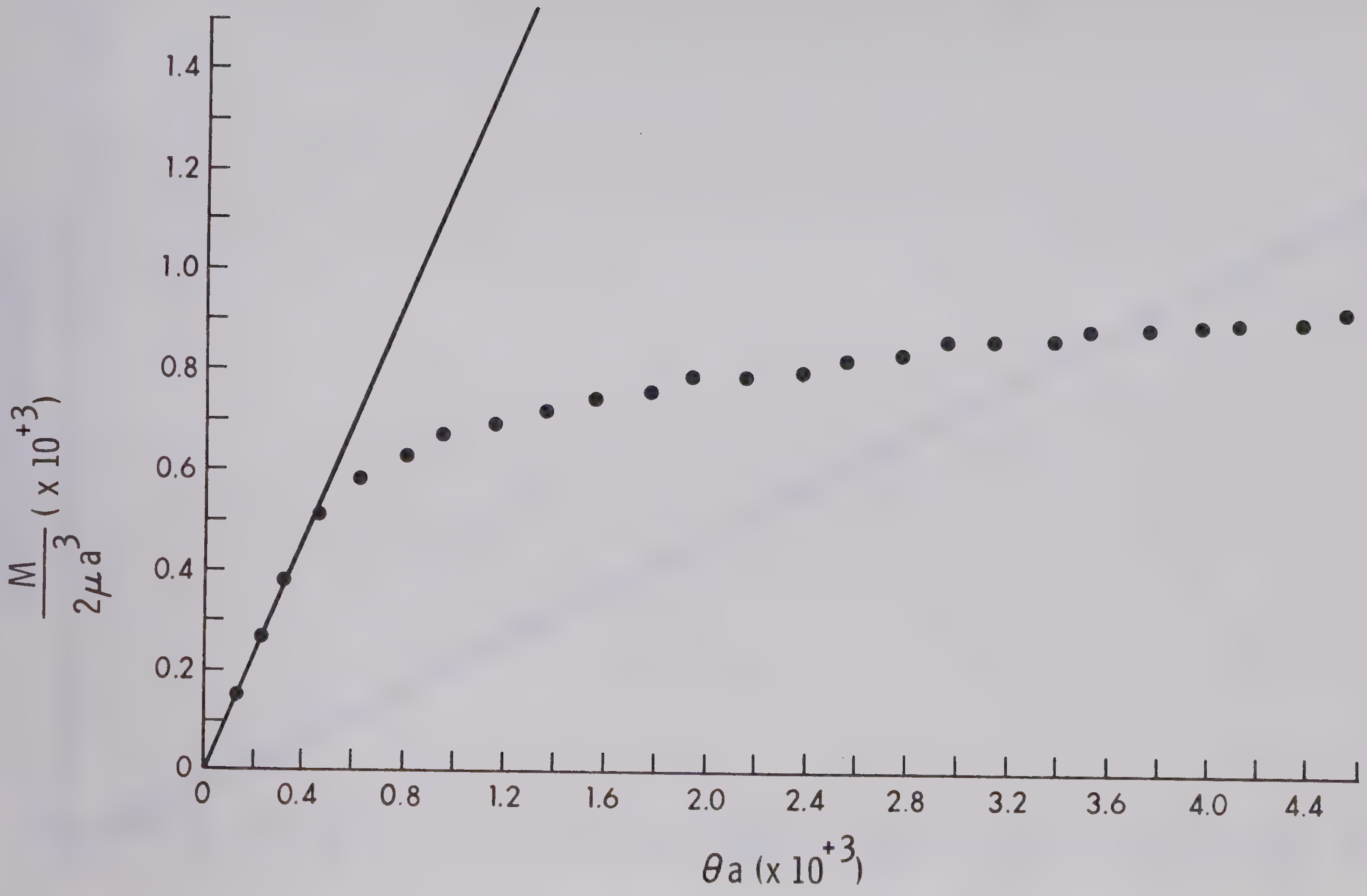

Fig. 4.11 Experimental Moment for Torsion of Square Specimen

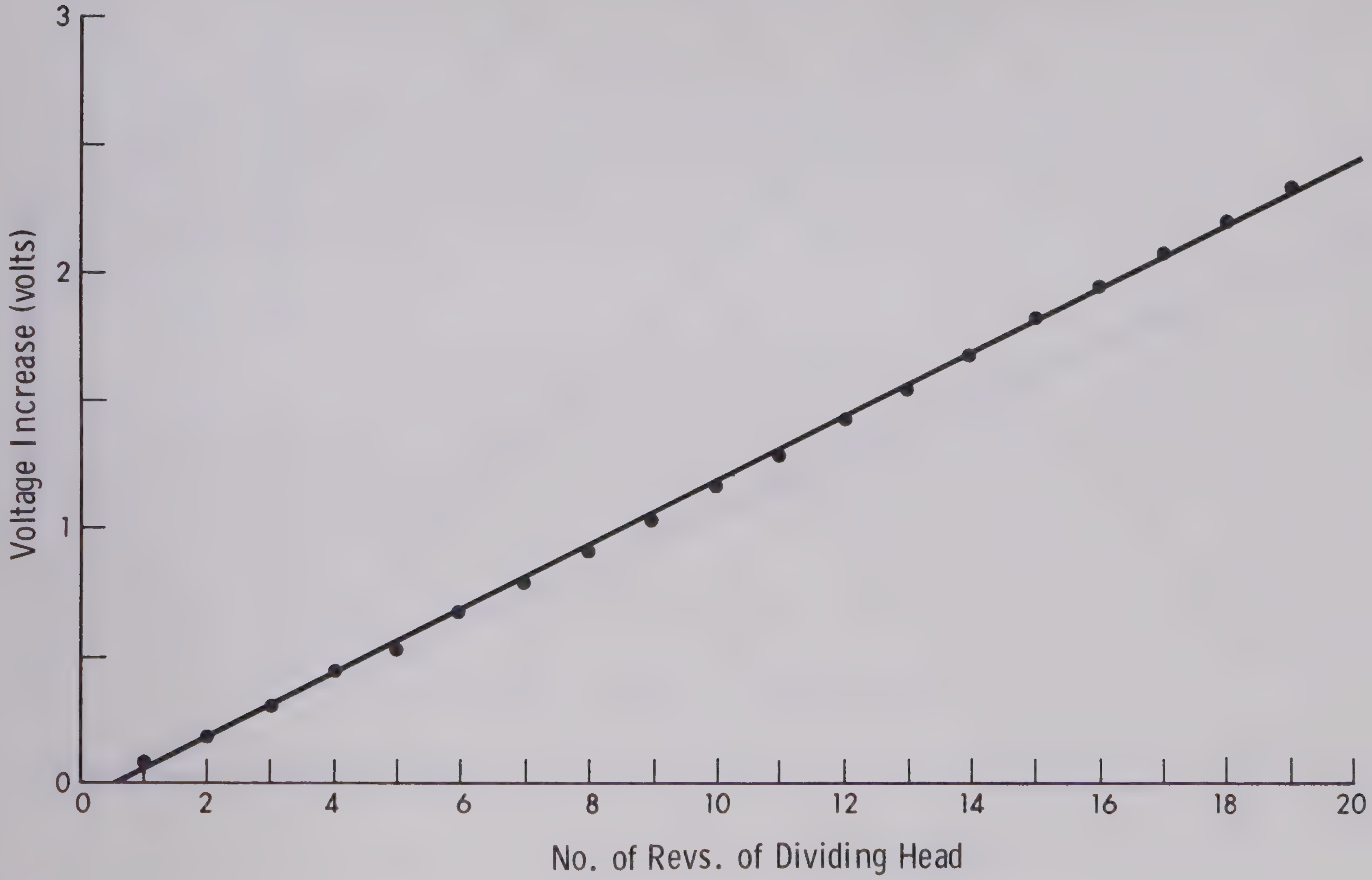

Fig. 4.12 Calibration of Angle of Twist for Lower Spider of Comparison Specimen

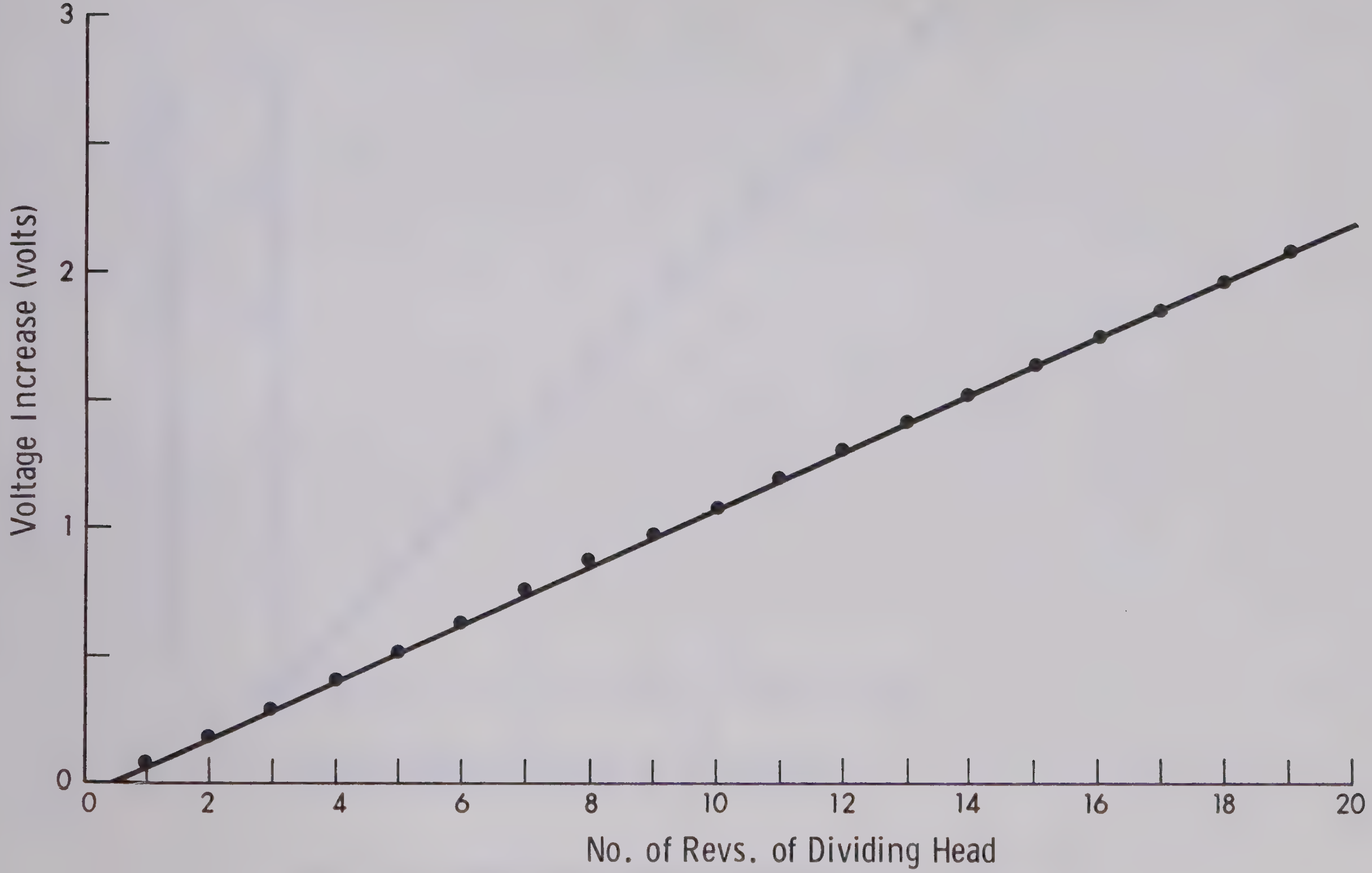

Fig. 4.13 Calibration of Angle of Twist for Upper Spider of Comparison Specimen

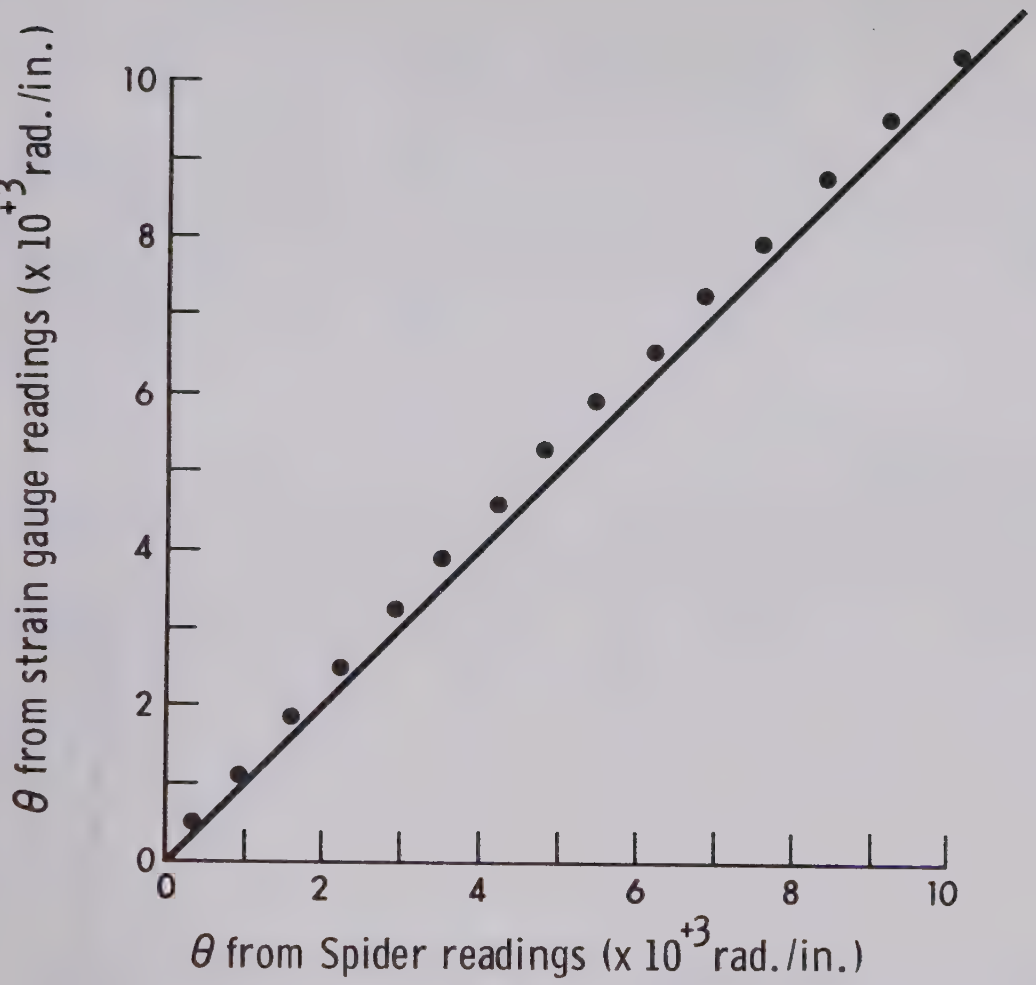

Fig. 4.14 Comparison of Angle of Twist Per Unit Length From Strain Gauges and Spider Apparatus

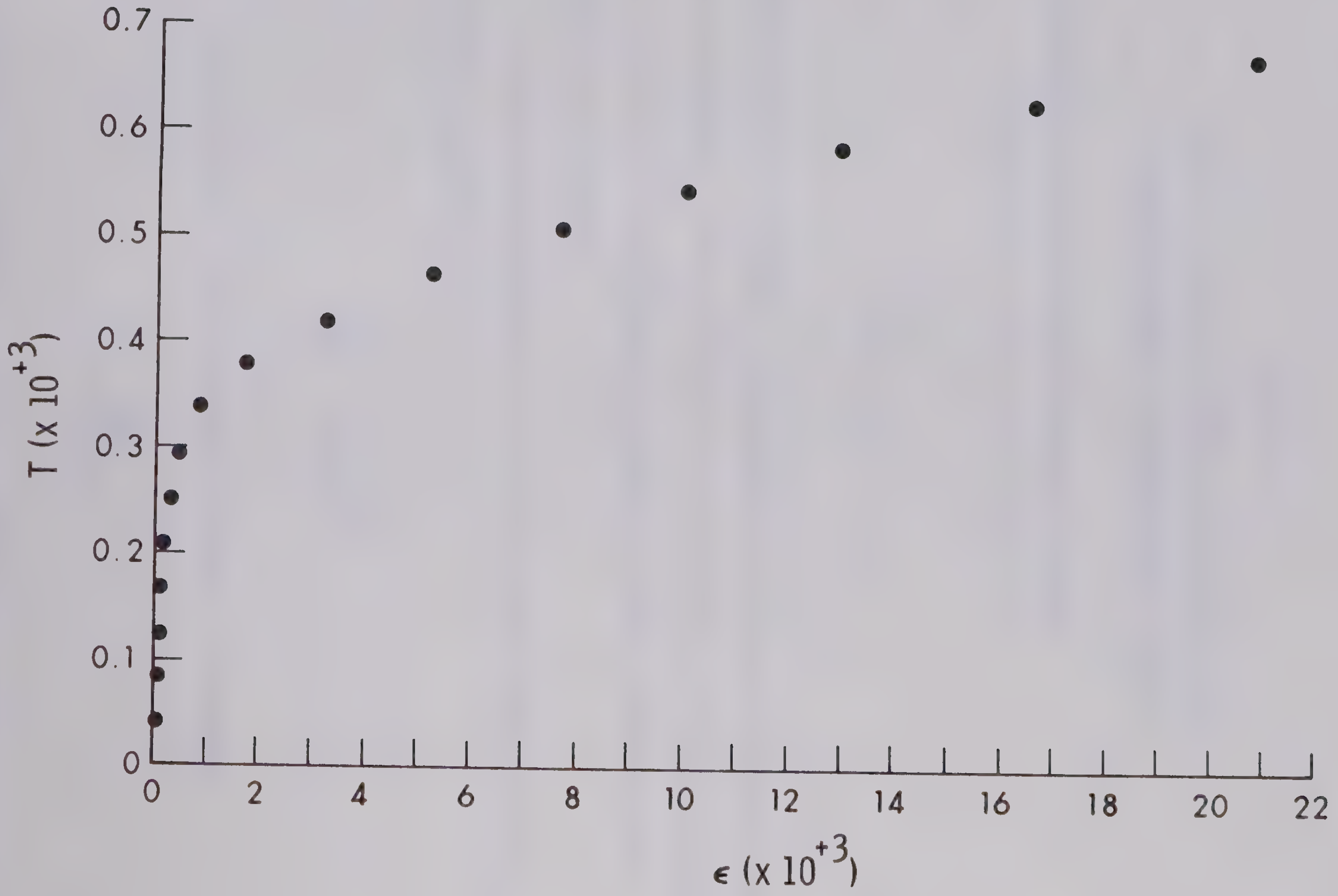

Fig. 4.17 Experimental Tensile Results for a Work-Hardening Material

CHAPTER V

SOLUTION OF SOME WORK-HARDENING PROBLEMS AND COMPARISON TO EXPERIMENTAL RESULTS

5.1 Determination of the Work-Hardening Function

The hypoelastic constitutive equation

$$\frac{\mathcal{D}T_{ij}}{\mathcal{D}t} = d'_{ij} + h\, M' T_{ij} \tag{5.1}$$

is applied, in this chapter, to Engineering problems involving work-hardening materials. The solutions are compared to the experimental results obtained for the tension and torsion tests involving commercially pure Aluminum.

In applying equation (5.1) to the simple tension problem, the resulting equation [14] is

$$\frac{dT}{d\varepsilon} = 1 + \frac{3}{2} hT^2$$

where $T = S_{11}/2\mu$ and ε is the deviatoric strain. Therefore

$$h = \frac{\frac{dT}{d\varepsilon} - 1}{2J}$$

where $J = \frac{1}{2} T_{k\ell}T_{k\ell} = \frac{3}{4} T^2$. If the slope $\frac{dT}{d\varepsilon}$ can be found from the

deviatoric stress-deviatoric strain data shown graphically in Figure 4.17, then h can be obtained as a function of J. However in the above form, h is indeterminate at the origin, and near the origin both the numerator and denominator are extremely small resulting in a large possible error in h. The following work-hardening function does not have this defect;

$$H = 2Jh = \frac{dT}{d\varepsilon} - 1 .$$

The hypoelastic constitutive equation (5.1) for a work-hardening material will then be written as

$$\frac{\mathcal{D}T_{ij}}{\mathcal{D}t} = d'_{ij} + H\left(\frac{M'}{2J}\right) T_{ij} \tag{5.2}$$

where $0 \geq H \geq -1$ and the second term on the right hand side vanishes when $J = 0$.

The slope $d\varepsilon/dT$ is approximated at each of the data points in Figure 4.17 by a fourth order Lagrange interpolation formula. The values are listed in Table 5.1 and plotted in Figure 5.1.

Let

$$g(T) = a + bT - \frac{d\varepsilon}{dT}$$

and let a and b take values so that the initial and final g(T) is zero.

A Fourier sine series,*

$$g(T) = \sum_{k=1}^{15} B_k \sin(\frac{k\pi T}{T_f}) ,$$

is fitted to the function g(T). Then

$$\frac{d\varepsilon}{dT} \equiv \frac{1}{1+H} = a + bT - \sum_{k=1}^{15} B_k \sin(\frac{k\pi T}{T_f}) . \tag{5.3}$$

Since $J = \frac{3}{4} T^2$,

$$\frac{1}{1+H} = a + b\sqrt{\frac{4}{3} J} - \sum_{k=1}^{15} B_k \sin(\frac{k\pi\sqrt{J}}{\sqrt{J_f}}) \tag{5.4}$$

where

$a = 1.000$

$b = 168.8 \times 10^3$

$B_1 = 40.57$

$B_2 = 0.1103$

$B_3 = 1.577$

$B_4 = -5.783$

$B_5 = 3.170$

$B_6 = 0.3168$

$B_7 = -0.9106$

$B_8 = 0.1436$

$B_9 = 0.1017$

---

*T_f is the final experimental value of T and in this particular case $T_f = 670.1 \times 10^{-6}$.

$B_{10} = -0.0474$

$B_{11} = 0.2405$

$B_{12} = -0.3466$

$B_{13} = 0.1637$

$B_{14} = -0.0012$

$B_{15} = -0.0329$

Figure 6.1 shows a plot of the work-hardening function H as a function of J.

Recall that for simple tension

$$\frac{dT}{d\varepsilon} = 1 + H \; .$$

Therefore

$$\varepsilon = \int_0^T \frac{dT}{1+H} = aT + \frac{bT^2}{2} + \sum_{k=1}^{15} \left(\frac{T_f}{k\pi}\right) B_k\left[\cos\left(\frac{k\pi T}{T_f}\right) - 1\right]. \qquad (5.5)$$

The stress-strain relationship (5.5) is shown graphically in Figure 5.2 and compared to the experimental results.

5.2 Simple Shear

Consider a material that obeys the constitutive relation

$$\frac{\mathcal{D}T_{ij}}{\mathcal{D}t} = d'_{ij} + H\left(\frac{M'}{2J}\right) T_{ij} \; .$$

For simple shear it follows that

$$\frac{dT}{dc} = H\left(\frac{ST}{T^2+S^2}\right) \tag{5.6}$$

$$\frac{dS}{dc} = 1 + H\left(\frac{S^2}{T^2+S^2}\right) \tag{5.7}$$

where

$$T_{ij} \equiv \frac{S_{ij}}{2\mu} = \begin{bmatrix} T & S & 0 \\ S & -T & 0 \\ 0 & 0 & 0 \end{bmatrix} \quad ,$$

$$d'_{ij} = \begin{bmatrix} 0 & \dot{c} & 0 \\ \dot{c} & 0 & 0 \\ 0 & 0 & 0 \end{bmatrix}$$

and $J = T^2+S^2$. The material derivative has been used to arrive at equations (5.6) and (5.7). It follows from equation (5.6) and the initial condition that $T = 0$ when $c = 0$, that $T = 0$ always. Therefore equation (5.7) becomes

$$\frac{dS}{dc} = 1 + H \quad .$$

It follows from equation (5.4) that

$$c = \int_0^S \frac{dS}{1+H} = aS + \frac{b}{\sqrt{3}} S^2 + \sum_{k=1}^{15} (\frac{S_f}{k\pi}) B_k [\cos(\frac{k\pi S}{S_f}) - 1] .$$

The relation between S and c is shown graphically in Figure 5.3.

5.3 Torsion of a Circular Bar

In the case of torsion of a circular bar equation (5.2) reduces to

$$\frac{\partial T}{\partial \theta} = \frac{r}{2} (1 + H) \tag{5.8}$$

where $T = S_{\theta z}/2\mu$ and θ is the angle of twist per unit length. Also $J = T^2$. Equation (5.8) can be integrated to yield

$$\frac{\theta r}{2} = aT + \frac{bT^2}{\sqrt{3}} + \sum_{k=1}^{15} (\frac{T_f}{k\pi}) B_k [\cos(\frac{k\pi T}{T_f}) - 1] .$$

Now since the moment is defined as

$$M = \int_0^a 2\pi r^2 S_{\theta z} \, dr$$

it follows that

$$\frac{M}{2\mu a^3} = 2\pi \int_0^1 T(\frac{r}{a})^2 d(\frac{r}{a}) . \tag{5.9}$$

Let T_0 represent the shear stress when $r = a$. Then

$$\frac{\theta a}{2} = aT_0 + \frac{b}{\sqrt{3}} T_0^{\,2} + \sum_{k=1}^{15} \left(\frac{T_f}{k\pi}\right) B_k\left[\cos\left(\frac{k\pi T_0}{T_f}\right) - 1\right] . \qquad (5.10)$$

Also for some particular angle of twist (θa)

$$\left(\frac{r}{a}\right) = \left(\frac{2}{\theta a}\right)\left[aT + \frac{b}{\sqrt{3}} T^2 + \sum_{k=1}^{15} \left(\frac{T_f}{k\pi}\right) B_k\left[\cos\left(\frac{k\pi T}{T_f}\right) - 1\right]\right].$$

From equation (5.9) it follows that

$$\frac{M}{2\mu a^3} = \frac{16\pi}{(\theta a)^3} \int_0^{T_0} T\left[aT + \frac{b}{\sqrt{3}} T^2 + \sum_{k=1}^{15} \left(\frac{T_f}{k\pi}\right) B_k\left[\cos\left(\frac{k\pi T}{T_f}\right) - 1\right]\right]^2 \cdot \qquad (5.11)$$

$$\cdot \left[a + b\sqrt{\frac{4}{3}}\, T - \sum_{k=1}^{15} B_k \sin\left(\frac{k\pi T}{T_f}\right)\right] dT .$$

For each T_0, (θa) can be found from equation (5.10). Then the integral in equation (5.11) is evaluated by Simpson's Rule with T_0 divided into 10 equal segments. As T_0 varies from 0 to T_f a corresponding (θa) and $M/2\mu a^3$ can be found. Some of these values are listed in Table 5.2 and a plot of moment versus angle of twist is shown in Figure 5.4 and compared with experimental torsion results.

5.4 Torsion of a Square Bar

The problem of torsion of a material that obeys the constitutive equation

$$\frac{\mathcal{D}T_{ij}}{\mathcal{D}t} = d'_{ij} - \alpha^2 M' T_{ij}$$

where $\alpha^2 = 2\mu^2/k^2$ was solved in Section 3.3.c and 3.3.d. In this section the problem is solved for a square bar where

$$\frac{\mathcal{D}T_{ij}}{\mathcal{D}t} = d'_{ij} + H\left(\frac{M'}{2J}\right) T_{ij} \; .$$

The solution proceeds as in Section 3.3.c up to equations (3.15) and (3.16) except that $-\alpha^2$ is replaced by (H/2J). Equations (3.15) and (3.16) become

$$\frac{\partial\phi}{\partial x_2} = -x_1 + \frac{\left(\frac{1}{2} + \frac{H}{2J} T_{13}^2\right) \frac{\partial T_{23}}{\partial\theta} - \frac{H}{2J} T_{13} T_{23} \frac{\partial T_{13}}{\partial\theta}}{\frac{1}{4}(1 + H)}$$

and

$$\frac{\partial\phi}{\partial x_1} = x_2 + \frac{\left(\frac{1}{2} + \frac{H}{2J} T_{23}^2\right) \frac{\partial T_{13}}{\partial\theta} - \frac{H}{2J} T_{13} T_{23} \frac{\partial T_{23}}{\partial\theta}}{\frac{1}{4}(1 + H)}$$

where $J = T_{13}^2 + T_{23}^2$. Define

$$\beta = \frac{2\left(1 + \frac{H}{J} T_{13}^2\right)}{(1 + H)}$$

$$\gamma = \frac{2 \frac{H}{J} T_{13} T_{23}}{(1 + H)}$$

$$\eta = \frac{2\left(1 + \frac{H}{J} T_{23}^2\right)}{(1 + H)} \; .$$

Then

$$\frac{\partial\phi}{\partial x_2} = - x_1 + \beta \frac{\partial T_{23}}{\partial\theta} - \gamma \frac{\partial T_{13}}{\partial\theta} \tag{5.12}$$

and

$$\frac{\partial\phi}{\partial x_1} = x_2 + \eta \frac{\partial T_{13}}{\partial\theta} - \gamma \frac{\partial T_{23}}{\partial\theta} . \tag{5.13}$$

Differentiating equation (5.12) with respect to x_1 yields

$$\frac{\partial^2\phi}{\partial x_1 \partial x_2} = - 1 + \beta \frac{\partial}{\partial x_1} (\frac{\partial T_{23}}{\partial\theta}) + \frac{\partial\beta}{\partial x_1} \frac{\partial T_{23}}{\partial\theta} - \gamma \frac{\partial}{\partial x_1} (\frac{\partial T_{13}}{\partial\theta}) - \frac{\partial\gamma}{\partial x_1} \frac{\partial T_{13}}{\partial\theta} . \tag{5.14}$$

Differentiating equation (5.13) with respect to x_2 yields

$$\frac{\partial^2\phi}{\partial x_2 \partial x_1} = 1 + \eta \frac{\partial}{\partial x_2} (\frac{\partial T_{13}}{\partial\theta}) + \frac{\partial\eta}{\partial x_2} \frac{\partial T_{13}}{\partial\theta} - \gamma \frac{\partial}{\partial x_2} (\frac{\partial T_{23}}{\partial\theta}) - \frac{\partial\gamma}{\partial x_2} \frac{\partial T_{23}}{\partial\theta} . \tag{5.15}$$

Upon eliminating ϕ from equations (5.14) and (5.15),

$$\begin{aligned} 2 + \eta \frac{\partial}{\partial x_2} (\frac{\partial T_{13}}{\partial\theta}) + \frac{\partial\eta}{\partial x_2} \frac{\partial T_{13}}{\partial\theta} - \gamma \frac{\partial}{\partial x_2} (\frac{\partial T_{23}}{\partial\theta}) - \frac{\partial\gamma}{\partial x_2} \frac{\partial T_{23}}{\partial\theta} \\ - \beta \frac{\partial}{\partial x_1} (\frac{\partial T_{23}}{\partial\theta}) - \frac{\partial\beta}{\partial x_1} \frac{\partial T_{23}}{\partial\theta} + \gamma \frac{\partial}{\partial x_1} (\frac{\partial T_{13}}{\partial\theta}) + \frac{\partial\gamma}{\partial x_1} \frac{\partial T_{13}}{\partial\theta} = 0 . \end{aligned} \tag{5.16}$$

Now since

$$T_{13} = \frac{\partial\psi}{\partial x_2} \qquad T_{23} = - \frac{\partial\psi}{\partial x_1} ,$$

equation (5.16) becomes

$$A \frac{\partial^2}{\partial x_1^2}\left(\frac{\partial\psi}{\partial\theta}\right) + 2B \frac{\partial^2}{\partial x_1 \partial x_2}\left(\frac{\partial\psi}{\partial\theta}\right) + C \frac{\partial^2}{\partial x_2^2}\left(\frac{\partial\psi}{\partial\theta}\right)$$
$$+ D \frac{\partial}{\partial x_1}\left(\frac{\partial\psi}{\partial\theta}\right) + E \frac{\partial}{\partial x_2}\left(\frac{\partial\psi}{\partial\theta}\right) + F = 0 \tag{5.17}$$

where $A = \beta$

$B = \gamma$

$C = \eta$

$D = \frac{\partial\beta}{\partial x_1} + \frac{\partial\gamma}{\partial x_2}$

$E = \frac{\partial\gamma}{\partial x_1} + \frac{\partial\eta}{\partial x_2}$

$F = 2$.

Since equation (5.17) is identical to equation (3.22) the rest of the solution is the same as in Section 3 except that the coefficients A, B, C, D and E depend on the work-hardening function H which is given by equation (5.4). The results are given in Figure 5.5 and compared with the experimental results.

5.5 An Elastic-Plastic Constitutive Equation for a Work-Hardening Material

From the classical theory of plasticity, the flow rule for a work-hardening material with a regular yield surface is

$$d^p_{ij} = 0 \quad \text{if} \quad f < 0 \quad \text{or if} \quad f = 0 \quad \text{and} \quad \dot{f} \equiv \frac{\partial f}{\partial \sigma_{ij}} \dot{\sigma}_{ij} \leq 0$$

$$d^p_{ij} = g \frac{\partial f}{\partial \sigma_{ij}} \dot{f} \quad \text{if} \quad f = 0 \quad \text{and} \quad \dot{f} \geq 0$$

where f is the plastic potential. If

$$f = f(II_s)$$

where

$$II_s = \frac{1}{2} S_{k\ell} S_{k\ell} ,$$

then

$$d^p_{ij} = g(\frac{\partial f}{\partial II_s})^2 \dot{II}_s S_{ij} \qquad (5.18)$$

during plastic flow. It follows that

$$S_{ij} d^p_{ij} = 2II_s g(\frac{\partial f}{\partial II_s})^2 \dot{II}_s$$

or

$$g(\frac{\partial f}{\partial II_s})^2 \dot{II}_s = \frac{S_{ij}d^p_{ij}}{2II_s} .$$

Equation (5.18) then becomes

$$d^p_{ij} = \frac{S_{k\ell}d^p_{k\ell}}{2II_s} S_{ij}$$

or in dimensionless form

$$d^p_{ij} = \frac{T_{k\ell}d^p_{k\ell}}{2J} T_{ij}$$

where $T_{ij} = S_{ij}/2\mu$ and $J = \frac{1}{2} T_{k\ell}T_{k\ell}$. The total deviatoric strain increment $d\varepsilon_{ij}$ is then given by

$$d\varepsilon_{ij} = dT_{ij} + \frac{T_{k\ell}d^p_{k\ell}}{2J} T_{ij} \ . \qquad (5.19)$$

In the dynamically correct form, equation (5.19) becomes

$$\frac{\mathcal{D}T_{ij}}{\mathcal{D}t} = d'_{ij} - \frac{T_{k\ell}d^p_{k\ell}}{2J} T_{ij}$$

for the elastic-plastic range and

$$\frac{\mathcal{D}T_{ij}}{\mathcal{D}t} = d'_{ij}$$

in the elastic range.

Consider a material that begins to yield immediately upon initial loading. (Commercially pure aluminum is an example). Then the constitutive equation

$$\frac{\mathcal{D}T_{ij}}{\mathcal{D}t} = d'_{ij} - \frac{T_{k\ell}d^{p}_{k\ell}}{2J}\,T_{ij} \tag{5.20}$$

applies for the complete range of loading. Now since

$$T_{k\ell}d'_{k\ell} = T_{k\ell}d'^{e}_{k\ell} + T_{k\ell}d^{p}_{k\ell} ,$$

let

$$T_{k\ell}d^{p}_{k\ell} = (-H)\,T_{k\ell}d'_{k\ell} \equiv -\,HM'$$

where $-1 \leq H \leq 0$.

Equation (5.20) becomes

$$\frac{\mathcal{D}T_{ij}}{\mathcal{D}t} = d'_{ij} + H\left(\frac{M'}{2J}\right)T_{ij} \tag{5.21}$$

where (-H) is the ratio of plastic work to the total work done.

Equation (5.21) for the elastic-plastic flow of a work-hardening material is identical to equation (5.2) for a hypoelastic body.

TABLE 5.1

Estimated Slopes of Tensile Results

$T(x10^{+6})$	$\frac{d\varepsilon}{dT}$
0	1.000 (*)
41.88	1.051
83.76	1.075
125.6	1.121
167.5	1.175
209.4	1.620
251.3	2.728
293.2	5.641
335.0	14.42
376.9	28.74
418.8	42.55
460.7	52.99
502.6	57.23
544.4	62.86
586.3	75.71
628.2	92.23
670.1	114.1

(*) $\frac{d\varepsilon}{dT}$ was set equal to 1.000 at the origin

TABLE 5.2

Results for Torsion of Circular Bar

$T_0(x10^{+6})$	$\theta a(x10^{+3})$	$\frac{M}{2\mu a^3}(x10^{+3})$
0	0	0
17.41	0.03563	0.02746
34.82	0.07220	0.05493
52.23	0.1087	0.08225
69.64	0.1455	0.1097
87.05	0.1834	0.1377
104.5	0.2222	0.1658
121.9	0.2612	0.1935
139.3	0.3005	0.2213
156.7	0.3421	0.2503
174.1	0.3896	0.2819
191.5	0.4473	0.3169
208.9	0.5204	0.3554
226.3	0.6158	0.3975
243.7	0.7460	0.4441
261.1	0.9375	0.4967
278.5	1.238	0.5532
296.0	1.708	0.6053
313.4	2.401	0.6459
330.8	3.339	0.6766
348.2	4.521	0.7046

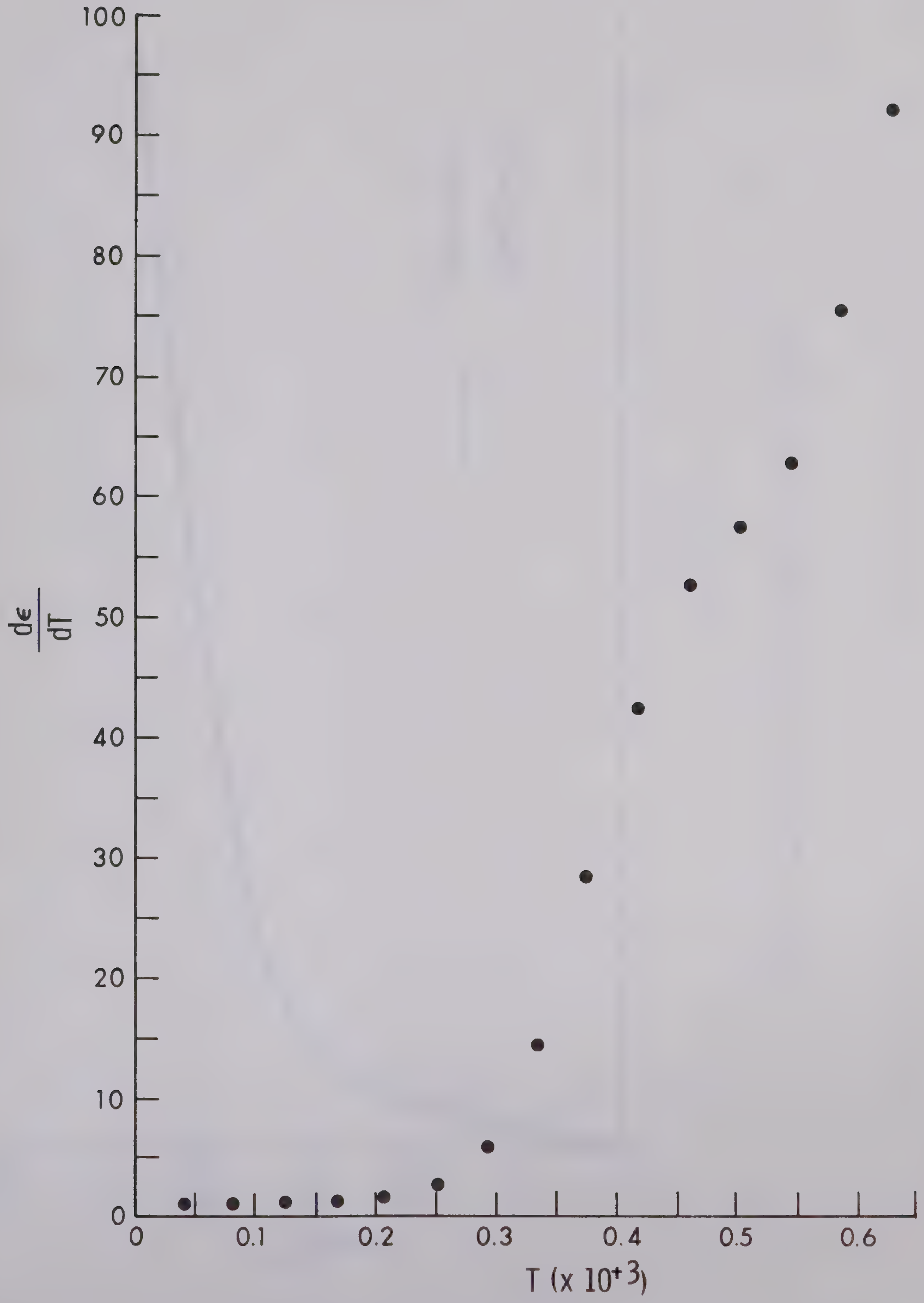

Fig. 5.1 Estimated Slopes of Tensile Results

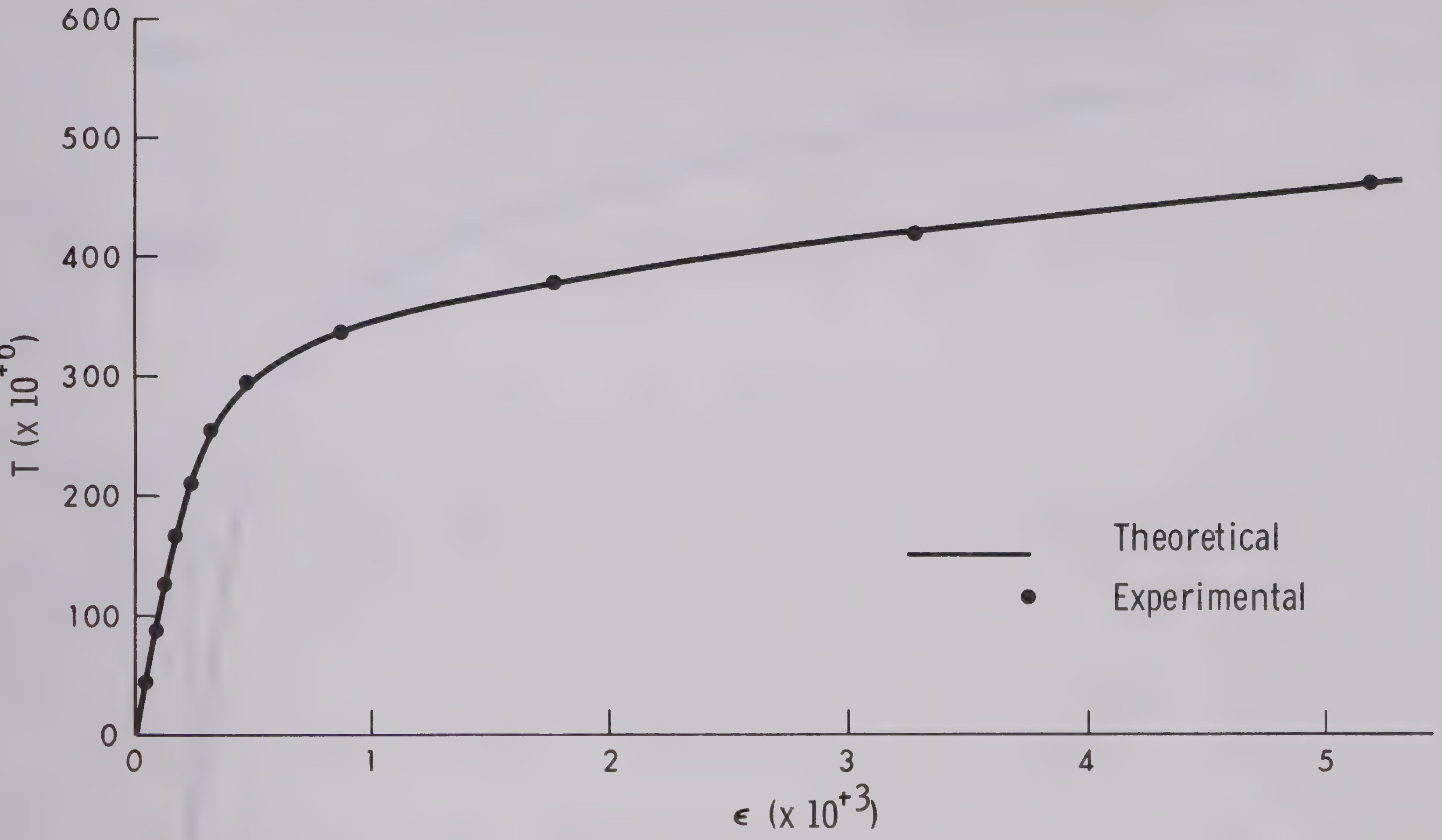

Fig. 5.2 Theoretical Curve for Simple Tension Problem

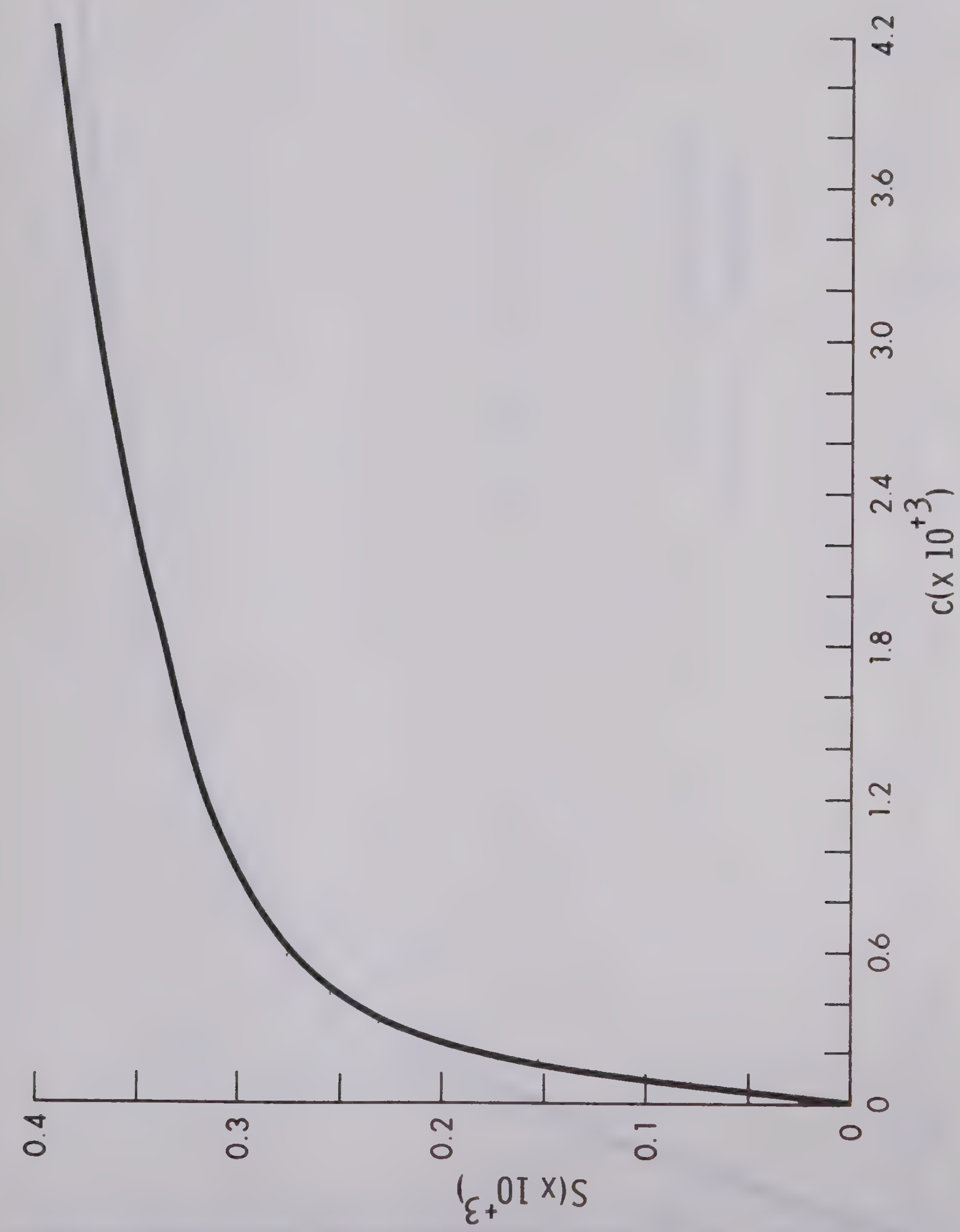

Fig. 5.3 Simple Shear - Work-Hardening Material

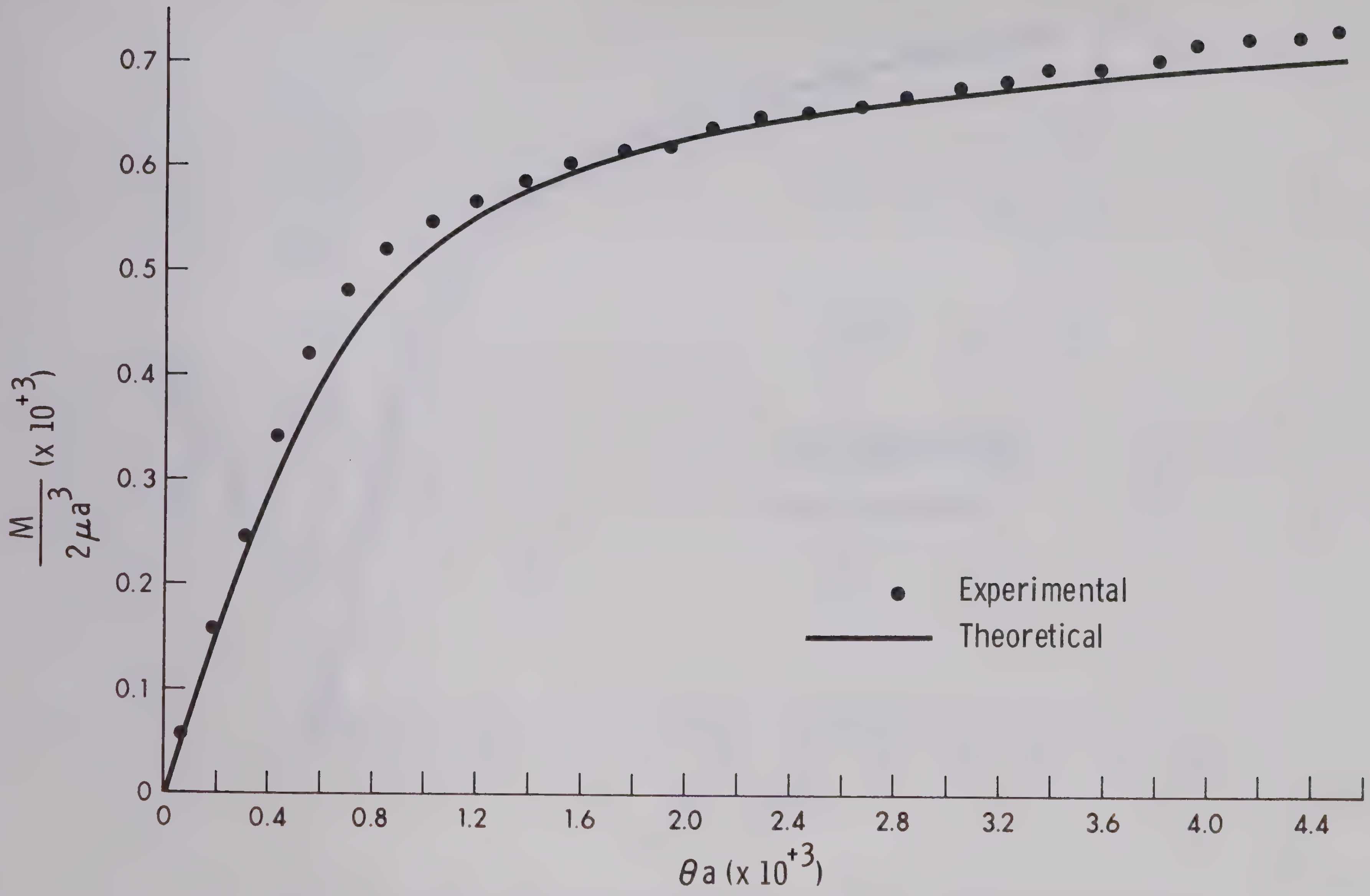

Fig. 5.4 Torsion of Work-Hardening Material With a Circular Cross-Section

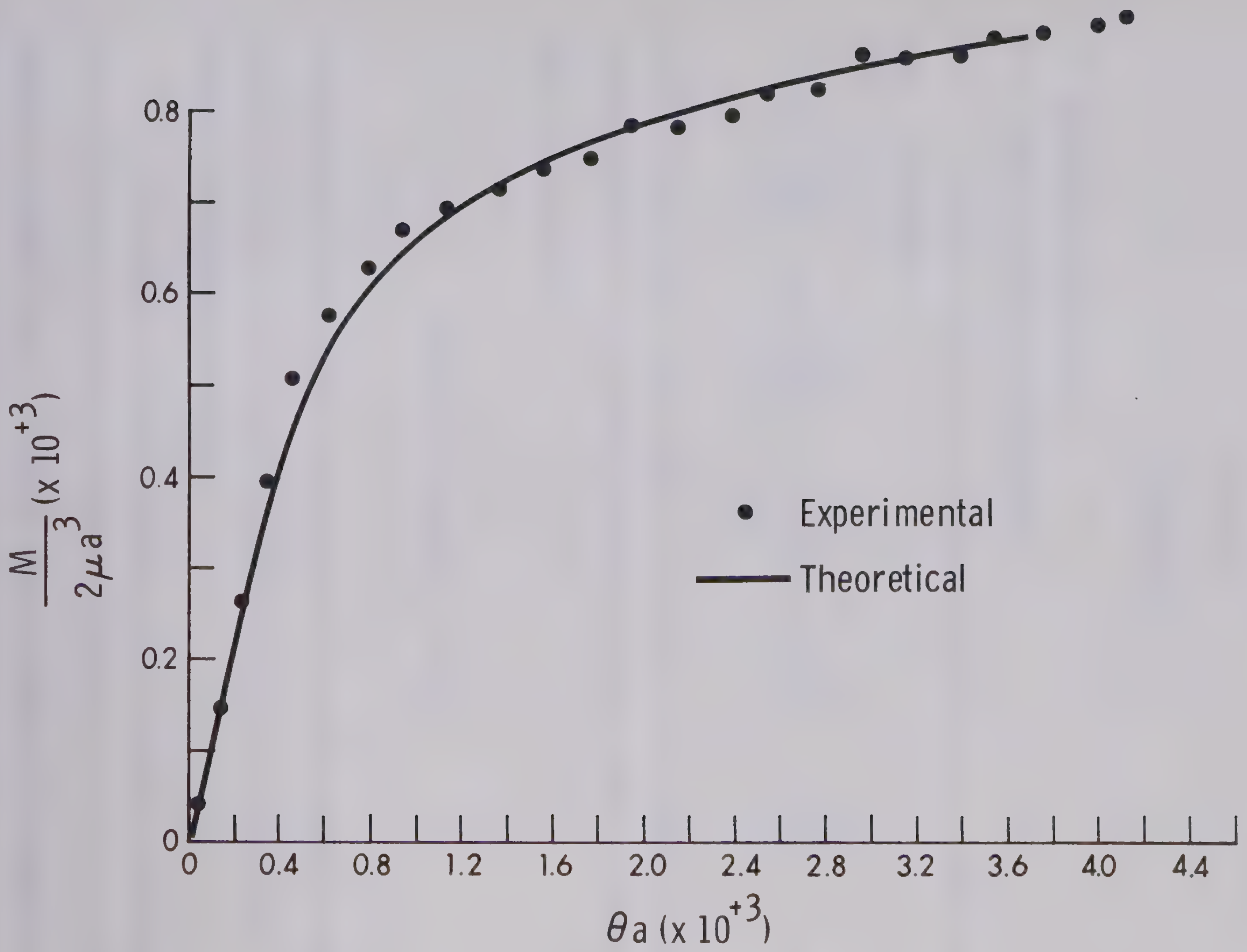

Fig. 5.5 Torsion of Work-Hardening Material With a Square Cross-Section

CHAPTER VI

CONCLUSION

6.1 Estimation of Errors

6.1.1 Errors in Numerical Procedure

For both the elastic-perfectly plastic and the work-hardening body, the equation

$$A \frac{\partial^2(\frac{\partial\psi}{\partial\theta})}{\partial x_1^2} + 2B \frac{\partial^2(\frac{\partial\psi}{\partial\theta})}{\partial x_1 \partial x_2} + C \frac{\partial^2(\frac{\partial\psi}{\partial\theta})}{\partial x_2^2} + D \frac{\partial(\frac{\partial\psi}{\partial\theta})}{\partial x_1} + E \frac{\partial(\frac{\partial\psi}{\partial\theta})}{\partial x_2} + F = 0 \quad (6.1)$$

was solved for $(\frac{\partial\psi}{\partial\theta})$ at each angle of twist per unit length in the torsion problem. A new stress function was calculated each time by applying the formula

$$\psi(\theta+\Delta\theta) = \psi(\theta-\Delta\theta) + 2\Delta\theta(\frac{\partial\psi}{\partial\theta}) \quad (6.2)$$

at each point in the square cross-section. A corresponding moment was then found by integrating the stress function over the cross-section by using Simpson's Rule.

An estimate of the truncation error introduced when replacing equation (6.1) by a finite difference approximation is obtained by changing the mesh size. In Chapter III and Chapter V a mesh size of 1/10 is used. The problem was also solved with a mesh size of 1/6.

It was found that a local truncation error of 0.2% is present in the calculated value of the rate of increase of the stress function at the center of the cross-section. After 800 increments in angle of twist per unit length this truncation error had accumulated to a value of 0.7%. These truncation errors are at least 1000 times as large as the error involved in using Simpson's Rule to find moments from the stress function.

The truncation errors in the stress function, as described above, caused a local error in the moment of 0.13%. After 800 increments in angle of twist the error became 0.3%.

The increment in angle of twist per unit length was then doubled for the case of the mesh size equal to 1/10. This made no significant change in any of the results. The computer program printed out results to eight significant figures and after one thousand increments in angle no change could be noticed in the eighth digit of the stress function or the moment.

Roundoff errors were minimized by using double precision accuracy when making the computer calculations. A computer library subroutine (DGELB), which is designed specifically for inverting matrices with a banded structure, was used to solve the 55 equations at each angle of twist per unit length. The solution of these equations was carried out with a precision of 10^{-15} [24].

In addition to the above, there are errors in the calculated moments due to errors in the work-hardening function H.

H is found from the slope of the stress-strain data from the

tension test as described in Chapter V. From equations (5.3) and (5.4)

$$\frac{d\varepsilon}{dT} \equiv \frac{1}{1+H} = 1 + b\sqrt{\frac{4}{3}J} - \sum_{k=1}^{15} Bk \sin\left(\frac{k\pi\sqrt{J}}{\sqrt{J_f}}\right) . \tag{6.3}$$

Consider

$$\left(\frac{d\varepsilon}{dT}\right)_1 = \frac{1}{1+H_1} = 1 + e_1\left[b\sqrt{\frac{4}{3}J} - \sum_{k=1}^{15} Bk \sin\left(\frac{k\pi\sqrt{J}}{\sqrt{J_f}}\right)\right] \tag{6.4}$$

and

$$\left(\frac{d\varepsilon}{dT}\right)_2 = \frac{1}{1+H_2} = 1 + e_2\left[b\sqrt{\frac{4}{3}J} - \sum_{k=1}^{15} Bk \sin\left(\frac{k\pi\sqrt{J}}{\sqrt{J_f}}\right)\right] \tag{6.5}$$

where $0 < e_1 < 1$ and $e_2 > 1$. Therefore

$$\left(\frac{d\varepsilon}{dT}\right)_1 \leq \frac{d\varepsilon}{dT} \leq \left(\frac{d\varepsilon}{dT}\right)_2 \tag{6.6}$$

where $\frac{d\varepsilon}{dT}$ are the calculated values from equation (6.3). It follows then that

$$H_1 \geq H \geq H_2 \tag{6.7}$$

where the equalities in equations (6.6) and (6.7) apply only when $J = 0$. During loading, for a positive angle of twist, $T_{13} \leq 0$,

$d'_{13} \leq 0$, $T_{23} \geq 0$ and $d'_{23} \geq 0$ in the quadrant $x_1 \geq 0$, $x_2 \geq 0$. Therefore, since

$$\left(\frac{\partial T_{13}}{\partial \theta}\right)_1 = \frac{d'_{13}}{\dot{\theta}} + \frac{H_1}{\dot{\theta}} \left(\frac{T_{k\ell} d'_{k\ell}}{2J}\right) T_{13}$$

and

$$\left(\frac{\partial T_{23}}{\partial \theta}\right)_1 = \frac{d'_{23}}{\dot{\theta}} + \frac{H_1}{\dot{\theta}} \left(\frac{T_{k\ell} d'_{k\ell}}{2J}\right) T_{23}$$

it follows that $M_1 \geq M$. Also since

$$\left(\frac{\partial T_{13}}{\partial \theta}\right)_2 = \frac{d'_{13}}{\dot{\theta}} + \frac{H_2}{\dot{\theta}} \left(\frac{T_{k\ell} d'_{k\ell}}{2J}\right) T_{13}$$

and

$$\left(\frac{\partial T_{23}}{\partial \theta}\right)_2 = \frac{d'_{23}}{\dot{\theta}} + \frac{H_2}{\dot{\theta}} \left(\frac{T_{k\ell} d'_{k\ell}}{2J}\right) T_{23}$$

it follows that $M_2 \leq M$, where M is the moment and M_1 and M_2 are the moments calculated when H_1 and H_2 are substituted respectively for H.

Equations (6.4) and (6.5) are imposing an error on $d\varepsilon/dT - 1$ for all J and yet the functions H_1 and H_2 are still bounded by the inequalities

$$0 \leq H_1 \text{ , } H_2 \leq -1 \text{ .}$$

If the function $d\varepsilon/dT - 1$ can be determined from the experimental tension data to within the imposed error at all points then M_1 and M_2 are certainly upper and lower estimates respectively for the moment.

It was found that M_1 and M_2 for the problem of torsion of a square bar varied only about 2.5% from the previously calculated moments M when a 20% error in $d\varepsilon/dT - 1$ was imposed by letting $e_1 = 0.80$ and $e_2 = 1.20$.

During the experimental tension tests, assume that the strains ε were obtained with an accuracy of ± 3%. The slope of the T vs ε data was obtained at each data point by a computer library subroutine which used a fourth order Lagrange interpolation formula. An estimate of the maximum errors in the calculated slopes $d\varepsilon/dT$ [25] is given below.

$$\text{truncation error in } \frac{d\varepsilon}{dT}(T_i) = \frac{(\Delta T)^4}{30} \frac{d^5\varepsilon}{dT^5}(\xi_i)$$

$$\xi_i \ \varepsilon(T_{i-2}, T_{i+2})$$

$$\text{roundoff error in } \frac{d\varepsilon}{dT} = \frac{3}{2} \frac{e_s}{|\Delta T|}$$

where e_s is the error in the ordinate ε and ΔT is the equally spaced intervals in stresses T.

Since the slope $\frac{d\varepsilon}{dT}$ is given by

$$\frac{d\varepsilon}{dT} = 1 + bT - \sum_{k=1}^{15} Bk \sin(\frac{k\pi T}{T_f})$$

the truncation error is given by

$$e_T = -\frac{\Delta^4}{30} \sum_{k=1}^{15} (\frac{k\pi}{T_f})^4 \, Bk \sin(\frac{k\pi T}{T_f}) \; .$$

Therefore since $T_f = 16\Delta$,

$$e_T = -\frac{\pi^4}{30(16)^4} \sum_{k=1}^{15} k^4 \, Bk \sin(\frac{k\pi T}{T_f}) \qquad (6.8)$$

and

$$e_R = \frac{3}{2} \times \frac{0.03}{41.8 \times 10^{-6}} \; \varepsilon_i \qquad (6.9)$$

where e_T and e_R are the maximum truncation and roundoff errors. Table 6.1 lists the slopes dε/dT and the corresponding errors* calculated at each point from equations (6.8) and (6.9). It appears that the error in (dε/dT - 1) may be approximately 100% when dε/dT is small. However as the slope increases, a 20% error may be assumed for the purpose of establishing bounds on the error in moment. The upper and lower estimates, M_1 and M_2, were calculated assuming 100% error in dε/dT - 1 when $J \leq 3 \times 10^{-8}$ and a 20% error when $J > 3 \times 10^{-8}$. The factors e_1 and e_2

---

*It may be noted that the fifth derivative in equation (6.8) is the fifth derivative of a best-fit curve through the calculated slopes.

in equations (6.4) and (6.5) take the following values;

$$e_1 = \begin{cases} 0.10 & (J \leq 3 \times 10^{-8}) \\ 0.80 & (J > 3 \times 10^{-8}) \end{cases}$$

$$e_2 = \begin{cases} 2.00 & (J \leq 3 \times 10^{-8}) \\ 1.20 & (J > 3 \times 10^{-8}) \end{cases} \quad .$$

The corresponding curves for H_1 and H_2 are shown in Figure 6.1. Table 6.2 shows the percentage errors in the moments as calculated by the equation

$$\text{(upper/lower) bound} = \frac{(M_i - M)}{M} \times 100 \qquad (i=1,2)$$

for a square bar at various angles of twist. It can be seen that the maximum difference between the calculated moments M and the moments M_1 and M_2 is approximately 6% and occurs at a relatively small angle of twist. The difference then tends to decrease towards approximately 2.5% as the angle of twist per unit length increases. It appears that the large possible error in H for small J has little effect at larger angles of twist.

The corresponding errors in moments for the circular bar behaved in the same manner. A table for the circular bar similar to Table 6.2 is not included because when H changes, the angles of twist

as well as the moments change and the moments could not be compared at any specific angle of twist.

6.1.2 Experimental Errors

An estimate of the errors for the tension test is given in Section 6.1.1.

The following discussion on errors for the experimental torsion problem applies to both the circular and square cross-section.

The non-dimensional moment is given by $M/2\mu a^3$. The moment M can be obtained from the expression M = 179 V to within 1% of the true moment where V is the voltage reading in m.v. and M is moment in units of in.-lb. Since "a" is measured to within ± 0.001", a^3 is within 1% of the true value. Also it is assumed that μ is correct to within 1%. The fact that the initial slope in Figure 4.9 compares so well with the classical elastic theory for torsion of a circular bar indicates that $\mu = 3.76 \times 10^6$ psi is a reasonable value to use. Therefore the expression $M/2\mu a^3$ may have a maximum error of 3%. However, the most probable error is approximately 1.7%.

Originally, neither of the experimental curves for moment versus angle of twist went through the origin. This can be seen in Tables 4.8 and 4.9 where a constant was added to the θa values. This may partially be due to a small moment induced in the specimens when the upper jaws of the torsion machine were tightened prior to the experiments. It may also be caused by one of the spider mechanisms having a different amount of slack than the other.

Section 4.1.5 compares the angle of twist measured by the spider apparatus to the angle of twist measured by strain gauges. Figure 4.14 shows that if a constant is added to the angles of twist determined by the spider apparatus, the two different methods give almost identical results.

From the above discussion and the close agreement of the calibration data with the calibration curves as shown in Chapter IV the author makes the assumption that the angles of twist (θa) are accurate to within 3%.

6.2 Discussion of Errors

It appears that the numerical calculations of the theoretical moments for the square cross-section could be improved by decreasing the mesh size. However, the numerical technique seems quite adequate until the error in H can be reduced for the case of the work-hardening solid.

The theoretical and experimental torsion results compare quite favorably. The theoretical moment curves for both the square and circular cross-sections deviate from the experimental results in the same manner and at approximately the same angle. The angle at which the greatest deviation occurs is approximately the same angle at which an error in H would cause the greatest error in moment, as seen in Table 6.2.

The calculations shown in Chapter III for the torsion problem of an elastic-perfectly plastic material would not involve errors due

to an estimated work-hardening function.

Error estimates in this chapter are concerned only with the torsion problem because this is the only problem to which results could be compared. An error analysis on the numerical methods used for the other minor problems in this thesis can be done using similar reasoning.

6.3 Discussion of Results

In Section 6.1.1 it was shown that if $H_2 \leq H$ for all J, the moment M_2 calculated by using H_2 in the hypoelastic constitutive equation would be a lower estimate for M. The same reasoning can be applied to the elastic-perfectly plastic results shown in Chapter III. It follows then that hypoelastic theory gives an underestimate for the torque of the classical elastic-perfectly plastic solution for the torsion problem. This is also true for the simple shear and the simple extension problem.

In Chapter III the simple shear problem was solved with the assumption that the material obeyed the constitutive equation

$$\frac{\mathcal{D}T_{ij}}{\mathcal{D}t} = d'_{ij} - \alpha^2 M'T_{ij} \qquad (6.10)$$

where $\alpha^2 = 2\mu^2/k^2$ and $M' = T_{k\ell}d'_{k\ell}$.

Truesdell [13] solved the same problem but interpreted the results differently than did the author of this thesis. The constitutive equation used by Truesdell [13] is identical to equation (6.10) except that the constant α^2 is replaced by $1/K^2$. Therefore

$$K^2 = \frac{k^2}{2\mu^2} \ .$$

From the results of Section 3.2 and the comments made at the end of that section it is clear that if the dynamically correct form of the stress rate is used the solution of the problem will consist of a shearing stress S and a tensile stress T. The ratio T/k approaches k/μ asymptotically from below while S/k rises above $\sqrt{1 - k^2/\mu^2}$ and then approaches $\sqrt{1 - k^2/\mu^2}$ asymptotically from above. The point at which S reaches a maximum is defined as the hypoelastic yield point by Truesdell [13] and the von Mises yield is obtained when $T^2 + S^2 = k^2$. It is shown in Section 3.2 that the asymptotic values shown above are valid for the hypoelastic theory and the classical elastic-plastic theory if the von Mises yield criteria and the Jaumann stress rate is used. However in the hypoelastic theory $(T^2 + S^2)/k^2$ approaches unity from below while in the classical elastic-plastic theory $(T^2 + S^2)/k^2 = 1$ once the yield point is reached. If the material or local stress rate is used, both of the above theories predict that $T = 0$.

Truesdell [13] compares the results of the hypoelastic theory in which the Jaumann stress rate is used to that of the classical elastic-plastic theory in which the material rate of stress is used. These comparisons lead to various incorrect deductions.

As is mentioned above, a normal stress T appears in Truesdell's solution because the Jaumann stress rate is used rather than the material derivative.

It can be shown that the hypoelastic yield always occurs at a smaller strain than does the von Mises yield as predicted by elastic-plastic theory. Truesdell deduces then that since the hypoelastic yield is a maximum for shearing stress S, it is impossible for the shear stress to increase continuously to the von Mises yield as observed by T.Y. Thomas [22]. Although this statement is true, it is trivial because S is merely a measure of shear on a particular plane. From the Mohr circle shown in Figure 6.2 it is clear that the normal stress T induces a further shear at each point in the body.

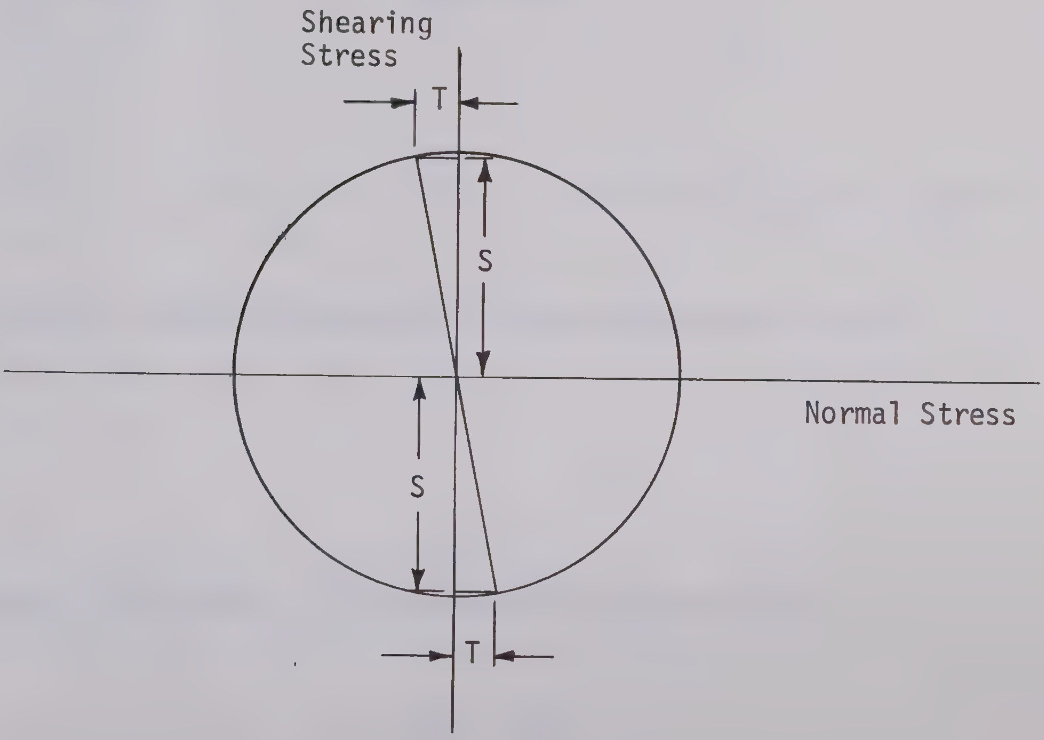

Fig. 6.2 Mohr Circle for the Simple Shear Problem

The Mohr circle in Figure 6.2 is for a typical element in the body as shown in Figure 6.3.

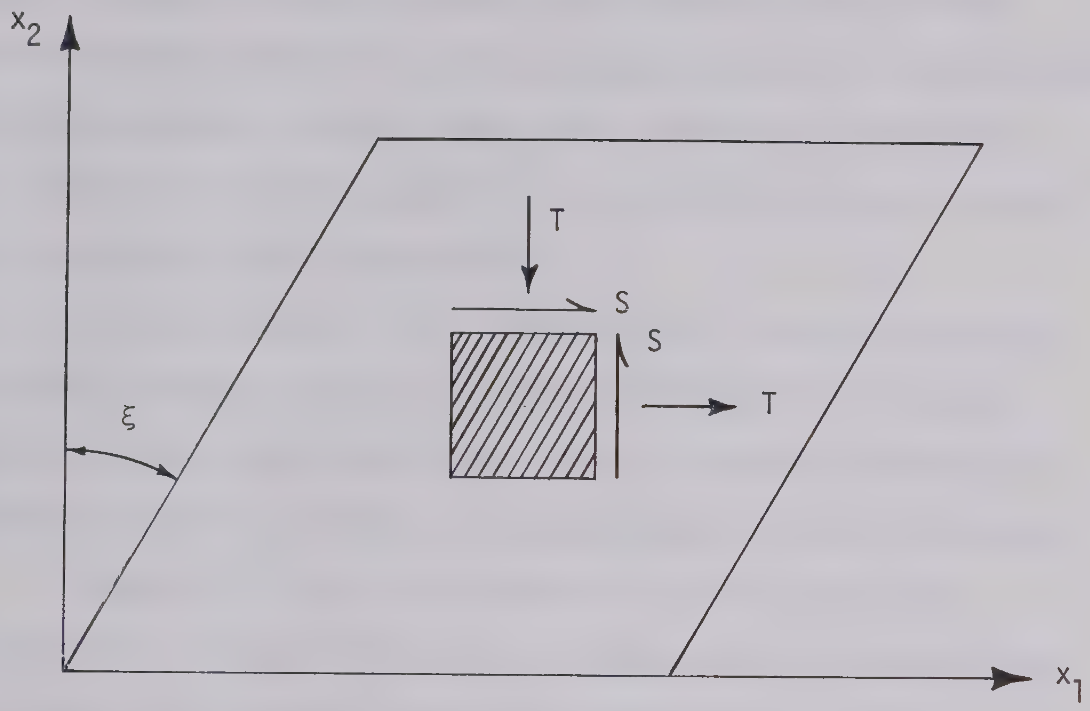

Fig. 6.3 Typical Element in a Body During Simple Shear

The maximum shear stress τ is found from the relationship

$$\tau^2 = T^2 + S^2$$

and it was shown in Section 3.2 that τ approaches k asymptotically

from below.

Simple shear consists of pure shear with a rotation. If the problem of pure shear was solved, no normal stress T would appear since the Jaumann stress rate would reduce to the material rate of stress. The resulting shear stress for a shearing angle of $\phi/2$ would be identical to the maximum shear τ for the simple shear problem at a shear angle of ϕ. Therefore the normal stress T arises in the simple shear problem due to a rotation through the angle $\phi/2$.

For most metals $\frac{\mu}{k} \approx 10^3$. Therefore K is very small and for the problems solved in Chapter III, the stresses get very large before the rotations become significant. One is then justified in using the material derivative in place of the dynamically correct stress rate.

Truesdell [13] also concludes that "since for very small K, the shear stress at hypoelastic yield is substantially the same as the shear stress at the von Mises yield, the shear stress as a function of shear strain will rise quickly to a value approximately $K/\sqrt{2}$, overshoot to a slightly larger value, and then level off again". Regardless of whether Truesdell is considering the shear stress S or the maximum shear stress τ, this conclusion is erroneous for any permissible value of K. Section 3.2 of this thesis shows that τ approaches k from below. Therefore $\tau/2\mu$ approaches $k/2\mu$ or $K/\sqrt{2}$ asymptotically from below.

Chapters IV and V consider the experimental measurement and the theoretical prediction respectively of problems involving a work-

hardening material. The results compare favorably and it is felt that the method described in Chapter V may be used quite confidently to predict the relation between $M/2\mu a^3$ and θa for a work-hardening material with a square cross-section. Since angles of twist are extremely difficult to measure for a square bar, it would be a simple matter to perform a tension test on the material and feed the resulting stress strain data into a computer program which would predict the performance of the same material under torsion. This technique, of course, is not restricted to the torsion problem. Torsion of a square bar was chosen as an example since experimental results are sometimes difficult to obtain. The results for simple shear, shown in Figure 5.4, would hopefully compare quite favorably with experimental results.

TABLE 6.1

Estimation of Maximum Errors in Slopes

$\frac{d\varepsilon}{dT}$	Truncation Error	Round Off Error
1.000	0.000	0.000
1.051	0.00894	0.0460
1.075	-0.0150	0.0940
1.121	0.0292	0.143
1.175	-0.0130	0.196
1.620	-0.00221	0.255
2.728	0.187	0.354
5.641	-0.160	0.533
14.42	-0.375	0.942
28.74	0.381	1.91
42.55	-0.313	3.53
52.99	0.662	5.69
57.23	-0.0958	8.24
62.86	-0.638	10.9
75.71	0.616	14.0
92.23	-0.548	17.8
114.1	0.000	22.4

TABLE 6.2

Estimation of Maximum Errors in Moments

θa $(\times 10^{+3})$	$\frac{(M_1-M)}{M} \times 100$	$\frac{(M_2-M)}{M} \times 100$
0.000	0.0	0.0
0.164	3.9	-4.0
0.329	6.0	-5.8
0.493	5.4	-5.5
0.657	4.6	-4.7
0.822	4.0	-4.0
0.986	3.7	-3.6
1.15	3.4	-3.3
1.31	3.3	-3.1
1.48	3.2	-2.9
1.64	3.1	-2.8

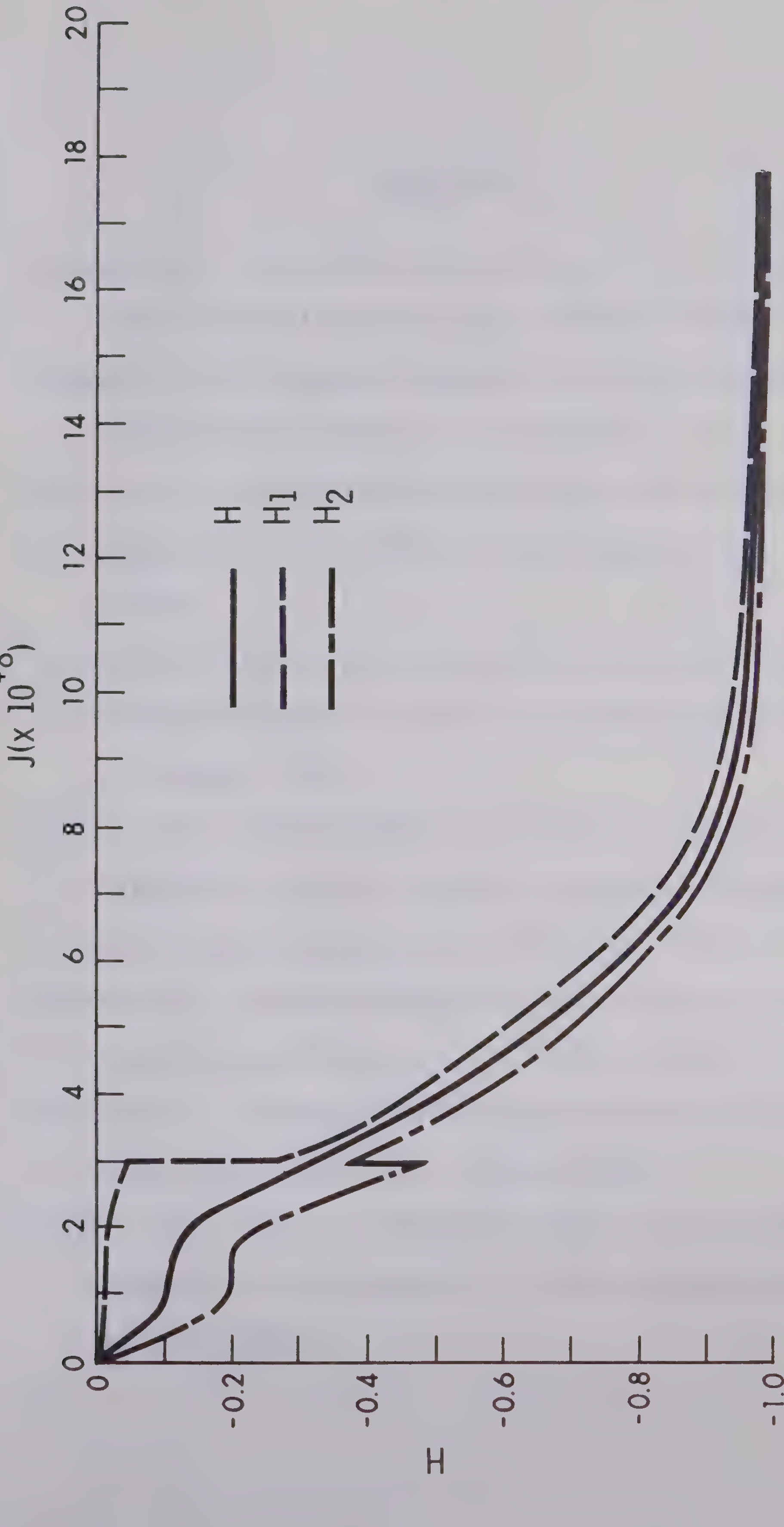

Fig. 6.1 Work-Hardening Function for Commercially Pure Aluminum

BIBLIOGRAPHY

1. Truesdell, C., The Simplest Rate Theory of Pure Elasticity, Comm. Pure Applied Math., 8; p. 123-132, (1955).
2. Prager, W., An Elementary Discussion of Definitions of Stress Rate, Quarterly Journal of Applied Math., 18; p. 403, (1960).
3. Noll, W., On the Continuity of the Solid and Fluid States, Journal of Rational Mechanics and Analysis, 4; p. 3-81, (1955).
4. Jaumann, G., Geschlossenes System Physikalischer und Chemischer Differenzialgesetze, Sitzber. Akad. Wiss. Wien. (IIa) 120; p. 385-530, (1911).
5. Rivlin, R.S., Further Remarks on the Stress-Deformation Relations for Isotropic Materials, Journal of Rational Mechanics and Analysis, 4; p. 681-702, (1955).
6. Bernstein, B., Hypoelasticity and Elasticity, Arch. of Rational Mechanics and Analysis, 6; p. 90-104, (1960).
7. Bernstein, B., Relations Between Hypoelasticity and Elasticity, Trans. Soc. Rheol., 4; p. 23-28, (1960).
8. Koiter, W.T., General Theorems for Elastic-Plastic Solids, Progress in Solid Mechanics, p. 167, Amsterdam, North Holland, (1960).

9. Hill, R., The Mathematical Theory of Plasticity, Oxford University Press, Oxford Engineering Science Series, (1950).

10. Thomas, T.Y., Plastic Flow and Fracture in Solids, New York; Academic Press, p. 94, (1961).

11. Green, A.E. and Adkins, J.E., Large Elastic Deformations and Non-linear Continuum Mechanics, Clarendon Press, Oxford (1960), p. 340.

12. Truesdell, C., Second Order Effects in the Mechanics of Materials, International Symposium on Second Order Effects in Elasticity, Plasticity and Fluid Dynamics, Haifa, (1962), p. 16, Permagon Press, (1964).

13. Truesdell, C., Hypoelastic Shear, Journal of Applied Physics, 27; p. 441, (1956).

14. Green, A.E., Hypoelasticity and Plasticity, Proc. Roy. Soc., A234; p. 46-59, (1956).

15. Green, A.E., Hypoelasticity and Plasticity II, Journal of Rational Mechanics and Analysis, 5; p. 725-734, (1956).

16. Ramberg, W. and Osgood, W.R., Description of Stress-Strain Curves by Three Parameters, N.A.C.A. Technical Note No. 902, (1943).

17. Saint-Venant, B., Mém. Savants Éstrangers, vol. 14; (1855).

18. Prandtl, L., Physik. Z., vol. 4; (1903).

19. Timoshenko, S. and Goodier, J.N., Theory of Elasticity, McGraw-Hill, New York, (1951).

20. Metals Handbook, 1948 Edition, The American Society for Metals, p. 811.

21. Esser, Hans, and Ahrend, H., Kann die 0.2% Grenze durch eine übereinkommenfreie Dehngrenze ersetzt werden, Arch. f. Eisenhüttenw, vol. 13, no. 10, p. 425-428, (1939-40).

22. Thomas, T.Y., Proc. Natl. Acad. Sci., 41; p. 720, (1955).

23. Saint Venant, B., Comptes Rendus Acad. Sci. Paris, 70, (1870), p. 473; Journal Math pures et app., 16, (1871), p. 308; Comptes Rendus Acad. Sci. Paris, 74, (1872), p. 1009 and 1083.

24. Subroutine DGELB from I.B.M. System/360 Scientific Subroutine Package.

25. Subroutine DDET5 from I.B.M. System/360 Scientific Subroutine Package.

26. Fröberg, C.E., Introduction to Numerical Analysis, Second Edition, Addison-Wesley Publishing Company, (1969), p. 336.

27. Ralston, A., A First Course in Numerical Analysis, McGraw-Hill, Inc. (1965).

28. Lanczos, C., Applied Analysis, Sir Isaac Pitman and Sons Ltd., (1957).

29. Greenberg, H.J., Dorn, W.S., and Wetherell, E.H., A Comparison of Flow and Deformation Theories in Plastic Torsion of a Square Cylinder, Plasticity: Proceedings of the Second Symposium on Naval Structural Mechanics, Brown University, R.I., (1960), p. 279-296.

30. Herakovich, C.T. and Hodge, P.G. Jr., Elastic-Plastic Torsion of Hollow Bars by Quadradic Programming, Int. J. Mech. Sci., 11, (1969), p. 53-63.

31. Leigh, D.C., Nonlinear Continuum Mechanics, McGraw-Hill, New York, (1968).

32. Hodge, P.G. Jr., Herakovich, C.T., and Stout, R.B., On Numerical Comparisons in Elastic-Plastic Torsion, Journal of Applied Mechanics, 35, (1968), p. 454-459.

B30003